UC Santa Cruz

UC Santa Cruz Electronic Theses and Dissertations

Title
Investigating the role of Lipoxygenase and oxylipins in platelet aggregation

Permalink
https://escholarship.org/uc/item/9913d44g

Author
Tran, Michelle

Publication Date
2023

Peer reviewed|Thesis/dissertation

UNIVERSITY OF CALIFORNIA

SANTA CRUZ

DOCTOR OF PHILOSOPHY

in

Molecular, Cellular, and Developmental Biology

by

Michelle Tran

September 2023

The Dissertation of Michelle Tran

is approved:

_____

Theodore Holman

_____

Manual Ares

_____

Seth Rubin

_____

Peter Biehl
Vice Provost and Dean of Graduate Studies

Table of Contents

List of Figures

List of tables

Abstract:

Investigation of the role of oxylipins and Lipoxygenase in platelet aggregation

Michelle Tran

Platelet aggregation and thrombosis are critical processes in hemostasis and wound healing, but their dysregulation can lead to the formation of obstructive blood clots with severe health consequences. To maintain control over these processes, the body relies on specialized pro-resolving mediators (SPMs) derived from polyunsaturated fatty acids (PUFAs) such as arachidonic acid (AA), eicosapentaenoic acid (EPA), and docosahexaenoic acid (DHA). Lipoxygenase (LOX) enzymes, which are non-heme iron-containing enzymes, play a vital role in the generation of specific oxylipins, including specialized resolvins, that act as important regulators of platelet function and thrombus resolution.

The interplay between LOX enzymes and platelet aggregation is complex. These enzymes can produce both pro-inflammatory and pro-thrombotic lipid mediators, as well as specialized resolvins that have anti-inflammatory and pro-resolving effects. Targeting LOX activity and promoting the production of specialized resolvins holds promise as potential therapeutic strategies to regulate platelet function and enhance thrombus resolution. Moreover, essential fatty acids like linoleic acid (LA) and α-linolenic acid (ALA) play crucial roles as precursors for

the synthesis of bioactive lipid mediators, including omega-6 and omega-3 fatty acids. Understanding the catalytic mechanisms, expression patterns, and allosteric regulation of LOX enzymes is essential for uncovering their physiological functions and developing targeted therapeutic interventions.

In line with these investigations, recent research has focused on the impact of a single nucleotide polymorphism (SNP) in human platelet 12-lipoxygenase (h12-LOX). This SNP results in a tyrosine-to-cysteine mutation at a buried site (Y649C) and has been associated with reduced levels of 12(S)-hydroxyeicosatetraenoic acid (12S-HETE) production in isolated platelets. Detailed characterization of the Y649C mutant revealed that it exhibits reduced catalytic rates, altered membrane affinity, and decreased protein stability compared to the wild-type (WT) h12-LOX enzyme. These subtle changes in activity and protein properties may contribute to the significant physiological alterations observed in platelet biology associated with the Y649C SNP.

Furthermore, lipid metabolism and the involvement of acyl-coenzyme A (acyl-CoA) molecules have gained attention in the context of LOX biochemistry and inflammation. Acyl-CoAs have been found to bind to LOX enzymes, and their inhibitory effects on various LOX isozymes have been investigated. C18 acyl-CoA derivatives were identified as potent inhibitors of h12-LOX, human reticulocyte 15-LOX-1 (h15-LOX-1), and human endothelial 15-LOX-2 (h15-LOX-2), while C16 acyl-CoAs showed higher potency against human 5-LOX. Notably, oleoyl-CoA (18:1) was the most potent inhibitor of h12-LOX and h15-LOX-2, while stearoyl-CoA showed high potency against h15-LOX-1. Additionally, linoleoyl-CoA (18:2)

acted as a weak inhibitor but a rapid substrate for h15-LOX-1. These findings

highlight the significant role of acyl-CoAs in regulating LOX activity and suggest

their involvement in the formation of oxylipin-CoAs, which may serve as novel

signaling molecules.

Moreover, omega-3 fatty acids, including docosahexaenoic acid (DHA) and

docosapentaenoic acid (DPAn6), have been studied for their health benefits and their

oxidation by LOX enzymes to form bioactive oxylipins. The impact of saturation on

the kinetic properties and product profiles of h12-LOX, h15-LOX-1, and h15-LOX-2

was investigated using fatty acid substrates with varying degrees of unsaturation. The

loss of $\Delta 4$ and $\Delta 19$ double bonds led to a significant reduction in the kinetic activity

of h12-LOX, while h15-LOX-1 and h15-LOX-2 exhibited lower kcat/KM values

upon the loss of $\Delta 4$ and $\Delta 19$. The product profiles varied with the degree of saturation

and revealed a preference for 14-oxylipins by h12-LOX, an increase in 14-oxylipin

production with loss of saturation by h15-LOX-1, and predominant production of 17-

oxylipins by h15-LOX-2.

Additionally, the effects of various 17-oxylipins on platelet activation were

investigated, revealing distinct properties of different oxylipins. For instance, 17(S)-

hydroxy-4Z,7Z,10Z,13Z,15E,19Z-DHA and 17(S)-hydroxy-4Z,7Z,10Z,13Z,16Z-

DPAn6 demonstrated anti-aggregation properties, while 17(S)-hydroxy-

7Z,10Z,13Z,15E,19Z-DPAn3 exhibited agonistic effects. The effects of 17(S)-

hydroxy-7Z,10Z,13Z,15E-DTA varied depending on concentration, inhibiting

aggregation at lower concentrations but promoting it at higher concentrations. In

comparison, 17(S)-hydroxy-13Z,15E,19Z-DTrA and 17(S)-hydroxy-13Z,15E-DDiA

induced platelet aggregation. Notably, 14-oxylipin counterparts of certain 17-oxylipins, such as 14(S)-hydroxy-13Z,15E,19Z-DTrA, exhibited inhibitory properties when stimulated with collagen or thrombin.

These findings provide valuable insights into the role of oxylipins in platelet aggregation and reveal the influence of fatty acid saturation and specific LOX isozyme activity on their physiological activity. The degree of unsaturation and the location of oxidation appear to influence the physiological properties of these oxylipins, with more unsaturated compounds generally inhibiting aggregation while less unsaturated compounds promoting it. Understanding the mechanisms underlying LOX enzyme regulation, the impact of acyl-CoAs, and the physiological effects of different oxylipins contributes to our knowledge of platelet aggregation and thrombosis, offering potential avenues for the development of targeted therapeutic interventions and improvements in cardiovascular health.

Acknowledgements

I would like to to express my sincere appreciation to the individuals who have been instrumental in shaping my academic and research journey and my family. I would not be the person I am today if it was not for you.

I extend my deepest gratitude to Professor Theodore Holman, my primary advisor, for his exceptional mentorship and unwavering commitment to scientific excellence. Your guidance and expertise have been invaluable, and I am grateful for the opportunities you have provided me to grow as a researcher.

I would also like to thank the members of the Holman Lab, including Dylan Simpson, Chris Van Hoorbeke, Robert Jenkins, Drewv Desai. and Steve Perry, for their collaboration and support. Your scientific expertise and camaraderie have enhanced my research experience.

To my friends in the Rubin Lab, particularly Peter Ngoi (Summer) and Tilini Wijeratne, I want to express my heartfelt appreciation. Your friendship, encouragement, and shared scientific experiences have been a constant source of inspiration. I am grateful to my friends in the Partch Lab and Grant Koch in Lokey Lab for their support and scientific insights.

Finally, I want to express my deepest gratitude to my friends, Emilio Arroyo-Fang, Alex Billings, Jonathan Wickes, Brian Le, Alexander Moran, Natalie Lillig, David Dong, Megan Tran, Brandon Wolfinger, and Savannah Love. You all have

been a driving force in helping me finish this degree and making life worth living. To

Johnathan, Emilio, Alex, and Savannah, I would willingly venture everything to

safeguard your lives, as the immeasurable good you can bring to the world is truly

remarkable.

The text of this dissertation [or thesis] includes reprint[s] of the following

previously published material: [*Cryo-EM structures of human arachidonate 12S-

Lipoxygenase (12-LOX) bound to endogenous and exogenous inhibitors*]. The co-

author listed in this publication directed and supervised the research which

forms the basis for the dissertation [or thesis]

Chapter 1: Introduction:

1.1   Platelet aggregation and thrombosis

Thrombosis is a prevalent medical condition that can have severe and even fatal consequences[1]. Its occurrence is widespread, affecting individuals of different ages, genders, and ethnicities. The exact prevalence of thrombosis can vary depending on various factors, including population demographics, risk factors, and diagnostic methods[1–4]. Venous thrombosis, which includes deep vein thrombosis (DVT)[5] and pulmonary embolism (PE)[6], is estimated to affect millions of people worldwide each year. DVT occurs when blood clots form in the deep veins, typically in the legs[5,7,8], while PE happens when these clots travel to the lungs[6,7,9,10]. Together, DVT and PE constitute venous thromboembolism (VTE)[11]. It is estimated that VTE affects around 1 to 2 individuals per 1,000 in the general population annually, making it a significant health concern[1,3,11,12] .

Arterial thrombosis, on the other hand, involves the formation of blood clots in the arteries[4], leading to conditions such as heart attack[13,14], stroke[15,16], and peripheral arterial disease[17,18]. These events are major causes of morbidity and mortality worldwide. Coronary artery thrombosis, leading to heart attacks, is another common and life-threatening manifestation of arterial thrombosis[14]. The consequences of thrombosis can be fatal, particularly if the clot occludes a vital blood vessel[4].

Platelet aggregation, a critical process in hemostasis and wound healing, can also contribute to the formation of blood clots, known as thrombosis[19,20]. Thrombosis

occurs when platelet aggregation and clotting factors become dysregulated, leading to the formation of an obstructive clot within a blood vessel[4,21]. Under normal circumstances, platelets play a crucial role in maintaining the integrity of blood vessels. When a blood vessel is damaged, platelets adhere to the exposed collagen fibers at the site of injury, forming a platelet plug[21–23]. This initial aggregation is essential for preventing excessive bleeding.[24] However, in the case of thrombosis, platelet aggregation becomes excessive and uncontrolled, leading to the formation of an occlusive blood clot[25,26]. The process of platelet aggregation involves several steps. Upon vascular injury, platelets are activated, leading to changes in their shape and the exposure of receptors on their surface[21,27,28]. These activated platelets release chemical messengers, such as adenosine diphosphate (ADP), thromboxane A2 (TXA2), and serotonin, which attract and activate other platelets in the vicinity[23,27,29–31] (Figure 1.1).

One of the key mechanisms underlying platelet aggregation is the binding of the glycoprotein IIb/IIIa receptors on the surface of platelets to fibrinogen and von Willebrand factor[27,28,30,32,33]. Fibrinogen is a soluble protein present in blood plasma, while von Willebrand factor is secreted by endothelial cells and platelets[34–36]. The binding of these adhesive proteins to the glycoprotein IIb/IIIa receptors facilitates the cross-linking of platelets, forming stable aggregates[32,32,34]. In addition to fibrinogen and von Willebrand factor, other molecules and signaling pathways contribute to platelet aggregation[21,22,34,34]. These include the activation of G protein-coupled receptors, such as the P2Y12 receptor, by ADP, leading to further platelet activation and recruitment[35–38]. Thromboxane A2, generated by the enzymatic action of

cyclooxygenase-1 (COX-1) on arachidonic acid, acts as a potent platelet agonist, promoting aggregation and vasoconstriction[39–41].

1.2   Spatial resolving mediators:

Platelet aggregation and thrombosis are critical processes in hemostasis and wound healing. However, when dysregulated, they can lead to the formation of obstructive blood clots, resulting in serious health complications. To control these processes, the body employs various mechanisms, including the involvement of oxylipins known as specialized pro-resolving mediators (SPMs) or specialized resolving mediators (SRMs) (Figure 1.2).

In recent years, research has highlighted the role of SPMs, specifically a group of oxylipins called specialized resolvins, in the resolution of inflammation and regulation of platelet aggregation and thrombosis.[42–44] SPMs are derived from polyunsaturated fatty acids (PUFAs), such as arachidonic acid (AA), eicosapentaenoic acid (EPA), and docosahexaenoic acid (DHA)[45,46]. These lipid mediators act as potent signaling molecules that promote the resolution of inflammation and contribute to the restoration of homeostasis[42,47–49].

Among the SPMs, specialized resolvins have been identified as important regulators of platelet function and thrombus resolution[44,50,51]. These resolvins are generated through the action of various enzymes, including lipoxygenases (LOX)[52–

3

[54]. LOX enzymes are a family of non-heme iron-containing enzymes that catalyze the oxygenation of PUFAs, leading to the formation of specific oxylipins[55,56].

The interplay between LOX enzymes and platelet aggregation is complex. LOX enzymes, such as 5-lipoxygenase (5-LOX) and 12-lipoxygenase (12-LOX), can produce both pro-inflammatory and pro-thrombotic lipid mediators, as well as specialized resolvins that exert anti-inflammatory and pro-resolving effects[57–60]. The balance between these lipid mediators determines the outcome of platelet activation and thrombus resolution[61–63]. By modulating the activity of LOX enzymes and promoting the production of specialized resolvins, it may be possible to control platelet aggregation and enhance thrombus resolution[50,64]. Targeting specific LOX isoforms or manipulating the metabolism of PUFAs can influence the production of lipid mediators, thereby regulating platelet function and thrombotic processes[65–68].

1.3   Essential Fatty Acids

Mammalian cells have the ability to synthesize most of the lipids they require through de novo synthesis using fatty acid synthase and various modifying enzymes[69,70]. However, there are two important exceptions: linoleic acid (LA) and α-linolenic acid (ALA). These fatty acids cannot be synthesized from precursors within the body and are therefore classified as essential fatty acids[71,72]. The discovery of these essential fatty acids dates back to 1923 when researchers found that rats fed a fat-free diet developed skin problems[73–75].

LA, an omega-6 polyunsaturated fatty acid (PUFA), contains two sites of unsaturation and serves as a precursor for the synthesis of arachidonic acid (AA), a major omega-6 product[46,46,76,77]. On the other hand, ALA is an omega-3 PUFA with three sites of unsaturation that can be converted into important omega-3 products such as eicosapentaenoic acid (EPA), docosapentaenoic acid (DPAω3), and docosahexaenoic acid (DHA)[78,79]. These omega-3 fatty acids play crucial roles in various signaling pathways[78].

Both LA and ALA can be obtained through dietary sources. They can be synthesized by plants and subsequently consumed by animals or obtained directly by consuming plant-based foods. Once ingested, LA and ALA undergo a series of elongation and desaturation steps, resulting in the conversion to longer-chain fatty acids with higher degrees of unsaturation[46,73,76,77].

1.4   Lipoxygenase role and mechanism

Lipoxygenases (LOX) are a family of non-heme iron-containing enzymes that are found abundantly in animals, plants, and certain bacteria[80,81]. They play a crucial role in the biosynthesis of lipid mediators involved in various physiological and pathological processes, including inflammation, immune response, and cell signaling[55]. Lipoxygenases primarily catalyze the dioxygenation of polyunsaturated fatty acids (PUFA) containing a 1,4 cis-cis pentadiene moiety[82,83].

In humans, the genome encompasses six known functional LOX genes: ALOXE3, ALOX5, ALOX12B, ALOX12, ALOX15, and ALOX15B. These genes encode for different LOX isoforms, each with distinct enzymatic properties and tissue

expression patterns. For instance, h5-LOX, h12-LOX, h15-LOX-1, and h15-LOX-2 are isoforms named based on the location of enzymatic molecular oxygen insertion with the canonical substrate, arachidonic acid (AA)[55,55,83,84] .

The mechanism of lipoxygenase catalysis involves a series of reactions. Initially, the LOX enzyme abstracts a bis-allylic hydrogen from the 1,4 cis-cis pentadiene moiety of the PUFA substrate[65,65,85]. This hydrogen abstraction is a proton-coupled electron transfer (PCET) reaction, which is the rate-limiting step in the catalytic cycle. Following hydrogen abstraction, a radical rearrangement occurs, and molecular oxygen is inserted two carbons away from the site of abstraction, generating a hydroperoxide product (HpETE)[65,85] (Figure 1.3).

The hydroperoxide products generated by LOX are stereospecific, except for the h12R-LOX isoform, which produces a product in the R-chirality[85–87]. The LOX isoforms exhibit substrate selectivity, and different isoforms can react with a variety of substrates, leading to the formation of diverse products[57 ,62]. For example, h5-LOX predominantly reacts with AA to form 5S-HpETE, while h12-LOX and h15-LOX-1 metabolize AA to create mixtures of 12S-HpETE and 15S-HpETE.[88–91]

It is important to note that LOX isoforms can also react with their own products and the products of other isoforms, leading to the formation of secondary metabolites. This complexity adds to the diversity of LOX products and their biological functions. Moreover, the fidelity of LOX reactions with the canonical substrate AA can be affected when longer substrates, such as docosahexaenoic acid (DHA), are metabolized, resulting in the formation of a variety of products[57,65,85,85–87].

6

The structure of LOX enzymes plays a crucial role in their catalytic activity. The enzymes consist of two domains: the smaller N-terminal polycystin-1, lipoxygenase, alpha toxin (PLAT) domain and the larger C-terminal catalytic domain. The PLAT domain is involved in interacting with cellular membranes and micelle-bound substrates. The catalytic domain contains the active site where the iron ion, coordinated by histidine residues and a carboxylate group, catalyzes the oxygenation reactions[82,88,92–94].

Elucidating the structure and function of LOX enzymes has facilitated the design of therapeutic strategies targeting these enzymes[68,95,96]. Modulating LOX activity and the production of specific LOX products can have implications in various diseases, including inflammatory disorders[97,98], cancer[98,99], and cardiovascular diseases[100,101]. By understanding the intricate mechanisms of lipoxygenase catalysis, researchers can explore the potential of developing selective inhibitors and therapeutic interventions to regulate LOX-mediated pathways and their associated pathologies[95,96].

1.5   Lipoxygenase expression and genes

The tissue expression and cellular localization of lipoxygenase (LOX) genes in humans have been extensively studied[55,102–106], shedding light on their roles in different physiological and pathological contexts.

Among the LOX genes, ALOX5, located on chromosome 10, is expressed in high abundance in neutrophils, dendritic cells, macrophages, and other immune cells. It is primarily localized in the nucleus[101,102,107,108]. While in vitro experiments have demonstrated that h5-LOX can be active in the absence of five-lipoxygenase activating protein (FLAP), the in vivo activity of h5-LOX is dependent on FLAP. FLAP acts as a cofactor that facilitates the translocation of arachidonic acid (AA) to the active site of h5-LOX, thereby enhancing its enzymatic activity[109–111].

ALOX12, located on chromosome 17, is highly expressed in platelets, as suggested by its alternative name "platelet-type h12-LOX." [112,113–115] It is also found in certain endothelial cells[113]. Similarly, ALOX15 and ALOX15B, also located on chromosome 17, are expressed in macrophages. ALOX15B is constitutively expressed, while the expression of ALOX15 is dependent on signaling by interleukin-4 (IL-4) and interleukin-13 (IL-13). ALOX15 expression has also been observed in eosinophils and has been implicated in various cancers and neurological conditions[116]. ALOX15B, on the other hand, is primarily expressed in epithelial cells, including the skin and hair roots[117,118]. Both ALOX15 and ALOX15B have been found to be upregulated in various cancers[59,119,119–121].

Less extensively studied are the ALOXE3 and ALOX12B genes, which are co-clustered with ALOX15B on chromosome 17. These genes are expressed in epithelial cells. ALOXE3 is particularly associated with skin and hair follicles, while ALOX12B has been implicated in various cancers as well[80,122,123] (Table 1.1).

The sequence identity and similarity of LOX genes in humans and other species provide valuable information for comparative studies. For instance, h15-LOX-1 shares high sequence conservation (85% similarity, 74% identity) [124–126]with the main lipoxygenase found in mice, known as 12/15-LOX. However, despite their high sequence similarity, there are significant catalytic differences between the two species, which complicate translational research and therapeutic testing.

1.6   Lipoxygenase catalysis and mechanism

The catalysis of lipoxygenase (LOX) enzymes involves a series of reactions that lead to the oxygenation of polyunsaturated fatty acids (PUFAs) and the formation of various bioactive lipid mediators. Understanding the catalytic mechanism of LOX is essential for unraveling its physiological functions and developing targeted therapeutic strategies.

The primary catalytic cycle of LOX is centered around a four-reaction mechanism. It begins with the activation of the non-heme iron in the Fe^{3+} (ferric) stateThe activated LOX iron selectively abstracts a pro-S hydrogen atom from the bis-allylic methylene carbon of the PUFA substrate. This hydrogen abstraction generates an inactive ferrous enzyme and a carbon-centered fatty acid radical [83,92,94,107].

Following the hydrogen abstraction, a radical rearrangement occurs within the fatty acid radical, leading to the positioning of the molecular oxygen near the radical

site. The molecular oxygen then reacts with the carbon radical, resulting in the formation of a peroxy-radical on the terminal oxygen. This peroxy-radical is rapidly reduced by the ferrous iron, leading to the generation of a hydroperoxy fatty acid (HpETE) and the regeneration of the ferric enzyme[94].

It is important to note that the hydroperoxy products generated by LOX enzymes are rapidly reduced to hydroxy fatty acids (HETEs) in the cellular environment by antioxidants and enzymes like glutathione peroxidase. The stereochemistry of the hydroperoxy products depends on the specific LOX isoform and substrate involved[88,88,107].

The catalytic rate-limiting step in the LOX reaction is the stereoselective abstraction of the pro-S hydrogen atom, which occurs through a proton-coupled electron transfer (PCET) reaction[127]. The localization of molecular oxygen in the active site has been the subject of extensive research. Studies on soybean 15-lipoxygenase (sLO) have suggested the presence of an oxygen channel that facilitates the diffusion of molecular oxygen to the active site[128–130]. Although the presence of an oxygen channel in human LOX is not fully elucidated, the conservation of critical residues known to be involved in oxygen channeling in sLO suggests a similar mechanism in human LOX enzymes[130].

The complexity of LOX catalysis arises from the fact that a single isoform can react with multiple substrates, leading to the formation of diverse products. The fidelity of LOX reactions with the canonical substrate AA is compromised when longer or shorter PUFAs are metabolized, resulting in the oxygenation of different

carbon positions. The nomenclature of LOX isoforms is based on the carbon number of the primary oxygenation site relative to the methyl end of the substrate[104].

Moreover, LOX isoforms can also react with their own products and the LOX products of other isoforms, giving rise to additional metabolites and increasing the diversity of lipid mediators generated[62,62,85].

The structure of LOX enzymes plays a critical role in catalysis. LOX enzymes consist of a single polypeptide chain that folds into a two-domain structure. The N-terminal domain, known as the polycystin-1, lipoxygenase, alpha toxin (PLAT) domain, facilitates the interaction of LOX with cellular membranes and micelle-bound substrates. The C-terminal domain contains the catalytically active site, including the iron-binding site and residues involved in substrate recognition and binding[92,131,132] (Figure 1.4) .

1.7   Lipoxygenase allostery

Allosteric regulation plays a significant role in the activity and function of lipoxygenase (LOX) enzymes. Allostery refers to the modulation of enzyme activity through the binding of molecules at sites other than the catalytic site, known as allosteric sites. These allosteric interactions can either enhance or inhibit the catalytic activity of LOX enzymes[133–136].

One of the key allosteric regulators of LOX enzymes is calcium (Ca2+).

Calcium ions have been shown to enhance the enzymatic activity of certain LOX

isoforms, such as 5-lipoxygenase (5-LOX), by promoting enzyme activation and

substrate binding. Calcium ions bind to specific sites on the enzyme, inducing

conformational changes that facilitate substrate recognition and positioning within the

active site[57,137–139].

In addition to calcium, other small molecules and ions can also modulate LOX

activity through allosteric mechanisms. For example, ATP has been shown to activate

certain LOX isoforms, while glutathione has been found to inhibit LOX activity.

These molecules bind to allosteric sites on the enzyme and induce conformational

changes that affect substrate binding and catalysis[140].

Furthermore, the interaction of LOX enzymes with membrane surfaces can

also exert allosteric effects on their activity. The presence of lipid membranes

enhances the catalytic activity of LOX enzymes by promoting their association with

substrates and providing a suitable environment for catalysis. Membrane interactions

can induce conformational changes in the enzyme that optimize its catalytic

efficiency[57].

Understanding the allosteric regulation of LOX enzymes is important for

several reasons. First, it provides insights into the intricate control mechanisms that

govern LOX activity and lipid mediator production. Allosteric regulation allows for

the fine-tuning of LOX activity in response to cellular signals and environmental

cues. Second, targeting allosteric sites on LOX enzymes can serve as a potential

strategy for modulating their activity and developing therapeutic interventions. By selectively binding to allosteric sites, it is possible to enhance or inhibit LOX activity, thereby influencing the production of bioactive lipid mediators. This approach holds promise for the development of novel drugs targeting LOX enzymes and their associated pathologies.

1.8 Lipoxygenase and platelets

Lipoxygenase (LOX) enzymes play a crucial role in platelet function and contribute to platelet activation and aggregation. Platelets express various LOX isoforms, including h12-LOX, h15-LOX-1, and h5-LOX, which have been implicated in platelet-related processes.

The interaction between LOX enzymes and platelets is complex and multifaceted. LOX-derived products, such as 12S-HpETE, can act as signaling molecules and contribute to platelet activation and aggregation[141,142]. These products can induce platelet shape change, increase intracellular calcium levels, promote platelet adhesion to injured blood vessels, and enhance the release of platelet granules containing prothrombotic factors[44,62] (Figure 1.5).

The precise roles of different LOX isoforms in platelet function are still being elucidated. While h12-LOX has been extensively studied in platelets[141,142], recent research has also highlighted the involvement of h15-LOX-1[143] and h5-LOX in

13

platelet activation[144]. Understanding the interplay between LOX enzymes and

platelets is of great importance in the context of hemostasis, thrombosis, and other

platelet-related disorders. Dysregulation of LOX activity or altered LOX product

signaling can contribute to pathological conditions characterized by excessive platelet

activation and clot formation[142].

Figures and Tables
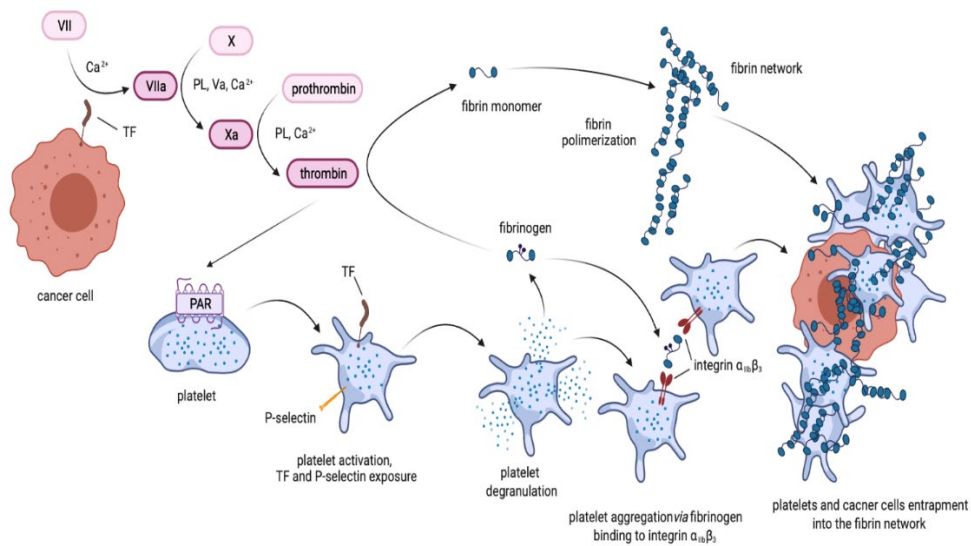
Figure 1.1: Platelet activation mechanism
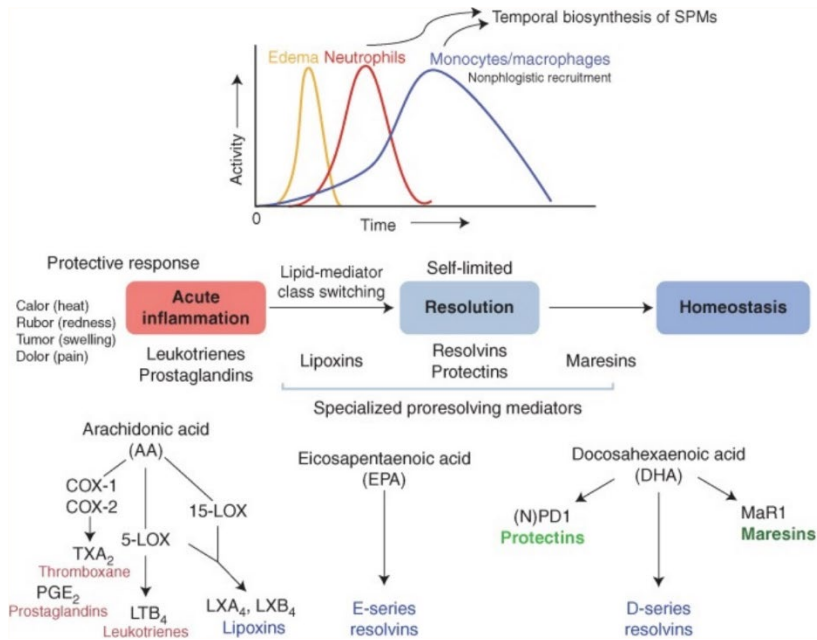
Figure 1.2: Role of specialized pro resolving mediators (SPMs) and specialized

resolving mediators (SRMs) in inflammation
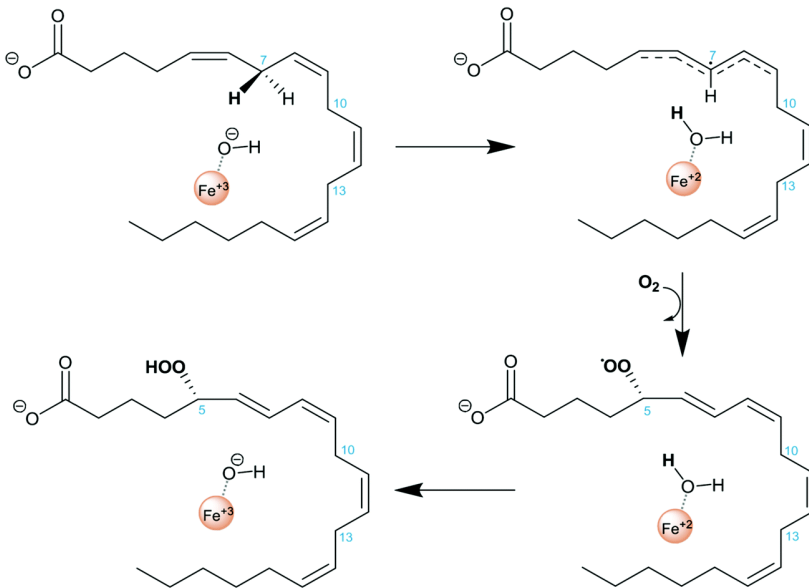
Figure 1.3: Mechanism of catalysis of lipoxygenase
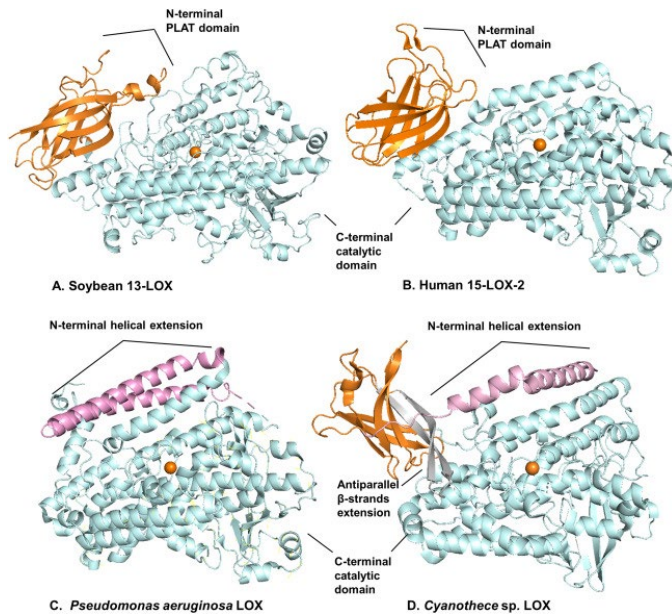
Figure 1.4: Structural characteristics of lipoxygenase
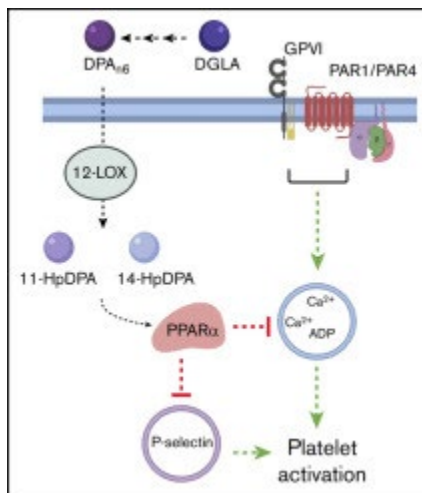
Figure 1.5: Role of 12-LOX in platelet activation

Gene	Enzyme	Expression tissue
ALOX5	h5-LOX	Macrophages, neutrophils
ALOX12	h12-LOX	Platelets
ALOX12B	h12R-LOX	Epithelial (skin)
ALOX15	h15-LOX-1	Macrophages, eosinophils
ALOX15B	h15-LOX-2	Macrophages, epithelial
ALOXE3	eLOX3	Epithelial (skin)

Table 1.1: Localization of lipoxygenases in the body

16

References

(1) Heit, J. A. The Epidemiology of Venous Thromboembolism in the Community. *Arterioscler. Thromb. Vasc. Biol.* **2008**, *28* (3), 370–372. https://doi.org/10.1161/ATVBAHA.108.162545.

(2) *Recurrent Venous Thromboembolism: What Is the Risk and How to Prevent It - PMC*. https://www.ncbi.nlm.nih.gov/pmc/articles/PMC3820456/ (accessed 2023-07-07).

(3) Previtali, E.; Bucciarelli, P.; Passamonti, S. M.; Martinelli, I. Risk Factors for Venous and Arterial Thrombosis. *Blood Transfus.* **2011**, *9* (2), 120–138. https://doi.org/10.2450/2010.0066-10.

(4) Ashorobi, D.; Ameer, M. A.; Fernandez, R. Thrombosis. In *StatPearls*; StatPearls Publishing: Treasure Island (FL), 2023.

(5) *Deep Vein Thrombosis - StatPearls - NCBI Bookshelf*. https://www.ncbi.nlm.nih.gov/books/NBK507708/ (accessed 2023-07-07).

(6) *Pulmonary embolism - PMC*. https://www.ncbi.nlm.nih.gov/pmc/articles/PMC3665123/ (accessed 2023-07-07).

(7)   General (US), O. of the S.; National Heart, L. SECTION I: Deep Vein

Thrombosis and Pulmonary Embolism as Major Public Health Problems. In

The Surgeon General's Call to Action to Prevent Deep Vein Thrombosis and

Pulmonary Embolism; Office of the Surgeon General (US), 2008.

(8)   *Deep vein thrombosis: pathogenesis, diagnosis, and medical management -*

PMC. https://www.ncbi.nlm.nih.gov/pmc/articles/PMC5778510/ (accessed

2023-07-07).

(9)   *Acute Pulmonary Embolism - StatPearls - NCBI Bookshelf*.

https://www.ncbi.nlm.nih.gov/books/NBK560551/ (accessed 2023-07-07).

(10)   *Pulmonary Embolism: Epidemiology, Pathophysiology, and Natural History of*

Pulmonary Embolism - PMC. https://www.ncbi.nlm.nih.gov/p

mc/articles/PMC5986574/ (accessed 2023-07-07).

(11)   Phillippe, H. M. Overview of Venous Thromboembolism. *Am. J. Manag. Care*

2017, *23* (20 Suppl), S376–S382.

(12)   *Prevention of Venous Thromboembolism in 2020 and Beyond - PMC*.

https://www.ncbi.nlm.nih.gov/pmc/articles/PMC7465935/ (accessed 2023-07-

07).

(13)   Nagareddy, P.; Smyth, S. S. Inflammation and Thrombosis in Cardiovascular Disease. *Curr. Opin. Hematol.* **2013**, *20* (5), 457–463. https://doi.org/10.1097/MOH.0b013e328364219d.

(14)   Adnan, G.; Singh, D. P.; Mahajan, K. Coronary Artery Thrombus. In *StatPearls*; StatPearls Publishing: Treasure Island (FL), 2023.

(15)   *Ischemic Stroke - StatPearls - NCBI Bookshelf*. https://www.ncbi.nlm.nih.gov/books/NBK499997/ (accessed 2023-07-07).

(16)   *Thrombotic Stroke: Neuroprotective Therapy by Recombinant Activated Protein C - PMC*. https://www.ncbi.nlm.nih.gov/pmc/articles/PMC5119536/ (accessed 2023-07-07).

(17)   Lowe, G. D.; Reid, A. W.; Leiberman, D. P. Management of Thrombosis in Peripheral Arterial Disease. *Br. Med. Bull.* **1994**, *50* (4), 923–935. https://doi.org/10.1093/oxfordjournals.bmb.a072934.

(18)   *Peripheral Arterial Disease - StatPearls - NCBI Bookshelf*. https://www.ncbi.nlm.nih.gov/books/NBK430745/ (accessed 2023-07-07).

(19)   Periayah, M. H.; Halim, A. S.; Mat Saad, A. Z. Mechanism Action of Platelets and Crucial Blood Coagulation Pathways in Hemostasis. *Int. J. Hematol.-Oncol. Stem Cell Res.* **2017**, *11* (4), 319–327.

(20)   LaPelusa, A.; Dave, H. D. Physiology, Hemostasis. In *StatPearls*; StatPearls
       Publishing: Treasure Island (FL), 2023.

(21)   *Interplay between platelets and coagulation - PMC*.
       https://www.ncbi.nlm.nih.gov/pmc/articles/PMC7354275/ (accessed 2023-07-
       07).

(22)   *Regulation of platelet activation and coagulation and its role in vascular injury
       and arterial thrombosis - PMC*.
       https://www.ncbi.nlm.nih.gov/pmc/articles/PMC5154246/ (accessed 2023-07-
       07).

(23)   *Physiology, Platelet Activation - StatPearls - NCBI Bookshelf*.
       https://www.ncbi.nlm.nih.gov/books/NBK482478/ (accessed 2023-07-07).

(24)   *Bleeding Disorders - StatPearls - NCBI Bookshelf*.
       https://www.ncbi.nlm.nih.gov/books/NBK541050/ (accessed 2023-07-07).

(25)   *Factors Affecting the Formation and Treatment of Thrombosis by Natural and
       Synthetic Compounds - PMC*.
       https://www.ncbi.nlm.nih.gov/pmc/articles/PMC7663413/ (accessed 2023-07-
       07).

(26)   *Atherosclerosis, platelets and thrombosis in acute ischaemic heart disease -*
       PMC. https://www.ncbi.nlm.nih.gov/pmc/articles/PMC3760546/ (accessed
       2023-07-07).

(27)   Rumbaut, R. E.; Thiagarajan, P. Platelet Aggregation. In *Platelet-Vessel Wall*
       Interactions in Hemostasis and Thrombosis; Morgan & Claypool Life
       Sciences, 2010.

(28)   *Platelet Activation: The Mechanisms and Potential Biomarkers - PMC*.
       https://www.ncbi.nlm.nih.gov/pmc/articles/PMC4925965/ (accessed 2023-07-
       07).

(29)   *Platelet Aggregation - Platelet-Vessel Wall Interactions in Hemostasis and*
       Thrombosis - NCBI Bookshelf.
       https://www.ncbi.nlm.nih.gov/books/NBK53449/ (accessed 2023-07-07).

(30)   *Effects of the interactions between platelets with other cells in tumor growth*
       and progression - PMC.
       https://www.ncbi.nlm.nih.gov/pmc/articles/PMC10158495/ (accessed 2023-07-
       07).

(31)   *Serotonin and thromboxane A2 stimulate platelet-derived microparticle-*
       induced smooth muscle cell proliferation - PubMed.
       https://pubmed.ncbi.nlm.nih.gov/15275628/ (accessed 2023-07-07).

(32) *Glycoprotein IIb-IIIa content and platelet aggregation in healthy volunteers and patients with acute coronary syndrome - PubMed.* https://pubmed.ncbi.nlm.nih.gov/21329420/ (accessed 2023-07-07).

(33) *Of von Willebrand factor and platelets - PMC.* https://www.ncbi.nlm.nih.gov/pmc/articles/PMC4284388/ (accessed 2023-07-07).

(34) *Current Understanding of Hemostasis - PMC.* https://www.ncbi.nlm.nih.gov/pmc/articles/PMC3126677/ (accessed 2023-07-07).

(35) *Central role of the P2Y12 receptor in platelet activation - PMC.* https://www.ncbi.nlm.nih.gov/pmc/articles/PMC324551/ (accessed 2023-07-07).

(36) *P2 receptors and platelet function - PMC.* https://www.ncbi.nlm.nih.gov/pmc/articles/PMC3166986/ (accessed 2023-07-07).

(37) *G-Protein–Coupled Receptors Signaling Pathways in New Antiplatelet Drug Development - PMC.* https://www.ncbi.nlm.nih.gov/pmc/articles/PMC4836833/ (accessed 2023-07-07).

(38)   *The Role of P2Y12 Receptor and Activated Platelets During Inflammation -*
       PMC. https://www.ncbi.nlm.nih.gov/pmc/articles/PMC5681251/ (accessed
       2023-07-07).

(39)   *IJMS | Free Full-Text | The Role of Thromboxane in the Course and Treatment*
       of Ischemic Stroke: Review. https://www.mdpi.com/1422-0067/22/21/11644
       (accessed 2023-07-07).

(40)   *Thromboxane and the thromboxane receptor in cardiovascular disease - PMC.*
       https://www.ncbi.nlm.nih.gov/pmc/articles/PMC2882156/ (accessed 2023-07-
       07).

(41)   *Physiology, Thromboxane A2 - StatPearls - NCBI Bookshelf.*
       https://www.ncbi.nlm.nih.gov/books/NBK539817/ (accessed 2023-07-07).

(42)   Yang, A.; Wu, Y.; Yu, G.; Wang, H. Role of Specialized Pro-Resolving Lipid
       Mediators in Pulmonary Inflammation Diseases: Mechanisms and
       Development. *Respir. Res.* **2021**, *22* (1), 204. https://doi.org/10.1186/s12931-
       021-01792-y.

(43)   *E-series resolvin metabolome, biosynthesis and critical role of stereochemistry*
       of specialized pro-resolving mediators (SPMs) in inflammation-resolution:
       Preparing SPMs for long COVID-19, human clinical trials, and targeted
       precision nutrition - PMC.

https://www.ncbi.nlm.nih.gov/pmc/articles/PMC8847098/ (accessed 2023-07-07).

(44) Bannenberg, G.; Serhan, C. N. Specialized Pro-Resolving Lipid Mediators in the Inflammatory Response: An Update. *Biochim. Biophys. Acta* **2010**, *1801* (12), 1260–1273. https://doi.org/10.1016/j.bbalip.2010.08.002.

(45) Weylandt, K. H.; Chiu, C.-Y.; Gomolka, B.; Waechter, S. F.; Wiedenmann, B. Omega-3 Fatty Acids and Their Lipid Mediators: Towards an Understanding of Resolvin and Protectin Formation. *Prostaglandins Other Lipid Medi*
at. **2012**, *97* (3), 73–82. https://doi.org/10.1016/j.prostaglandins.2012.01.005.

(46) *Polyunsaturated fatty acids, specialized pro-resolving mediators, and targeting inflammation resolution in the age of precision nutrition - PMC.*
https://www.ncbi.nlm.nih.gov/pmc/articles/PMC8496879/ (accessed 2023-07-07).

(47) *These lipid mediators act as potent signaling molecules that promote the resolution of inflammation and contribute to the restoration of homeostasis. -*
Google Search.
https://www.google.com/search?q=These+lipid+mediators+act+as+potent+sig
naling+molecules+that+promote+the+resolution+of+inflammation+and+contri
bute+to+the+restoration+of+homeostasis.&rlz=1C1SQJL_enUS877US877&o
q=These+lipid+mediators+act+as+potent+signaling+molecules+that+promote

+the+resolution+of+inflammation+and+contribute+to+the+restoration+of+ho

meostasis.&aqs=chrome..69i57.225j0j9&sourceid=chrome&ie=UTF-8

(accessed 2023-07-07).

(48)   *Maresin - an overview | ScienceDirect Topics*.

https://www.sciencedirect.com/topics/veterinary-science-and-veterinary-

medicine/maresin (accessed 2023-07-07).

(49)   *Novel lipid mediators promote resolution of acute inflammation: impact of*

aspirin and statins - PMC.

https://www.ncbi.nlm.nih.gov/pmc/articles/PMC3027152/ (accessed 2023-07-

07).

(50)   Yeung, J.; Hawley, M.; Holinstat, M. The Expansive Role of Oxylipins on

Platelet Biology. *J. Mol. Med.* **2017**, *95* (6), 575–588.

https://doi.org/10.1007/s00109-017-1542-4.

(51)   *Resolvin E1 Regulates ADP Activation of Human Platelets - PMC*.

https://www.ncbi.nlm.nih.gov/pmc/articles/PMC2982748/ (accessed 2023-07-

07).

(52)   *Resolvins in inflammation: emergence of the pro-resolving superfamily of*

mediators - PMC. https://www.ncbi.nlm.nih.gov/pmc/articles/PMC6025982/

(accessed 2023-07-07).

(53)   *Resolvins and protectins: mediating solutions to inflammation - PMC.*

https://www.ncbi.nlm.nih.gov/pmc/articles/PMC2785519/ (accessed 2023-07-
07).

(54)   *Resolvins: Endogenously-Generated Potent Painkilling Substances and their*

Therapeutic Perspectives - PMC.

https://www.ncbi.nlm.nih.gov/pmc/articles/PMC3849791/ (accessed 2023-07-
07).

(55)   Mashima, R.; Okuyama, T. The Role of Lipoxygenases in Pathophysiology;

New Insights and Future Perspectives. *Redox Biol.* **2015**, *6*, 297–310.

https://doi.org/10.1016/j.redox.2015.08.006.

(56)   *Inhibition of lipoxygenases and cyclooxygenases by linoleyl hydroxamic acid:*

comparative in vitro studies - PMC.

https://www.ncbi.nlm.nih.gov/pmc/articles/PMC2386902/ (accessed 2023-07-
07).

(57)   *Biochemical and hydrogen-deuterium exchange studies of the single nucleotide*

polymorphism Y649C in human platelet 12-lipoxygenase linked to a bleeding

disorder - PMC. https://www.ncbi.nlm.nih.gov/pmc/articles/PMC9888433/

(accessed 2023-07-07).

(58) *Hydroxyeicosatetraenoic acids (HETE), oxylipins, epoxides, docosanoids, octadecanoids, lipoxygenases, CYP450 oxidases - composition and biochemistry*. https://www.lipidmaps.org/resources/lipidweb/lipidweb_html/lipids/fa-eic/eic-hete/index.htm (accessed 2023-07-07).

(59) *Frontiers | Regulation and Functions of 15-Lipoxygenases in Human Macrophages*. https://www.frontiersin.org/articles/10.3389/fphar.2019.00719/full (accessed 2023-07-07).

(60) *Anti-Inflammatory and Pro-Resolving Lipid Mediators - PMC*. https://www.ncbi.nlm.nih.gov/pmc/articles/PMC2739396/ (accessed 2023-07-07).

(61) *The resolution of inflammation: the devil in the flask and in the details - PMC*. https://www.ncbi.nlm.nih.gov/pmc/articles/PMC3228345/ (accessed 2023-07-07).

(62) Chiang, N.; Serhan, C. N. Specialized Pro-Resolving Mediator Network: An Update on Production and Actions. *Essays Biochem.* **2020**, *64* (3), 443–462. https://doi.org/10.1042/EBC20200018.

(63) Heimerl, S.; Höring, M.; Kopczynski, D.; Sigruener, A.; Hart, C.; Burkhardt, R.; Black, A.; Ahrends, R.; Liebisch, G. Quantification of Bulk Lipid Species in Human Platelets and Their Thrombin-Induced Release. *Sci. Rep.* **2023**, *13*, 6154. https://doi.org/10.1038/s41598-023-33076-4.

(64) *12-Lipoxygenase: A Potential Target for Novel Anti-Platelet Therapeutics - PMC*. https://www.ncbi.nlm.nih.gov/pmc/articles/PMC3171607/ (accessed 2023-07-07).

(65) Joshi, N.; Hoobler, E. K.; Perry, S.; Diaz, G.; Fox, B.; Holman, T. R. Kinetic and Structural Investigations into the Allosteric and PH Effect on the Substrate Specificity of Human Epithelial 15-Lipoxygenase-2. *Biochemistry* **2013**, *52* (45), 8026–8035. https://doi.org/10.1021/bi4010649.

(66) *In Vitro Biosynthetic Pathway Investigations of Neuroprotectin D1 (NPD1) and Protectin DX (PDX) by Human 12-Lipoxygenase, 15-Lipoxygenase-1, and 15-Lipoxygenase-2 - PubMed*. https://pubmed.ncbi.nlm.nih.gov/34029049/ (accessed 2023-07-07).

(67) *Human 15-LOX-1 active site mutations alter inhibitor binding and decrease potency - PubMed*. https://pubmed.ncbi.nlm.nih.gov/27647374/ (accessed 2023-07-07).

(68)   *A potent and selective inhibitor targeting human and murine 12/15-LOX -*
        PubMed. https://pubmed.ncbi.nlm.nih.gov/26899595/ (accessed 2023-07-07).

(69)   *Fatty acid synthase is required for mammary gland development and milk*
        production during lactation - PMC.
        https://www.ncbi.nlm.nih.gov/pmc/articles/PMC4116404/ (accessed 2023-07-
        07).

(70)   *Lipoexpediency: de novo lipogenesis as a metabolic signal transmitter - PMC*.
        https://www.ncbi.nlm.nih.gov/pmc/articles/PMC3011046/ (accessed 2023-07-
        07).

(71)   *Alpha-Linolenic and Linoleic Fatty Acids in the Vegan Diet: Do They Require*
        Dietary Reference Intake/Adequate Intake Special Consideration? - PMC.
        https://www.ncbi.nlm.nih.gov/pmc/articles/PMC6835948/ (accessed 2023-07-
        07).

(72)   Rett, B. S.; Whelan, J. Increasing Dietary Linoleic Acid Does Not Increase
        Tissue Arachidonic Acid Content in Adults Consuming Western-Type Diets: A
        Systematic Review. *Nutr. Metab.* **2011**, *8* (1), 36. https://doi.org/10.1186/1743-
        7075-8-36.

(73) Burr, G. O.; Burr, M. M. ON THE NATURE AND RÔLE OF THE FATTY

ACIDS ESSENTIAL IN NUTRITION. *J. Biol. Chem.* **1930**, *86* (2), 587–621.

https://doi.org/10.1016/S0021-9258(20)78929-5.

(74) *Thematic Review Series: Living History of Lipids: Discovery of essential fatty*

acids - PMC. https://www.ncbi.nlm.nih.gov/pmc/articles/PMC4274059/

(accessed 2023-07-07).

(75) Spector, A. A.; Kim, H.-Y. Discovery of Essential Fatty Acids. *J. Lipid Res.*

2015, *56* (1), 11–21. https://doi.org/10.1194/jlr.R055095.

(76) Zhou, L.; Nilsson, Å. Sources of Eicosanoid Precursor Fatty Acid Pools in

Tissues. *J. Lipid Res.* **2001**, *42* (10), 1521–1542.

https://doi.org/10.1016/S0022-2275(20)32206-9.

(77) *Foods | Free Full-Text | The Sources, Synthesis and Biological Actions of*

Omega-3 and Omega-6 Fatty Acids in Red Meat: An Overview.

https://www.mdpi.com/2304-8158/10/6/1358 (accessed 2023-07-07).

(78) *Beneficial Outcomes of Omega-6 and Omega-3 Polyunsaturated Fatty Acids*

on Human Health: An Update for 2021 - PMC.

https://www.ncbi.nlm.nih.gov/pmc/articles/PMC8308533/ (accessed 2023-07-

07).

(79) *Overconsumption of Omega-6 Polyunsaturated Fatty Acids (PUFAs) versus Deficiency of Omega-3 PUFAs in Modern-Day Diets: The Disturbing Factor for Their "Balanced Antagonistic Metabolic Functions" in the Human Body - PMC*. https://www.ncbi.nlm.nih.gov/pmc/articles/PMC7990530/ (accessed 2023-07-07).

(80) *Mammalian lipoxygenases and their biological relevance - PMC*. https://www.ncbi.nlm.nih.gov/pmc/articles/PMC4370320/ (accessed 2023-07-07).

(81) *Evolutionary aspects of lipoxygenases and genetic diversity of human leukotriene signaling - PMC*. https://www.ncbi.nlm.nih.gov/pmc/articles/PMC7112624/ (accessed 2023-07-07).

(82) Chrisnasari, R.; Hennebelle, M.; Vincken, J.-P.; van Berkel, W. J. H.; Ewing, T. A. Bacterial Lipoxygenases: Biochemical Characteristics, Molecular Structure and Potential Applications. *Biotechnol. Adv.* **2022**, *61*, 108046. https://doi.org/10.1016/j.biotechadv.2022.108046.

(83) Wood, I.; Trostchansky, A.; Rubbo, H. Structural Considerations on Lipoxygenase Function, Inhibition and Crosstalk with Nitric Oxide Pathways. *Biochimie* **2020**, *178*, 170–180. https://doi.org/10.1016/j.biochi.2020.09.021.

(84) Maloberti, P. M.; Duarte, A. B.; Orlando, U. D.; Pasqualini, M. E.; Solano, A. R.; López-Otín, C.; Podestá, E. J. Functional Interaction between Acyl-CoA Synthetase 4, Lipooxygenases and Cyclooxygenase-2 in the Aggressive Phenotype of Breast Cancer Cells. *PloS One* **2010**, *5* (11), e15540. https://doi.org/10.1371/journal.pone.0015540.

(85) Perry, S. C.; Kalyanaraman, C.; Tourdot, B. E.; Conrad, W. S.; Akinkugbe, O.; Freedman, J. C.; Holinstat, M.; Jacobson, M. P.; Holman, T. R. 15-Lipoxygenase-1 Biosynthesis of 7S,14S-DiHDHA Implicates 15-Lipoxygenase-2 in Biosynthesis of Resolvin D5. *J. Lipid Res.* **2020**, *61* (7), 1087–1103. https://doi.org/10.1194/jlr.RA120000777.

(86) Tsai, W.-C.; Gilbert, N. C.; Ohler, A.; Armstrong, M.; Perry, S.; Kalyanaraman, C.; Yasgar, A.; Rai, G.; Simeonov, A.; Jadhav, A.; Standley, M.; Lee, H.-W.; Crews, P.; Iavarone, A. T.; Jacobson, M. P.; Neau, D. B.; Offenbacher, A. R.; Newcomer, M.; Holman, T. R. Kinetic and Structural Investigations of Novel Inhibitors of Human Epithelial 15-Lipoxygenase-2. *Bioorg. Med. Chem.* **2021**, *46*, 116349. https://doi.org/10.1016/j.bmc.2021.116349.

(87) Aleem, A. M.; Tsai, W.-C.; Tena, J.; Alvarez, G.; Deschamps, J.; Kalyanaraman, C.; Jacobson, M. P.; Holman, T. Probing the Electrostatic and Steric Requirements for Substrate Binding in Human Platelet-Type 12-

Lipoxygenase. *Biochemistry* **2019**, *58* (6), 848–857.

https://doi.org/10.1021/acs.biochem.8b01167.

(88)   Gilbert, N. C.; Gerstmeier, J.; Schexnaydre, E. E.; Börner, F.; Garscha, U.;
        Neau, D. B.; Werz, O.; Newcomer, M. E. Structural and Mechanistic Insights
        into 5-Lipoxygenase Inhibition by Natural Products. *Nat. Chem. Biol.* **2020**, *16*
        (7), 783–790. https://doi.org/10.1038/s41589-020-0544-7.

(89)   Coffa, G.; Imber, A. N.; Maguire, B. C.; Laxmikanthan, G.; Schneider, C.;
        Gaffney, B. J.; Brash, A. R. On the Relationships of Substrate Orientation,
        Hydrogen Abstraction, and Product Stereochemistry in Single and Double
        Dioxygenations by Soybean Lipoxygenase-1 and Its Ala542Gly Mutant. *J.
        Biol. Chem.* **2005**, *280* (46), 38756–38766.
        https://doi.org/10.1074/jbc.M504870200.

(90)   *IJMS | Free Full-Text | Inhibitory Investigations of Acyl-CoA Derivatives
        against Human Lipoxygenase Isozymes*. https://www.mdpi.com/1422-
        0067/24/13/10941 (accessed 2023-07-07).

(91)   *Functional characterization of genetic enzyme variations in human
        lipoxygenases - PMC*.
        https://www.ncbi.nlm.nih.gov/pmc/articles/PMC3840004/ (accessed 2023-07-
        07).

(92)   *Cryo-EM structures of human arachidonate 12S-Lipoxygenase (12-LOX) bound to endogenous and exogenous inhibitors | bioRxiv.* https://www.biorxiv.org/content/10.1101/2023.03.10.532002v1 (accessed 2023-05-26).

(93)   *Characterization of the lipoxygenase (LOX) gene family in the Chinese white pear (Pyrus bretschneideri) and comparison with other members of the Rosaceae | BMC Genomics | Full Text.* https://bmcgenomics.biomedcentral.com/articles/10.1186/1471-2164-15-444 (accessed 2023-07-07).

(94)   *The structural basis for specificity in lipoxygenase catalysis - PMC.* https://www.ncbi.nlm.nih.gov/pmc/articles/PMC4353356/ (accessed 2023-07-07).

(95)   *Discovery of ML351, a Potent and Selective Inhibitor of Human 15-Lipoxygenase-1 - Probe Reports from the NIH Molecular Libraries Program - NCBI Bookshelf.* https://www.ncbi.nlm.nih.gov/books/NBK190602/ (accessed 2023-07-07).

(96)   *12-HETrE inhibits platelet reactivity and thrombosis in part through the prostacyclin receptor - PubMed.* https://pubmed.ncbi.nlm.nih.gov/29296755/ (accessed 2023-07-07).

(97)   *Regulation of Tissue Inflammation by 12-Lipoxygenases - PMC.*
https://www.ncbi.nlm.nih.gov/pmc/articles/PMC8150372/ (accessed 2023-07-
07).

(98)   *Inflammation, Cancer and Oxidative Lipoxygenase Activity are Intimately
Linked - PMC.* https://www.ncbi.nlm.nih.gov/pmc/articles/PMC4190552/
(accessed 2023-07-07).

(99)   *Cyclooxygenases and lipoxygenases in cancer - PMC.*
https://www.ncbi.nlm.nih.gov/pmc/articles/PMC3798028/ (accessed 2023-07-
07).

(100)   *Cardiac 12/15 lipoxygenase–induced inflammation is involved in heart failure
- PMC.* https://www.ncbi.nlm.nih.gov/pmc/articles/PMC2715088/ (accessed
2023-07-07).

(101)   *5-Lipoxygenase as a putative link between cardiovascular and psychiatric
disorders - PubMed.* https://pubmed.ncbi.nlm.nih.gov/15581413/ (accessed
2023-07-07).

(102)   *Gene expression of 5-, 12-, and 15-lipoxygenases and leukotriene receptors
along the rat nephron | American Journal of Physiology-Renal Physiology.*
https://journals.physiology.org/doi/full/10.1152/ajprenal.00169.2005 (accessed
2023-07-07).

(103) Sigal, E.; Grunberger, D.; Highland, E.; Gross, C.; Dixon, R. A.; Craik, C. S. Expression of Cloned Human Reticulocyte 15-Lipoxygenase and Immunological Evidence That 15-Lipoxygenases of Different Cell Types Are Related. *J. Biol. Chem.* **1990**, *265* (9), 5113–5120. https://doi.org/10.1016/S0021-9258(19)34092-X.

(104) *Lipoxygenase - an overview | ScienceDirect Topics*. https://www.sciencedirect.com/topics/medicine-and-dentistry/lipoxygenase (accessed 2023-05-26).

(105) *The tissue expression and cellular localization of lipoxygenase (LOX) genes in humans have been extensively studied - Google Search*. https://www.google.com/search?q=The+tissue+expression+and+cellular+locali zation+of+lipoxygenase+(LOX)+genes+in+humans+have+been+extensively+s tudied&rlz=1C1SQJL_enUS877US877&oq=The+tissue+expression+and+cell ular+localization+of+lipoxygenase+(LOX)+genes+in+humans+have+been+ext ensively+studied&aqs=chrome..69i57.422j0j4&sourceid=chrome&ie=UTF-8 (accessed 2023-07-07).

(106) *Characterization of Epidermal Lipoxygenase Expression in Normal Human Skin and Tissue-Engineered Skin Substitutes - PMC*. https://www.ncbi.nlm.nih.gov/pmc/articles/PMC6213569/ (accessed 2023-07-07).

(107) Cruz, S. KINETIC, MECHANISTIC, AND STRUCTURAL INVESTIGATIONS OF HUMAN LIPOXYGENASES

(108) *The role of 5-lipoxygenase in the pathophysiology of COVID-19 and its therapeutic implications - PMC*. https://www.ncbi.nlm.nih.gov/pmc/articles/PMC8176665/ (accessed 2023-07-07).

(109) *Arachidonic acid promotes the binding of 5-lipoxygenase on nanodiscs containing 5-lipoxygenase activating protein in the absence of calcium-ions | PLOS ONE*. https://journals.plos.org/plosone/article?id=10.1371/journal.pone.0228607 (accessed 2023-07-07).

(110) *5-Lipoxygenase-activating protein rescues activity of 5-lipoxygenase mutations that delay nuclear membrane association and disrupt product formation - PubMed*. https://pubmed.ncbi.nlm.nih.gov/26842853/ (accessed 2023-07-07).

(111) Spanbroek, R.; Stark, H.-J.; Janßen-Timmen, U.; Kraft, S.; Hildner, M.; Andl, T.; Bosch, F.-X.; Fusenig, N. E.; Bieber, T.; Rådmark, O.; Samuelsson, B.; Habenicht, A. J. R. 5-Lipoxygenase Expression in Langerhans Cells of Normal Human Epidermis. *Proc. Natl. Acad. Sci.* **1998**, *95* (2), 663–668. https://doi.org/10.1073/pnas.95.2.663.

(112) *ALOX12 (Arachidonate 12-Lipoxygenase) Homo sapiens*.

https://atlasgeneticsoncology.org/gene/620/alox12-(arachidonate-12-

lipoxygenase)-homo-sapiens (accessed 2023-07-07).

(113) *ALOX12 Gene - GeneCards | LOX12 Protein | LOX12 Antibody*.

https://www.genecards.org/cgi-bin/carddisp.pl?gene=ALOX12 (accessed

2023-07-07).

(114) *ALOX12 - Polyunsaturated fatty acid lipoxygenase ALOX12 - Homo sapiens

(Human) | UniProtKB | UniProt*.

https://www.uniprot.org/uniprotkb/P18054/entry (accessed 2023-07-07).

(115) Zheng, Z.; Li, Y.; Jin, G.; Huang, T.; Zou, M.; Duan, S. The Biological Role of

Arachidonic Acid 12-Lipoxygenase (ALOX12) in Various Human Diseases.

Biomed. Pharmacother. **2020**, *129*, 110354.

https://doi.org/10.1016/j.biopha.2020.110354.

(116) *Regulation and Functions of 15-Lipoxygenases in Human Macrophages -

PMC*. https://www.ncbi.nlm.nih.gov/pmc/articles/PMC6620526/ (accessed

2023-07-07).

(117) *Arachidonic Acid 15-Lipoxygenase: Effects of Its Expression, Metabolites, and

Genetic and Epigenetic Variations on Airway Inflammation - PMC*.

https://www.ncbi.nlm.nih.gov/pmc/articles/PMC8419644/ (accessed 2023-07-07)

.

(118) *Expression and regulation of 12/15-lipoxygenases in human primary macrophages - ScienceDirect*. https://www.sciencedirect.com/science/article/pii/S0021915012004947?via%3Dihub (accessed 2023-07-07).

(119) *Both ALOX15 and ALOX15B have been found to be upregulated in various cancers. - Google Search*. https://www.google.com/search?q=Both+ALOX15+and+ALOX15B+have+been+found+to+be+upregulated+in+various+cancers.&rlz=1C1SQJL_enUS877US877&oq=Both+ALOX15+and+ALOX15B+have+been+found+to+be+upregulated+in+various+cancers.&aqs=chrome..69i57.326j0j9&sourceid=chrome&ie=UTF-8 (accessed 2023-07-07).

(120) *ALOX15 as a Suppressor of Inflammation and Cancer: Lost in the Link - PMC*. https://www.ncbi.nlm.nih.gov/pmc/articles/PMC5509529/ (accessed 2023-07-07).

(121) Vijil, C.; Hermansson, C.; Jeppsson, A.; Bergström, G.; Hultén, L. M. Arachidonate 15-Lipoxygenase Enzyme Products Increase Platelet

Aggregation and Thrombin Generation. *PloS One* **2014**, *9* (2), e88546.

https://doi.org/10.1371/journal.pone.0088546.

(122) *Development of an Ichthyosiform Phenotype in Alox12b-Deficient Mouse Skin Transplants - ScienceDirect*.

https://www.sciencedirect.com/science/article/pii/S0022202X15343840

(accessed 2023-07-07).

(123) *Meta-Analysis of Mutations in ALOX12B or ALOXE3 Identified in a Large Cohort of 224 Patients - PMC*.

https://www.ncbi.nlm.nih.gov/pmc/articles/PMC7826849/ (accessed 2023-07-07).

(124) *Genome-wide identification, classification and expression of lipoxygenase gene family in pepper - PMC*.

https://www.ncbi.nlm.nih.gov/pmc/articles/PMC6244800/ (accessed 2023-07-07).

(125) *IJMS | Free Full-Text | Identification, Phylogeny, and Comparative Expression of the Lipoxygenase Gene Family of the Aquatic Duckweed, Spirodela polyrhiza, during Growth and in Response to Methyl Jasmonate and Salt*.

https://www.mdpi.com/1422-0067/21/24/9527 (accessed 2023-07-07).

(126) Upadhyay, R. K.; Edelman, M.; Mattoo, A. K. Identification, Phylogeny, and Comparative Expression of the Lipoxygenase Gene Family of the Aquatic Duckweed, Spirodela Polyrhiza, during Growth and in Response to Methyl Jasmonate and Salt. *Int. J. Mol. Sci.* **2020**, *21* (24), 9527. https://doi.org/10.3390/ijms21249527.

(127) *Kinetic investigations of the rate-limiting step in human 12- and 15-lipoxygenase - PubMed*. https://pubmed.ncbi.nlm.nih.gov/12731864/ (accessed 2023-07-07).

(128) *Steric Control of Oxygenation Regiochemistry in Soybean Lipoxygen ase-1 | Journal of the American Chemical Society*. https://pubs.acs.org/doi/10.1021/ja003855k (accessed 2023-07-07).

(129) *Hydrogen–deuterium exchange reveals long-range dynamical allostery in soybean lipoxygenase - PMC*. https://www.ncbi.nlm.nih.gov/pmc/articles/PMC5787793/ (accessed 2023-07-07).

(130) *Molecular dioxygen enters the active site of 12/15-lipoxygenase via dynamic oxygen access channels - PubMed*. https://pubmed.ncbi.nlm.nih.gov/17675410/ (accessed 2023-07-07).

(131) Noh, Y. R. Comparison of Nanodisc and Liposome Interactions with 15-Lipoxygenase-2.

(132) *The Polycystin-1, Lipoxygenase, and α-Toxin Domain Regulates Polycystin-1 Trafficking - PMC*. https://www.ncbi.nlm.nih.gov/pmc/articles/PMC4814171/ (accessed 2023-07-07).

(133) *Molecular mechanism of 15-lipoxygenase allosteric activation and inhibition - Physical Chemistry Chemical Physics (RSC Publishing)*. https://pubs.rsc.org/en/content/articlelanding/2018/cp/c7cp08586a (accessed 2023-07-07).

(134) *Molecules | Free Full-Text | Fatty Acid Allosteric Regulation of C-H Activation in Plant and Animal Lipoxygenases*. https://www.mdpi.com/1420-3049/25/15/3374 (accessed 2023-07-07).

(135) *Allosteric Activation of 15-Lipoxygenase-1 by Boswellic Acid Induces the Lipid Mediator Class Switch to Promote Resolution of Inflammation - Börner - 2023 - Advanced Science - Wiley Online Library*. https://onlinelibrary.wiley.com/doi/full/10.1002/advs.202205604 (accessed 2023-07-07).

(136) *Characterization of Differential Dynamics, Specificity, and Allostery of Lipoxygenase Family Members | Journal of Chemical Information and*

Modeling. https://pubs.acs.org/doi/10.1021/acs.jcim.9b00006 (accessed 2023-07-07).

(137) *5-Lipoxygenase Binds Calcium | Biochemistry*. https://pubs.acs.org/doi/10.1021/bi9824700 (accessed 2023-07-07).

(138) *Activation of 5-lipoxygenase by cell stress is calcium independent in human polymorphonuclear leukocytes - PubMed*. https://pubmed.ncbi.nlm.nih.gov/11807011/ (accessed 2023-07-07).

(139) *Structure of a Calcium-dependent 11R-Lipoxygenase Suggests a Mechanism for Ca2+ Regulation - PMC*. https://www.ncbi.nlm.nih.gov/pmc/articles/PMC3381197/ (accessed 2023-07-07).

(140) *ATP Allosterically Activates the Human 5-Lipoxygenase Molecular Mechanism of Arachidonic Acid and 5(S)-Hydroperoxy-6(E),8(Z),11(Z),14(Z)-eicosatetraenoic Acid - PMC*. https://www.ncbi.nlm.nih.gov/pmc/articles/PMC4215895/ (accessed 2023-07-07).

(141) *Investigations of human platelet-type 12-lipoxygenase: role of lipoxygenase products in platelet activation - PMC*.

https://www.ncbi.nlm.nih.gov/pmc/articles/PMC3494251/ (accessed 2023-07-07).

(142) *Platelet 12-LOX scores a HIT | Blood | American Society of Hematology*.
https://ashpublications.org/blood/article/124/14/2166/33073/Platelet-12-LOX-scores-a-HIT (accessed 2023-07-07).

(143) *Fatty acids negatively regulate platelet function through formation of noncanonical 15-lipoxygenase-derived eicosanoids - PubMed*.
https://pubmed.ncbi.nlm.nih.gov/36708179/ (accessed 2023-07-07).

(144) *Zileuton, a 5-lipoxygenase inhibitor, increases production of thromboxane A2 and platelet aggregation in patients with asthma - Wu - 2003 - American Journal of Hematology - Wiley Online Library*.
https://onlinelibrary.wiley.com/doi/abs/10.1002/ajh.10370 (accessed 2023-07-07).

Chapter 2:

Biochemical and hydrogen-deuterium exchange studies of the single nucleotide polymorphism Y649C in human platelet 12-lipoxygenase linked to a bleeding disorder

[This chapter has been adapted from publication, **Biochemical and hydrogen-deuterium exchange** studies of the single nucleotide polymorphism Y649C in human platelet 12- lipoxygenase linked to a bleeding disorder, (Tran et al. 2023) Archives of Biochemistry and Biophysics]

Michelle Tran[1], Rachel L. Signorelli[2], Adriana Yamaguchi[3], Eefie Chen[1], Michael Holinstat[3], Anthony T. Iavarone[4], Adam R. Offenbacher[2], Theodore Holman[1],

1. Department of Chemistry and Biochemistry, University of California Santa Cruz, Santa Cruz, CA, 95064, USA

2. Department of Chemistry, East Carolina University, Greenville, NC, 27858, USA

3. Department of Pharmacology, University of Michigan Medical School, Ann Arbor, MI, 48109,

USA

4. QB3/Chemistry Mass Spectrometry Facility, University of California Berkeley, Berkeley, CA, 94720, USA

Biochemical and Hydrogen-Deuterium Exchange Studies of the Single Nucleotide Polymorphism Y649C in Human Platelet 12-Lipoxygenase Linked to a Bleeding Disorder

*Corresponding Authors:

TRH: Tel.: +1-831-459-5884, holman@ucsc.edu

ARO: Tel.: +1-252-737-5422, offenbachera17@ecu.edu

Abbreviations:

LOX, lipoxygenase; h12-LOX, human platelet 12S-lipoxygenase; r15-LOX-1 or r12/15-LOX or rALOX15, rabbit 15S-LOX-1; c11-LOX, coral 11R-LOX; AA, arachidonic acid; DHA, docosahexaenoic acid; 12(S)-HpETE, 12(S)-hydroperoxyeicosatetraenoic acid; 12(S)-HETE, 12(S)-hydroxyeicosatetraenoic acid; COX, cyclooxygenase; ML355, h12-LOX specific inhibitor; NSAIDs, nonsteroidal anti-inflammatory drugs; coxibs, COX-2 selective inhibitors; 13-HpODE, 13S-hydroperoxyoctadeca-9Z,11E-dienoic acid; 13-HODE, 13S-hydroxyoctadeca-9Z,11E-dienoic acid; TOP, a subdomain region in the helical bundle of the catalytic domain (residues 163-222); PLAT domain, Polycystin-1, Lipoxygenase, Alpha-Toxin; PDZ domain, PSD95, Dig1, Zo-1 domain; E_{cat}, catalytically active enzyme; E_{apo}, inactive Fe-free enzyme; SAXS, small angle X-ray scattering; ICP-MS, inductively coupled plasma mass spectroscopy; SEC, size exclusion chromatography; BSA, bovine serum albumin; DCM, dichloromethane; HDX-MS, hydrogen-deuterium exchange-mass spectrometry; WT h12-LOX, wild-type human platelet 12S-lipoxygenase; h15-LOX-2, human epithelial 15-lipoxygenase; SLO-1, soybean lipoxygense-1; SDS-PAGE, sodium dodecyl sulfate-polyacrylamide gel electrophoresis; DOPC, 1,2-dioleoyl-sn-glycero-3-phosphocholine; DOPE, 1,2-dioleoyl-sn-glycero-3-phosphoethanolamine; DOPS, 1,2-dioleoyl-sn-glycero-3-phospho-L-serine.

Highlights:

- **A human 12-LOX SNP forming a Y649C mutation is linked to a bleeding disorder**

- ***In vitro* kinetics show that Y649C exhibits reduced rates of 12S-HETE production at 37 ℃**

- **Y649C exhibits lowered liposome binding properties at 37 ℃**

- **HDX-MS reveals a long-range network of altered protein dynamics stemming from the mutation site**

- **Our results identify new structural and functional insights into this human 12-LOX SNP**

Abstract:

Human platelet 12-lipoxygenase (h12-LOX) is responsible for the formation of oxylipin products that play an important role in platelet aggregation. Single nucleotide polymorphisms (SNPs) of h12-LOX have been implicated in several diseases. In this study, we investigate the structural, dynamical, and functional impact of a h12-LOX SNP that generates a tyrosine-to-cysteine mutation at a buried site (Y649C) and was previously ascribed with reduced levels of 12(S)-hydroxyeicosatetraenoic acid (12S-HETE) production in isolated platelets. Herein, *in vitro* Michaelis-Menten kinetics show reduced catalytic rates for Y649C compared to WT at physiological or lower temperatures. Both proteins exhibited similar melting temperatures, metal content, and oligomerization state. Liposome binding for both proteins was also dependent upon the presence of calcium, temperature, and liposome composition; however, the Y649C variant was found to have lowered binding capacity to liposomes compared to WT at physiological temperatures. Further, hydrogen-deuterium exchange mass spectrometry (HDX-MS) experiments revealed a regional defined enhancement in the peptide mobility caused by the mutation. This increased instability for the mutation stemmed from a change in an interaction with an arched helix that lines the substrate binding site, located $\geq 15\text{Å}$ from the mutation site. Finally, differential scanning calorimetry demonstrated a reduced protein (un)folding enthalpy, consistent with the HDX results. Taken together, these results demonstrate remarkable similarity between the mutant and WT h12-LOX, and yet, subtle changes in activity, membrane affinity and protein stability may be responsible

for the significant physiological changes that the Y649C SNP manifests in platelet

biology.

1. Introduction

Platelet activation is essential to produce a platelet plug to restore hemostasis after injuries, however, uncontrolled platelet activation can also lead to the formation of an occlusive thrombus resulting in myocardial infarction or stroke. The importance platelets play in thrombotic disorders has been established through the decrease of thrombotic events with the use of antiplatelet therapeutics.[1, 2] In addition, the role of platelets in aggregation is underscored by single nucleotide polymorphisms (SNPs) which can affect platelet biology significantly.[3-7]

Human platelet 12-lipoxygenase (h12-LOX) is a non-heme, iron-containing enzyme that catalyzes the oxidation of polyunsaturated fatty acids (PUFAs) with cis-cis-1,4-pentadiene moieties, such as arachidonic acid (AA). These PUFA substrates are found in the phospholipid bilayer and can be released from the membrane by cleavage with a phospholipase.[8] h12-LOX is proposed to associate with the bilayer upon calcium release and react with the free PUFAs that are associated with the bilayer. It has been well documented that calcium leads to the translocation of h12-LOX from the cytosol to the membrane where free AA is associated with the bilayer;[9-11] however, h12-LOX has poor reactivity with PUFA molecules covalently attached to the phospholipid bilayer.[12]

The exact mechanism by which h12-LOX activates platelets is unknown. It has been postulated that 12(S)-hydroxyeicosatetraenoic acid (12S-HETE) activates NADPH oxidase to form reactive oxygen species, molecules known to lead to platelet activation, but it is not known whether NADPH oxidase is required for h12-LOX

activation.[13] 12S-HETE has also been hypothesized to bind to GPR31, an orphan

GPCR, causing a prothrombotic result.[14] Studies inhibiting the formation of 12S-

HETE showed a decrease in thrombus growth, vessel occlusion, and plug formation

in mice further supporting h12-LOX's prothrombotic behavior. It has also been

strongly suggested that 12-HETE leads to tissue-factor-dependent thrombin

Figure 1. A h12-LOX structural model with Y649 highlighted in pink, L407 (a critical active site residue) highlighted in

red and the active site iron in yellow. The proposed solution-state dimer is shown on the left, but only the monomer

is shown on the right for clarity of presentation.

generation due to its esterification into the membrane.[15-17] Further, transgenic mice

deficient in h12-LOX were not able to undergo normal platelet aggregation.[18] With

regards to possible physical protein-protein interactions, strong evidence has shown

that h12-LOX activates phospholipase C2, phosphokinase C, induces αIIbβ3

aggregation, and increases calcium concentrations.[18]

Figure 1. The enzymatic reaction of h12-LOX with AA, producing 12S-HpETE is

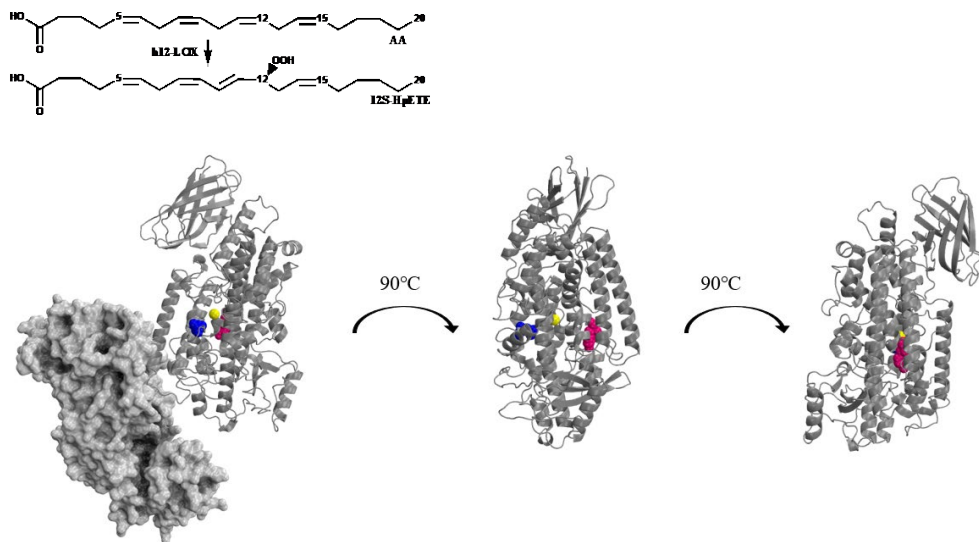shown (Top) and a h12-LOX structural model[19] with Y649 highlighted in pink, L407

(a critical active site residue) highlighted in blue and the active site iron in yellow.

The proposed solution-state dimer is shown on the left, with one monomer shown as a dimmed grey space-filling model and the other monomer shown as a blue ribbon model. The other two images are of only the cartoon monomer, for clarity of presentation.

SNPs in the wild-type h12-LOX (WT) coding region have been correlated with diseases such as human congenital toxoplasmosis,[20] breast cancer,[21] schizophrenia,[22] osteoporosis,[23] and early onset menopause.[24] However, a majority of the discovered SNPs, such as N322S, E259K, Q261R, and D134H, have been found on the surface of h12-LOX and their ability to produce 12-HpETE is comparable to WT ($101 \pm 23\%$, $60 \pm 18\%$, $91 \pm 10\%$, and $109 \pm 36\%$, respectively).[25] Recently, a study documenting a family with a dominantly inherited bleeding diathesis was linked to a h12-LOX SNP, Y649C.[26] A patient with this mutation experienced heavy menstrual bleeds and needed platelet transfusion during childbirth. In addition, both daughters of the patient developed purpura on their lower limbs. Unlike most documented SNPs of h12-LOX, Y649C is buried within the catalytic domain (**Figure 1**) and Y649C demonstrated a 25-35% loss of 12S-HETE production in patient-isolated platelets.[26] However, it was unclear why the mutation afforded this change in 12S-HETE production.[26] Due to the critical role 12S-HETE plays in regulating platelet aggregation and thrombosis, studying the correlation between the structure and function of the mutation is pertinent to understanding its role in the platelet and may potentially enable us to provide a more accurate and precise treatment to patients. In the current study, we examine the role of this mutation on the enzyme's temperature-dependent kinetic properties and membrane binding capacity. The

regional peptide flexibility of the SNP was also investigated with the goal of relating it to the protein folding enthalpy and catalytic activity. In combination, our cumulative results shed important new light on the structural, functional, and dynamical impact of this SNP of h12-LOX and its potential relationship to the pathological condition

2. Experimental Procedures

2.1 Chemicals

Fatty acids used in this study were purchased from Nu Chek Prep, Inc. (MN, USA). Deuterium oxide (99.9%) was purchased from Cambridge Isotope Laboratories (Tewksbury, MA, USA). All other solvents and chemicals were reagent grade or better and were used as purchased without further purification.

2.2 Site-Directed Mutagenesis, Protein Expression/Purification, and Metal Content

The h12-LOX mutation, Y649C, was introduced using the same residue numbering convention as used in UniProt for the h12-LOX sequence (accession number P18054). The online QuikChange Primer Design tool (http://www.genomics.agilent.com/primerDesignProgram.jsp) from Agilent Technologies (CA, USA) was used to design the primers for the Y649C mutant. The mutation was introduced using a QuikChange®II XL site-directed mutagenesis kit

from Agilent Technologies by following the instructions in the provided protocol. The mutation was confirmed by sequencing the LOX insert in the pFastBac3.2 shuttle vector (Eurofins Genomics, KY, USA).

Expression of the N_t-6His-tag recombinant enzymes was performed in an Sf9 system, with chromatographic purification and enzymatic activity assays performed as described previously.[27] All proteins were aliquoted and stored in 25 mM HEPES (pH 8) and samples from the same purification batch were used for all analyses. The reaction time course of enzymatic activity was monitored continuously at 234 nm using a Perkin-Elmer Lambda 45 UV/Vis spectrophotometer to observe the production of conjugated dienes (epsilon at 234 nm = 27,000 mM^{-1} cm^{-1} for 12S-HpETE) in a cuvette containing a 2 mL solution of 25 mM HEPES (pH 8), 10 μM AA and 20-30 μg of WT or Y649C h12-LOX. Iron content was determined by inductively coupled plasma mass spectrometry (ICP-MS), using an internal Co standard and external standardized Fe solutions. Iron concentrations were compared with standardized iron solutions and all kinetic data were normalized to the iron content. The Bradford assay, with bovine serum albumin (BSA) as the protein standard, was used to determine the protein concentration.

2.3 Steady-State Kinetics and Temperature Stability

h12-LOX reactions were performed at 22, 37, and 42 °C in a 1 cm^2 quartz cuvette containing 2 mL of 25 mM HEPES (pH 7.5) with substrate (docosahexaenoic acid (DHA) and AA). DHA and AA concentrations were varied from 0.25 to 10 μM.

Concentrations of DHA and AA were determined by measuring the amount of oxylipins produced from complete reaction with soybean lipoxygenase-1 (SLO-1). Concentrations of oxylipins were determined by measuring the absorbance at 234 nm. Reactions were initiated by the addition ~20 μg of WT and ~30 μg of Y649C and were monitored on a Perkin-Elmer Lambda 45 UV/Vis spectrophotometer. Product formation was determined by the increase in absorbance at 234 nm for oxylipin products (ε_{234nm} = 25,000 M^{-1} cm^{-1}). KaleidaGraph (Synergy) was used to fit initial rates (at less than 20% turnover), to the Michaelis-Menten equation for the calculation of kinetic parameters. For the stability assay, all reactions were conducted using a Cary-UV Vis spectrophotometer, which was set to 37 °C, with 25 mM HEPES buffer (pH 8) and stirred continuously. Stocks of WT and Y649C at 133nM and 200nM respectively were incubated at 37 °C and 6000 mL were withdrawn at each time point. The fastest rates over 15 second intervals were plotted versus the enzyme incubation time at 37 °C.

2.4 Enzymatic Products Determination and Competitive Substrate Specificity by LC-MS

To determine the products formed, WT and the Y649C enzymes were reacted with 10 μM of AA in 25 mM HEPES buffer (pH 7.5) for 10 min, in triplicate. The reactions were quenched with 1% glacial acetic acid and extracted three times with dichloromethane (DCM). The products were then reduced with trimethylphosphite and evaporated under a stream of nitrogen gas. The reaction products were reconstituted in methanol and analyzed via liquid chromatography-tandem mass spectrometry (LC-MS/MS). Chromatographic separation was performed using a

Sciex Excion LC system, using a C18 column (Phenomenex Kinetex, 4 μm, 150 × 2.0 mm). Mobile phase A consisted of water with 0.1% (v/v) formic acid, and mobile phase B was acetonitrile with 0.1% formic acid. The flow rate was 0.4 mL/min with initial conditions (15% B) maintained for 0.75 min. Mobile phase B was held at 15% over 1 min and then ramped to 30% over 0.75 min, to 47% over 2 min, to 54% over 1.5 min, to 60% over 4.5 min, to 70% over 4.5 min, to 80% over 1 min, to 100% over 1 min, held at 100% for 2 min, and finally returned to 15% to equilibrate for 2 min. The chromatography system was coupled to a Sciex PDA and x500B qTOF MS. Analytes were ionized through electrospray ionization with a −4.0 kV spray voltage and 50, 50, and 20 PSI for ion source gases 1 and 2 and the curtain gas, respectively. The CAD gas was set to 7, while the probe temperature was 550 °C. DP was −60 V, and CE was set to −10 V with a 5 V spread. MS2 acquisition was performed using SWATH, and mass lists containing the following m/z ratios of 343.2 ± 0.5 (HDHAs) and 359.2 ± 0.5 (HETEs) were used. All analyses were performed in negative ionization mode at the normal resolution setting. Matching retention times, UV spectra, and fragmentation patterns to known standards with at least six common fragments were used to identify the products. For the competitive substrate specificity assay, a similar procedure to product formation was used. A mixture of 10 mM AA and 10 mM DHA was incubated with enzyme, with the reaction being quenched with 1% glacial acetic acid after a third of the total substrate turnover.

2.5 IC$_{50}$ Determination

IC50 values for the h12-LOX specific inhibitor, ML355, against WT and Y649C

were determined in the same manner as the steady-state kinetic values. The reactions were

carried out in 25 mM HEPES buffer (pH 8.00), 0.01% Triton X-100, and 10 μM AA. IC50 values were obtained by determining the enzymatic rate at six inhibitor concentrations and plotting rate against their inhibitor concentration, followed by a hyperbolic saturation curve fit. The data used for the saturation curve fits were performed in duplicate or triplicate, depending on the quality of the data. Triton X-100 was used to ensure proper solubilization of the inhibitor.

2.6 Oligomeric State Determination

Size exclusion chromatography (SEC) was performed on the affinity-purified proteins

using an AKTA Pure system. After centrifugation at 13000 rpm for 5 mins (to sediment any

debris), the purified protein was loaded onto a SuperdexTM 75, 10/300 GL column (GE Healthcare), pre-equilibrated with 25 mM HEPES (pH 8) at a flow rate of 0.3 mL/min. The time of elution of WT and Y649C was compared with a gel filtration standard containing bovine thyroglobulin (MW 670 kDa), bovine γ-globulin (158 kDa), chicken ovalbumin (44 kDa), ribonuclease A type I-A from bovine pancreas (17 kDa) and p-aminobenzoic acid (1.35 kDa).

2.7 Protein Melting Temperature Determination with Circular Dichroism

Thermal denaturation spectra were measured on a CD spectrophotometer (J1500, JASCO, Inc., Easton, Maryland) using a 1 mm quartz cuvette in the 180-300 nm spectral region and the 25-81 °C temperature range. The temperature was controlled using a Peltier thermostatted cell holder, the thermal ramp rate was 0.6 °C/min, and the step size was 2 °C. Spectra were measured with a scan speed of 100 nm/min every 0.1 nm using a 4 nm bandwidth and a data integration time of 4 s. A 25 mM sodium phosphate buffer (pH 7.5) background CD spectrum was subtracted from each 10 µM WT or Y649 h12-LOX temperature-dependent CD spectrum. Phosphate buffers lacking sodium chloride were used for CD because chloride ions and common organic buffers, such as HEPES, interferes with CD signal in the UV region. Two to three sets of thermal melts were acquired for each of the WT and Y649 proteins.

2.8 Synthetic Liposome Preparation and h12-LOX Binding

Lipid suspensions were prepared from commercial sources with the following molar ratios; 60:30:9.9:0.1 DOPC:DOPE:DOPA:DSPE-PEG (DOPE); 60:30:9.9:0.1 DOPC:DOPS:DOPA:DSPE-PEG (DOPS); 99.9:0.1 DOPC: DSPE-PEG (DOPC). Each lipid mixture was dissolved in chloroform and the solutions were left under N_2 for 20 min and placed in a vacuum chamber for at least 12 h at room temperature to remove all traces of solvent. Lipid mixtures were dissolved in 25 mM HEPES buffer (pH 8) to a concentration of 10 mg/mL and incubated in glass vials on a tube rotator for 1 h to facilitate homogenization. Liposomes were created using the literature protocol,[28] using a 100 nm filter. For liposome membrane binding assays conducted at 37 °C, liposomes were extruded at 37 °C and remained at that temperature for the

assay. Liposome suspension volumes were adjusted to have a final concentration of 10 mg/mL and their size were determined by dynamic light scattering (DLS).

Liposome suspensions were placed on a DynaMag™-2 for 15 min at room temperature to bind the liposomes. Supernatant was removed and 1 mL of 25 mM HEPES buffer (pH 8) was added. This washing step was repeated five times. When calcium (10 μM) was added, it was stirred for 15 min before use. WT (30 μg) or Y649C (30 μg) were added to 1 mL of a 10 mg/mL liposome suspension. The sample was rocked over ice for 10 min and then placed on a DynaMag™-2 for 10 min. 25 μL of the supernatant was saved, and the beads were resuspended to a final volume of 1 mL. 25 μL of the resuspended beads were saved and the saved samples were subjected to SDS-PAGE. Using ImageLab, ratios of the supernatant to pellet were determined. All conditions were done in triplicate. In parallel, the remainder of the supernatant was added to a cuvette, its volume raised to 2 mL, and the sample tested for enzymatic activity with 10 μM AA. Rates of reactions were determined using the same protocol as used for steady-state kinetics.

2.9 HDX-MS of h12-LOX

Aliquots of WT or Y649C h12-LOX (3-5 mg/mL) were thawed and were diluted 10-fold (5 μL into 45 μL) in 10 mM HEPES, 150 mM NaCl, 5 mM dithiothreitol (DTT), pD 7.4 D_2O (99% D) buffer (corrected; pD = pH_{read} + 0.4). Samples were incubated randomly at 10 time points (0, 10, 20, 45, 60, 180, 600, 1800, 3600, and 7200 s) at 10 and 25 °C using a water bath. For each variant and temperature, time points were randomized and prepared once (see **Table S1**). At the designated incubation time, all samples were then treated identically; the samples

59

were rapidly cooled (5-6 s in a -20 °C bath) and acid quenched (to pH 2.4, confirmed with pH electrode, with 0.32 M citric acid stock solution to 90 mM final concentration). Procedures from this point were conducted near 4 °C. Prior to pepsin digestion, guanidine HCl (in citric acid, pH 2.4) was mixed with the samples to a final concentration of 0.5 M. h12-LOX HDX samples were digested with pre-equilibrated (10 mM citrate buffer, pH 2.4), immobilized pepsin for 2.5 min. The peptide fragments were filtered with spin cups (cellulose acetate) by centrifugation for 10 s at 4 °C, to remove pepsin. Samples were flash frozen immediately in liquid nitrogen and stored at -80 °C until data collection.

Deuterated, pepsin-digested samples of h12-LOX were analyzed using a 1200 series LC system (Agilent, Santa Clara, CA) that was connected in-line with the LTQ Orbitrap XL mass spectrometer (Thermo), as described by our laboratory previously.[19, 29] Mass spectral data corresponding to the HDX measurements were analyzed using HDX Workbench.[30] The percent deuterium incorporation was calculated for each of these peptides, taking into account the number of amide linkages (excluding proline residues), and the calculated number of deuterons incorporated. The values were normalized for 100% D_2O and corrected for peptide-specific back-exchange, HDX% = (observed, normalized extent of deuterium incorporation {in percent})/(1-{BE/100}).[31] Back-exchange values ranged from 2 to 53%, for an average value of 22% (**Supporting Information, HDX Summary Table; Table S1**). The resulting data were plotted as deuterium exchange versus time using Igor Pro software.

2.10 Protein Stability Determined by Differential Scanning Calorimetry (DSC)

DSC experiments were performed on the WT and Y649C h12-LOX variants using a NanoDSC microcalorimeter from TA Instruments. Protein samples were dissolved at 20-30 µM concentrations in 50 mM HEPES, 150 mM NaCl, pH 7.5. For a given experiment, the temperature was scanned from 30 to 90 °C, with a 1 °C/min ramp rate at constant pressure (3 atm). Experiments were performed in heating only mode because h12-LOX denatures and does not reversibly refold. The raw data was analyzed using NanoAnalyze software from TA instruments. Thermodynamic data was determined from Gaussian fit models of the raw data that had been corrected by using a fourth-order polynomial baseline. Each experiment was run in duplicate.

3. Results and Discussion

3.1-3.2 Protein Purification and Expression

Using standard protein purification methods as used previously,[27] the purity of WT and Y649C h12-LOX were assessed by SDS-PAGE gels to be greater than 90%. The metal content was determined to be 22% for WT and 20% for Y649C by inductively coupled plasma mass spectrometry (ICP-MS). All kinetic data were normalized to the iron content, and the protein concentrations were determined by Bradford assay with a bovine serum albumin protein standard.

3.3.1 Determining k_{cat} and k_{cat}/K_M for WT and Y649C at 22 °C, 37 °C, and 42 °C
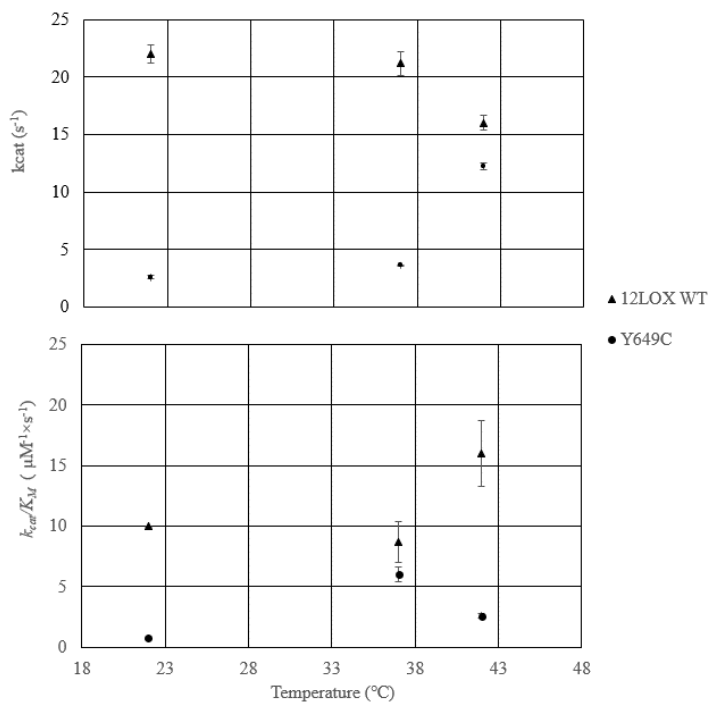
Figure 2: k_{cat} and k_{cat}/K_M values for WT (triangles) and Y649C (circles) at 22 °C, 37 °C, and 42 °C.

It was proposed that the activity of Y649C was markedly lower than WT, which manifested in the disease presentation.[10] Based on this hypothesis, the *in vitro* kinetic properties of the two enzymes were determined and compared (**Table 0, Figure 2**). The k_{cat} for WT and Y649C with AA at 22 °C was 22 ± 4 and 2.6 ± 6 s^{-1}, respectively, with the WT values correlating well with our previous work.[32-37] The k_{cat}/K_M for WT and Y649C was 10 ± 0.2 and 0.76 ± 0.4 μM^{-1} s^{-1}, respectively. These data de monstrate that the k_{cat} and k_{cat}/K_M with AA for WT is ~10-fold greater than that of Y649C at 22 °C; however, the functional temperature in the human body is 37 °C. Therefore, the temperature dependences of k_{cat} and k_{cat}/K_M were determined with AA at 37 °C and 42 °C. At 37 °C, the k_{cat} for WT and Y649C was 21 ± 1 and 3.6 ±

0.1 s^{-1}, respectively. The k_{cat}/K_M for WT and Y649C was 8.7 ± 2 and 6 ± 0.6 µM^{-1} s^{-1}, respectively.

	k_{cat} (sec^{-1})		k_{cat}/K_M (mM^{-1}sec^{-1})	
Table 1: Steady-State kinetic parameters for WT and Y649C at three temperatures. Standard deviation errors are shown in parentheses from 3 replicates.				
Temperature (°C)	WT	Y649C	WT	Y649C
22	22 (4)	2.6 (6)	10 (0.2)	0.76 (0.4)
37	21 (1)	3.6 (0.1)	8.7 (2)	6 (0.6)
42	16 (0.6)	12 (0.3)	16 (3)	2.6 (0.2)

At 42 °C, the k_{cat} for WT and Y649C with AA was 16 ± 0.6 and 12 ± 0.3 s^{-1}, respectively. The k_{cat}/K_M for WT and Y649C was 16 ± 3 and 2.6 ± 0.2 µM^{-1} s^{-1}, respectively. The kinetics for WT displayed relatively constant kinetic values from 22 °C to 37 °C, but a decrease in k_{cat} and an increase in k_{cat}/K_M at 42 °C. The k_{cat} of Y649C also was relatively constant from 22 °C to 37 °, but increased at 42 °C. The k_{cat}/K_M of Y649C increased at 37 °C and then subsequently decreased at 42 °C. Overall, the kinetic parameters of WT are significantly greater than those of Y649C, with the k_{cat} of WT being over six-fold greater than that of Y649C at 37 °C.

The functional stability of the two enzymes at 37 °C was investigated by comparing how the initial rates changed with 37 °C degree incubation. Surprisingly, WT h12-LOX lost activity significantly faster than Y649C. WT lost 75% of its

activity after only 200 s, whereas it took 3500 s for the activity of Y649C to drop

75% (**Supporting Information, Figure S1**).

Table 2: Competitive kinetic product distribution with a mixture of 10 μM AA and 10 μM DHA with both WT and Y649C. Standard deviation errors are shown in parentheses from 3 replicates.

	AA products (%)	DHA products (%)
WT	65 (6)	35 (3)
Y649C	63 (6)	37 (4)

3.3.2 Determining k_{cat} and k_{cat}/K_M for WT and Y649C with DHA 22 °C

DHA oxylipins are predominately anti-inflammatory mediators, and AA

oxylipins are mainly pro-inflammatory mediators,[38] therefore the kinetics for the

reaction of Y649C with DHA were investigated at 22 °C. The k_{cat} for the reactions of

WT and Y649C with DHA was 11 s^{-1} and 1.2 s^{-1} respectively, while the k_{cat}/K_M for

WT and Y649C was 7.7 s^{-1} μM^{-1} and 0.96 s^{-1} μM^{-1}, respectively. These data

demonstrate that the WT variant is a more effective catalyst than Y649C with DHA,

consistent with the kinetic trends with AA as the substrate, and that both WT and

Y649C react with AA preferentially over DHA. To confirm this result, competitive

kinetics were also performed (**Table 1**). WT demonstrated a preference for AA over

DHA, producing 65% AA-oxylipins and 35% DHA-oxylipins, when both AA and

DHA were present in the same reaction vessel. Y649C had a similar profile producing 63% AA-oxylipins and 37% DHA-oxylipins (**Table 1**). There was approximately double the amount of oxylipins formed from AA than DHA which is consistent with the two-fold increase in k_{cat} and k_{cat}/K_M between AA and DHA for both WT and Y649C.[34, 35, 37]

3.4 Product Profile and Substrate Specificity of AA and DHA with WT and Y649C

Given the significant role that the oxylipin products of h12-LOX play in platelet aggregation, the product profile for the reactions of Y649C and WT with both AA and DHA were investigated. With AA as substrate, WT and Y649C produced mostly the 12-oxylipin with 12-HETE:15-HETE ratios of 88:12 and 81:19, respectively. For DHA, the 14-oxylipin was the major product for both WT and Y649C, with 14-HDHA:17-HDHA:20-HDHA:11-HDHA ratios of 76:11:0:13 and 74:8:8:10 respectively (**Table 2**), which are consistent with previous work.[34, 35, 37] Thus, there was no significant difference between the product profile for these h12-LOX variants with either substrate.

Table 3: Distribution of products created by reaction of either WT or Y649C with AA or DHA (10 µM). Percent values are presented. Standard deviation errors are shown in parentheses from 3 replicates.

	AA Products		DHA Products			
	12-HETE	**15-HETE**	**14-HDHA**	**17-HDHA**	**20-HDHA**	**11-HDHA**
WT	88 (2)	12 (2)	76 (2)	11 (0.5)	0	13 (2)
Y649C	81 (1)	19 (1)	74 (2)	8 (2)	8 (1)	10 (1)

3.5 IC50 Determination with WT and Y649C

ML355 is a potent/selective h12-LOX inhibitor[39] which binds to its active site and thus its IC50 would be sensitive to structural changes in the active site. The IC50 values of ML355 were determined with both WT and Y649C and found to be 0.9 ± 0.2 μM ($91 \pm 5\%$ maximum inhibition) and 1.1 ± 0.2 μM ($90 \pm 4\%$ maximum inhibition), respectively. Since there was no significant difference between the IC50 values of WT and Y649C, the data indicates minimal change in the active site for inhibitor recognition (**Table 3**). The inhibitor data of WT are consistent with previous reports.[39, 40]

Table 4. I_{50} values and maximum inhibition percentage of **ML355** against WT and Y649C. Standard deviation errors are shown in parentheses from 3 replicates.

	IC$_{50}$ μM (error)	**Maximum % inhibition**

WT	0.9 (0.2)	91 (5)
Y649C	1.1 (0.2)	90 (4)

3.6 Oligomeric States of WT and Y649C

It has previously been shown that WT remains mainly in the dimeric state.[19] The oligomeric state of WT and Y649C were determined by size exclusion chromatograph (SEC). No significant difference was observed in the elution volume. Therefore, both remained in the dimer form, supporting that the Y649C mutation does not change the oligomeric state of h12-LOX (**Supporting Information, Figure S2**).

3.7 Protein Melting Point Determination of WT and Y649C by Circular Dichroism

To investigate the effects this mutation might have on the structural temperature dependence of h12-LOX, circular dichroism was used to determine the melting temperature of both WT and Y649C. The temperature-dependent protein unfolding traces were obtained by averaging the measured CD spectral data (**Supporting Information, Figure S3**) from 205 to 225 nm. This spectral range encompasses the wavelengths absorbed by both major secondary structures (helix and sheet). By fitting the thermal traces to three-parameter sigmoidal functions, the temperature midpoints (T_m) were determined to be 48 ± 0.5 °C for WT and 48 ± 1 °C

for Y649C. These data dismiss any significant change in the melting of the secondary structure as the origin of the kinetic properties emerging from the replacement of the tyrosine residue at position 649 with cysteine.

3.8 Synthetic Membrane Association of WT and Y649C at 22 °C and 37 °C

In the presence of DOPC liposomes (at 22 °C), 16 ± 4% of WT h12-LOX was bound to the membrane in the absence of calcium, and 50 ± 3% was bound in the presence of calcium. For Y649C, 66 ± 3% was bound in the absence of calcium; this value increased to 91 ± 7% when calcium was added. A similar trend was observed
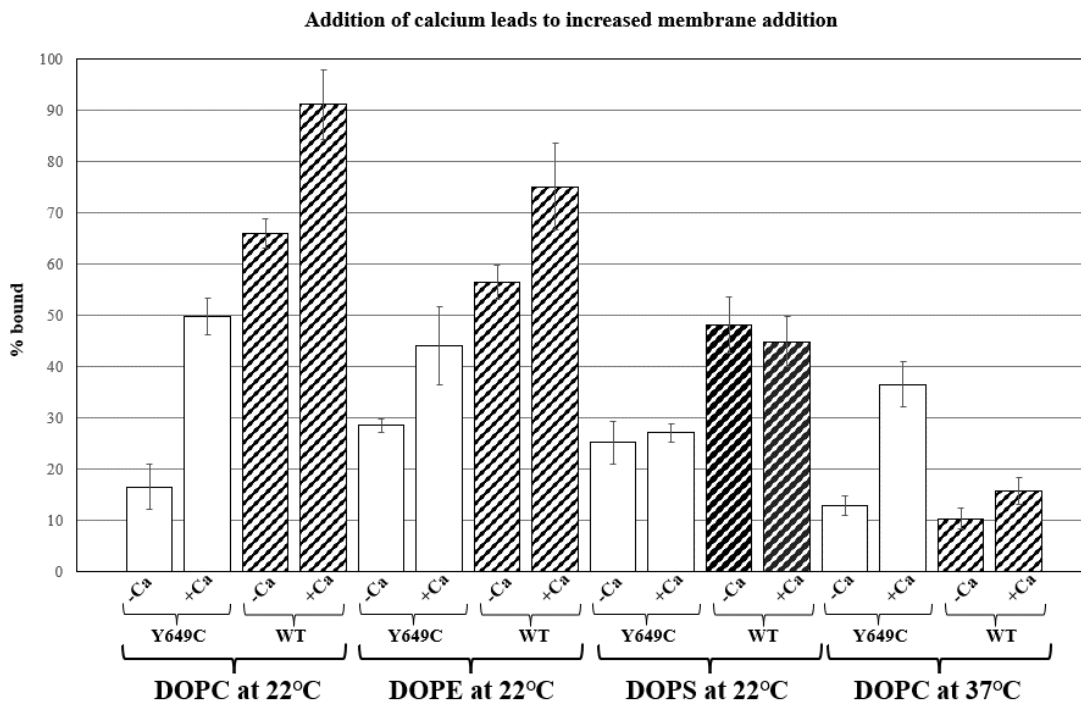

Figure 3: Percent of WT or Y649C bound to DOPC, DOPE, and DOPS liposomes at 22 °C. Membrane binding assays were conducted in 25 mM HEPES (pH 7.5) at room temperature in either the absence or presence of 10 μM calcium chloride.

with DOPE liposomes (**Figure 3**), though the impact of calcium addition did not have as significant an effect on h12-LOX association with PE liposomes compared to PC. Consistent with DOPC and DOPE, there was more Y649C associated with the DOPS liposomes than WT, but there was no effect from addition of 10 μM $CaCl_2$ (**Figure 3**). These data demonstrate that in general Y649C has a higher binding capacity to synthetic liposomes than WT at 22 °C and that calcium increases that affinity for both WT and Y649C, with DOPC and DOPE having the largest effect. This has been previously shown for WT with liposomes of comparable composition.[10, 11]

The temperature effect for DOPC liposome binding was investigated at 37 °C. At this temperature, $13 \pm 2\%$ of WT associated with the liposome, which increased to $36 \pm 4\%$ when calcium was added. For Y649C, $10 \pm 2\%$ was bound, which only
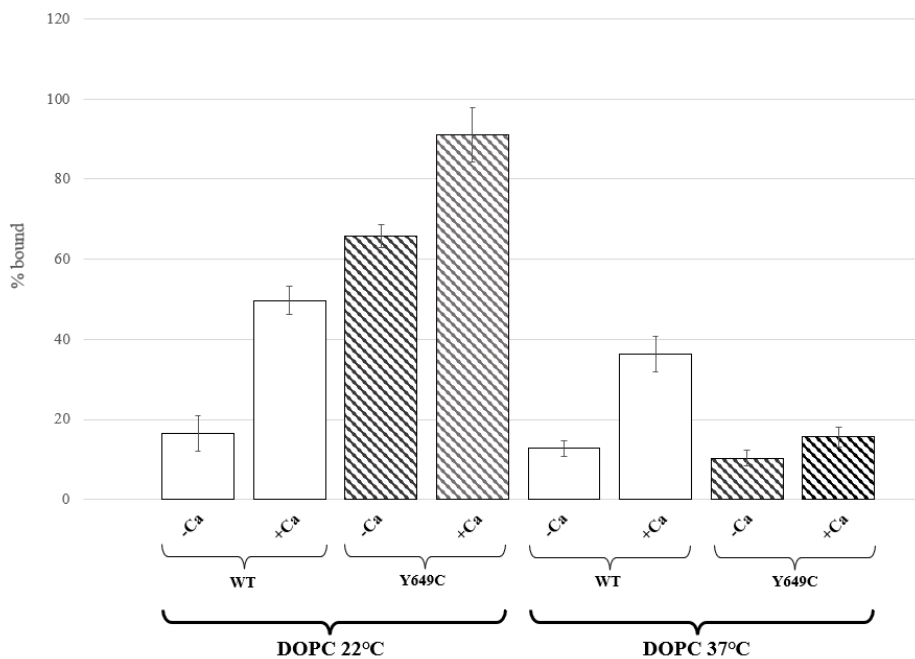

Figure 4: Percent of WT or Y649C bound to DOPC liposomes at 22 ℃ and 37 ℃. Membrane binding assays\ were conducted in 25 mM HEPES (pH 7.5) at room temperature in either the absence or presence of 10 μM

increased to $16 \pm 3\%$ when calcium was added (**Figure 4**). These data indicate that the binding affinity of WT is not significantly affected by the increase of temperature, which agrees with past literature.[11] However, the binding affinity of Y649C is significantly reduced at 37 °C and is nearly insensitive to the presence of calcium ions.

3.9 HDX-MS of h12-LOX Y649C

Based on an *in silico* model,[19] the site of mutation (Y649C) is 15-18 Å from the catalytic iron center and nearly 30 Å (Cα-Cα) from a conserved active site leucine, L407, that is critical for catalysis (**Figure 1**).[36] The rather distal location of Y649C relative to the active site raises the question as to how this mutation might influence h12-LOX activity through structural and/or dynamic regulation. As there is no X-ray structure of the h12-LOX, we pursued hydrogen-deuterium exchange mass spectrometry (HDX-MS). We had previously used HDX-MS to characterize the difference in exchange properties of a h12-LOX mutant, L183E/L187E, which forms an engineered monomeric form of the enzyme.[19] Room temperature HDX-MS helped to identify distinctive exchange properties between the WT dimer and the mutant monomer, thereby providing a map of the dimer interface, which was found to be localized along helix α2 and to serve as the gateway to substrate portal entrance. HDX-MS has been used to study the impact of disease-linked mutations on protein flexibility and dynamics for several other protein systems, and therefore offers an incisive method to examine the structural basis for this SNP of h12-LOX (Y649C).[41-44]

In the current study, using the same set of 45 non-overlapping peptides as previously identified,[19] we compared the HDX-MS properties of WT to the current mutant, Y649C, at two temperatures: 10 and 25 °C (**Table S1**). As described above, there was a notable shift in catalytic activity at 42 °C for WT compared to Y649C (**Figure 2A**). However, the functional stability for the WT variant at and above 37 °C (and higher) begins to drop after several minutes (**Supporting Information, Figure S4**), precluding reliable analysis[45] of longer incubation times at temperatures ≥ 37 °C. Thus, we limited our HDX measurements to 10 and 25 °C. The conditions of the described HDX-MS experiments, where exchange proceeds via the EX-2 mechanism,[31, 46] as indicated by the progressive shift in the isotopic mass spectral envelope, permit a temperature-dependent analysis of protein thermal fluctuations. This property is particularly informative for activity-altering protein mutations, as temperature-dependent HDX-MS can reveal mutation-induced changes on the temperature dependence of regional transient fluctuations of the protein linked to enzyme function.[47-49]

Note that non-conserved mutations, as in the case of Tyr-to-Cys, can influence the liquid chromatography (LC) retention times and/or intrinsic back-exchange values for the peptide(s) that contain the site of mutation, which could influence the true exchange properties of a given peptide. For example, the peptide containing the mutation, 645-650, exhibited no significant shift in LC retention time, with ~6.8 and ~6.6 min for the WT and mutant, respectively. However, there was a modest change in the back-exchange value seen for the peptide containing the Cys mutation, with a

~31% value compared to 20% for WT h12-LOX, despite nearly identical LC retention times. Peptide specific back-exchange values, collected for both WT and Y649C, were used to correct for the HDX at each peptide (**Supporting Information,** HDX Summary Table).

From the inspection of the time dependent HDX traces, there were 12 non-overlapping peptides that exhibited distinct hydrogen exchange behavior for Y649C relative to WT 12LOX. To be considered a significant difference between variants, at least three time points must deviate by >5% exchange at both temperatures. The most notable difference in exchange properties was centered at the site of mutation, peptide 645-650, particularly at longer incubation times of ≥ 10 min (**Figure 5A, B**). In fact, the extent of exchange for this peptide at nearly every time point for Y649C at 10 °C was elevated relative to the WT values at 25 °C. In addition, the peptide immediately adjacent to the mutation (i.e., 632-644) shows comparable exchange behavior to 645-650 (*cf*. **Figure 5A-C**). To further corroborate the impact of the mutation at the mutation site, we also present HDX analysis of two additional peptides that overlap the 645-650 peptide: 632-650 and 635-650 (**Supporting Information, Figure S4**). Note that the mutant effect on exchange properties is more prominent for the shorter of the two peptides, 635-650, in which the HDX time-dependent pattern of the Y649C protein at 10 °C nearly matches the exchange property of WT at 25 °C. Because HDX apparent rates and/or extent are often expected to increase with temperature, these data support that the Y649C mutant loosens up the local structure and dynamics of the peptides containing or surrounding the site of mutation.
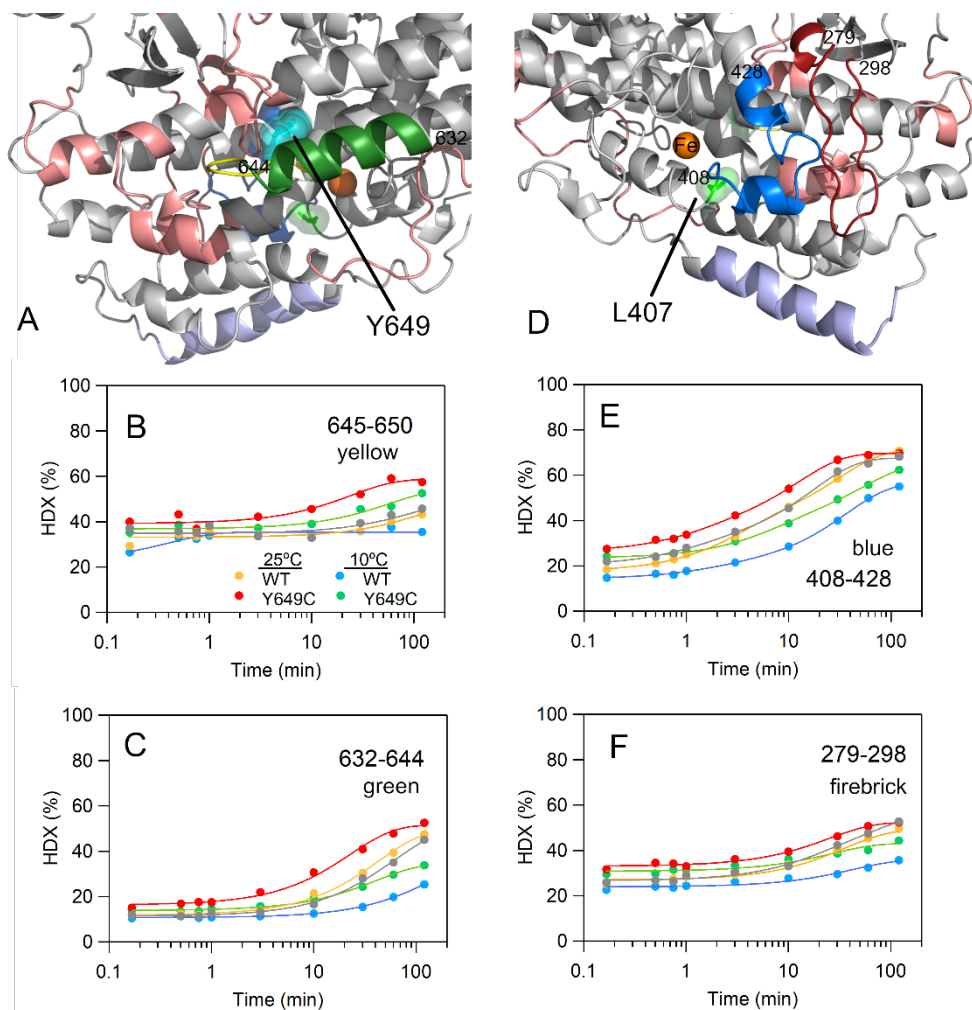
Figure 5. HDX-MS maps (A, D) and representative traces (B, C, E, and F) displaying differences in exchange properties between WT and the Y649C SNP variant of h12-LOX. Y649, the site of mutation, is shown as spheres in (A) for reference. The active site residue, L407, is represented by green spheres in (D). In A and D, the numbering of the colored peptides corresponds to the peptides displaying altered exchange properties and are shown in the other panels. The raw MS data for each of these peptides is presented in **Figure S5-S8**. The peptides colored in salmon also exhibited altered exchange patterns, as shown in **Figure S9**. Helix α2 is colored as light blue and represents the dimer-dimer

73

interface of 12-LOX.In (B-C, E-F), the gray trace represents WT 12-LOX collected at 25°C from our previous work[19] and represents a biological replicate.

Further, this behavior is seen to radiate from the site of mutation to several spatially adjacent peptides, ultimately influencing the exchange properties of select peptides on the front face of the enzyme (**Figure 5A** and **D**, salmon). One such peptide is 408-428 (**Figure 5E**, blue) which encompasses part of the arched helix 11. An overlapping peptide, 415-428, shows similar behavior (**Supporting Information, Figure S4**), corroborating the long-range mutational effect. Altered dynamics at this peptide have potential functional importance as helix 11 contains a fully conserved leucine, L407, in h12-LOX (**Figure 5D**, green spheres), that is responsible for positioning the reactive carbon of substrate AA close to the Fe(OH) cofactor for efficient catalysis. The role of L407 in catalysis is underscored by a previous kinetic study that reported k_{cat} values decreased by 100-fold for the mutation of this leucine to volume-reducing alanine or glycine.[19] A spatially adjacent peptide, 279-298 (**Figure 5F**), also tracks the mutant-induced exchange pattern at 408-428. The former peptide shares hydrophobic packing and some cross-stranded H-bonding with the active site peptide.

It is notable that peptide 186-194, which comprises part of helix α2, also exhibits some slight changes in exchange upon Tyr-to-Cys substitution at 649 (**Supporting Information, Figure S9**). However, these effects are modest compared to the dramatic increases in exchange properties previously observed from the

monomeric mutant (i.e., L183E/L187E).[19] Our HDX-MS analysis of Y649C further

supports the SEC results that the variant maintains the dimeric form and eliminates

the possibility of a change in oligomeric state as the origins for the altered kinetic

and/or membrane binding behaviors.

Figure 6. Map of network of h12-LOX derived peptides with altered exchange patterns emerging from the Y649C SNP (A). Panel (B) is rotated 90 degrees with respect to A along the y-axis. Panel (C) represents the cartoon model of space-filling mode from (B) and has the site of mutation, iron center, and L407 represented as spheres and labeled for reference. The peptide coloring is reproduced from **Figure 5**. Panel (D) displays the predicted packing environment surrounding Y649, which is represented as yellow spheres.

3.10 Protein Stability Determined by Differential Scanning Calorimetry

DSC thermograms of WT h12-LOX produced two distinct T_m values of 55 and 58-59 °C, respectively. We assign these thermal transitions to the melting of the dimeric and monomeric species, respectively. Note that these values are slightly elevated relative to the T_m values determined from CD melting traces (WT = 48 ± 0.5 °C and Y649C = 48 ± 1 °C). DSC has the advantage over CD melting traces as the technique is not limited by solution conditions that may stabilize protein structures. Importantly, the WT and Y649C 12-LOX variants produced nearly identical T_m values, consistent with the trends in the CD experiment. In addition to the T_m, DSC also reports on the thermodynamics of thermal unfolding of proteins and is thus complementary to the structural changes that are measured from temperature-dependent CD.[50] DSC has been used to provide quantitative estimates of the structural impact resulting from changes to the sidechain volume on protein (un)folding enthalpy (ΔH°) relative to the native enzyme.[51-53] The Y649C variant shows a significantly reduced ΔH° relative to WT (**Table 4**). The destabilization of protein inferred from the folding thermodynamics is consistent with the regionally defined enhanced peptide flexibility as detected by HDX, not only at the site of mutation, but extending throughout regions of the protein, including peptides lining the active site (**Figure 6**).

Table 5. DSC thermodynamics for WT and Y649C h12-LOX unfolding.			
	$T_{m,dimer}$ (°C)	$T_{m,monomer}$ (°C)	ΔH° (kJ/mol)
WT	55	58-59	1200
Y649C	55	60-61	350

3.11 Structural and Dynamical Consequences of Y649C in 12-LOX

For the current study of this 12-LOX SNP, the mutation of Tyr to Cys is a non-conservative, hydrophobic substitution. The mutation does not lead to increased protein aggregation as the SEC data support a predominant elution peak corresponding to a dimeric form (**Supporting Information, Figure S3**). Further, protein migration in SDS-PAGE under non-reducing conditions is identical to migration of WT and Y649C under reducing conditions (**Supporting Information, Figure S10**). The environment surrounding of Y649 (**Figure 6D**) is predicted to be primarily hydrophobic. The mutation likely disrupts the packing of these hydrophobic residues through loss of sidechain bulk and/or through infiltration of water molecules, as previously seen for a Tyr-to-Ser mutation in ketosteroid isomerase.[54] In either case, the Y649C mutation in 12-LOX loosens up the peptide to which Y649 resides, thereby eliciting enhanced flexibility of adjacent (and remote) peptides.

Relevant to the current work, a previous mutational study examined the structural and functional consequences of the substitution of a conserved tyrosine, located in the P+1 loop of a Ser/Thr kinase, for a more hydrophobic residue, alanine (i.e., Y204A).[55] This tyrosine is expected to stabilize the substrate through H-bonding interactions. Loss of this hydrogen bonding capability of the Y204 sidechain, upon Ala mutation, was accompanied by an impaired catalytic rate and altered (enhanced) global dynamic properties of the protein as assessed by NMR and HDX-MS.[55, 56] Conversely, there were no notable changes in protein structure through the comparison of X-ray structures.[57] This is a classic example of a dynamic allostery

mechanism,[58] one in which allostery is mediated without large changes in conformation or oligomerization.[59, 60] Notable, the P loop is a hot spot for kinase SNPs linked to disease, in which mutations presumably alter the dynamic landscape of kinases.[61]

Herein, the patterns of enhanced exchange stemming from Y649C are reminiscent to this dynamic allosteric mechanism.[62-64] Similarly, dynamic allostery has also been inferred for another human LOX isoform for its interaction with a natural anti-inflammatory[65] and for the regulation of SLO-1 by allosteric modulator, oleyl sulfate.[66] The comparative HDX-MS traces for WT and Y649C as a function of time and temperature reveal networks on two faces of the protein surface, one surrounding the site of mutation and another set of peptides proximal to the active site. Note that the connectivity between these two sets of peptides is not immediately apparent (**Figure 6A-C**). Typically, HDX-MS reveals the end points of allosteric pathways in proteins since HDX reports on the changes in H-bonding in peptides, with the most dramatic effects arising from regions that are more solvent accessible (i.e., ends of the pathway).[67] Taken together, the HDX-MS study presented herein for the 12-LOX SNP resulting in a Tyr-to-Cys mutation at position 649 presents a long-range network of peptides with enhanced protein flexibility, extending from the site of mutation to peptides as far as 40-50 Å away and includes those lining the active site (**Figure 6**). Our results expand upon previously characterized dynamic 'allosteric-like' networks of catalysis-altering peptide flexibility originating from protein mutations that have been detected by mutant-dependent HDX-MS for several

other systems, such as TIM barrels,[48, 68] kinases,[56, 69] thrombin,[67, 70] and tRNA synthetases.[71]

Conclusions

An SNP of h12-LOX, Y649C, was discovered in a patient suffering from a bleeding disorder stemming from impaired platelet aggregation.[26] It was proposed that this clinical symptom was due to a lowering of the enzymatic rate of the Y649C in the platelet but the molecular basis of the lower function was unclear. To investigate this *in vivo* observation, Y649C was expressed/purified, and its biochemical properties were determined. Y649C manifested a similar preference for AA catalysis over that of DHA and displayed comparable product profiles for both AA and DHA. The inhibitor response to ML355 was also similar to WT, suggesting similar active site structure with respect to inhibitor constraints. Synthetic membrane affinity of Y649C was also comparable to WT displaying a preference (PC and PE over PS) and a modest calcium effect. Y649C did display a greater membrane affinity than WT at 22 °C, however, at 37 °C its affinity was slightly lower than WT. The steady-state kinetic parameters of Y649C were lower than that of WT at 37 °C, with k_{cat} being over 6-fold lower. Interestingly, Y649C displayed greater catalytic stability to temperature, however, its protein stability as measured by DSC was significantly lower than that of WT. Finally, H/D exchange measured greater peptide mobility near the site of mutation that propagated to the active site for the Y649C compared to WT, providing a structural basis for the dynamic, allosteric-like effects stemming from this SNP. In summary, many of the biochemical traits of Y649C were similar to WT at 37

°C, except for lowered kinetic parameters, lowered synthetic membrane affinity, and enhanced regional peptide flexibility associated with decreased structural stability. Considering that h12-LOX most likely obtains its fatty acid substrate from the phospholipid bilayer and the biological temperature is 37 °C, it is possible that the lower activity of Y649C observed in patient platelets could be due to a combination of its lower activity, lower membrane affinity and its lower protein folding stability.

TOC Graphic
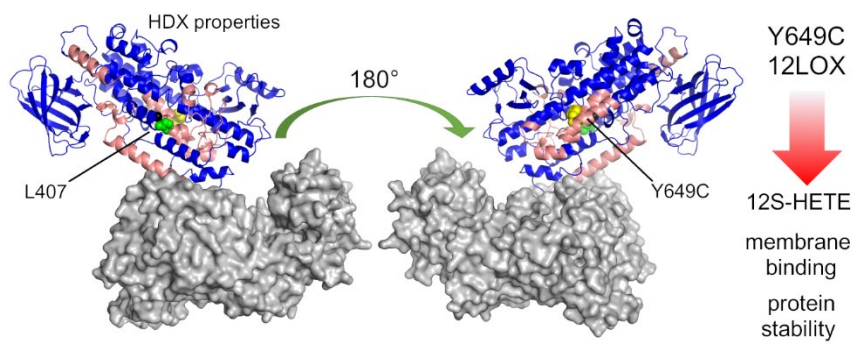
Supporting Information

Biochemical and hydrogen deuterium exchange studies of the single nucleotide polymorphism Y649C in human platelet 12-lipoxygenase linked to an impaired bleeding disorder

Michelle Tran,[1] Adriana Yamaguchi,[2] Eefie Chen,[1] Michael Hollinstat,[2] Rachel L. Signorelli,[3] Anthony T. Iavarone[4], Adam R. Offenbacher,[3]* Theodore Holman[1]*

[1]Department of Chemistry and Biochemistry, University of California Santa Cruz, Santa Cruz, CA 95064, United States

[2] Department of Pharmacology, University of Michigan Medical School, Ann Arbor, MI, 48109

[3]Department of Chemistry, East Carolina University, Greenville, NC 27858, United States

[4]QB3/Chemistry Mass Spectrometry Facility, University of California Berkeley, Berkeley, CA 94720, United States

*Corresponding Authors:

TRH: Tel.: +1-831-459-5884, holman@ucsc.edu

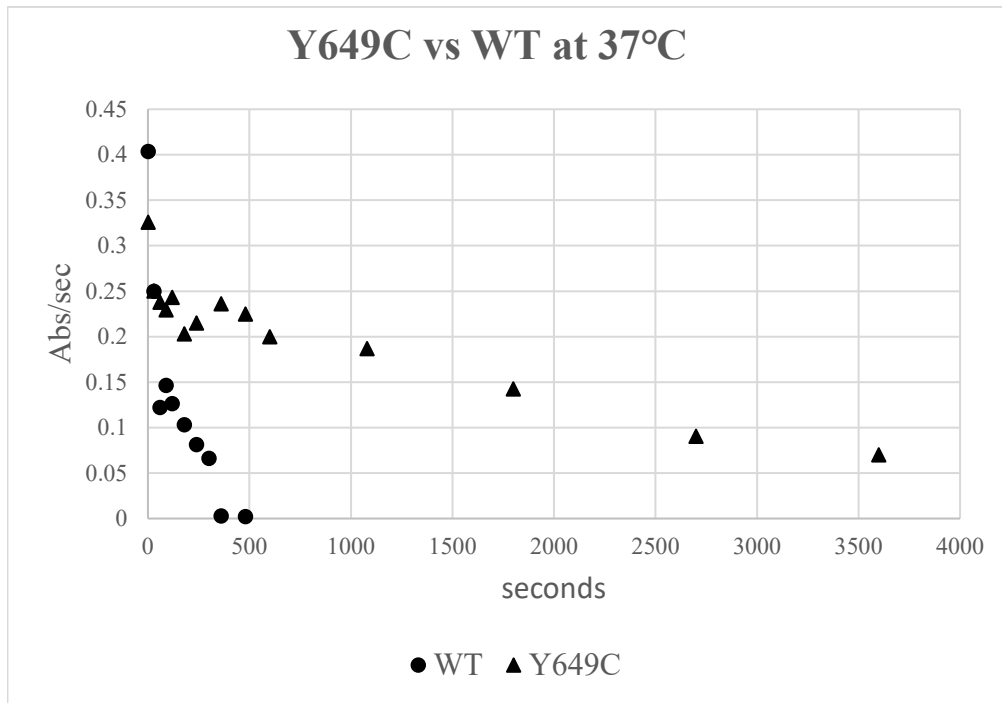ARO: Tel.: +1-252-737-5422, offenbachera17@ecu.edu

Figure S1: Temperature dependence of enzymatic activity for WT and Y649C.
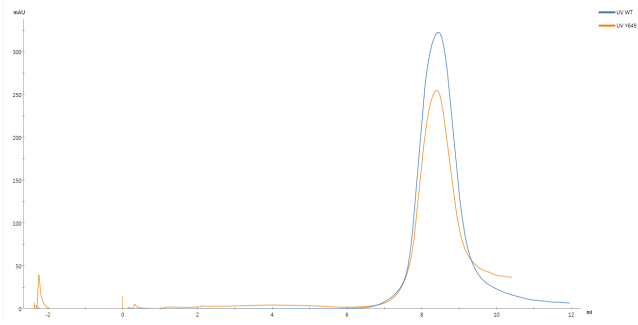
Figure S2: Size exclusion chromatogram of WT and Y649C demonstrating dimeric form for both enzymes.
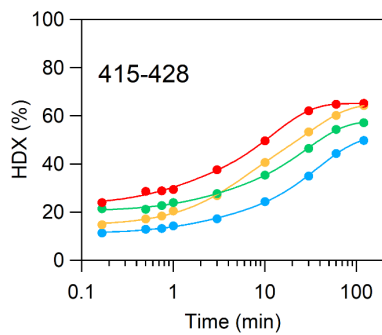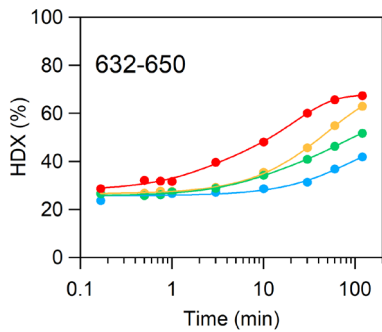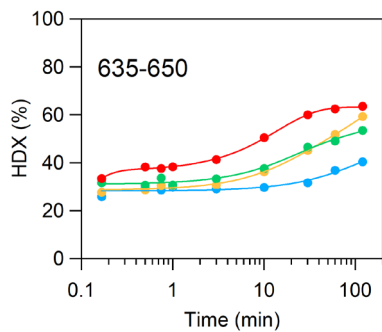
Figure S4. Temperature dependence of select overlapping peptides for wt and Y649C h12-LOX (red:, orange, green, blue).
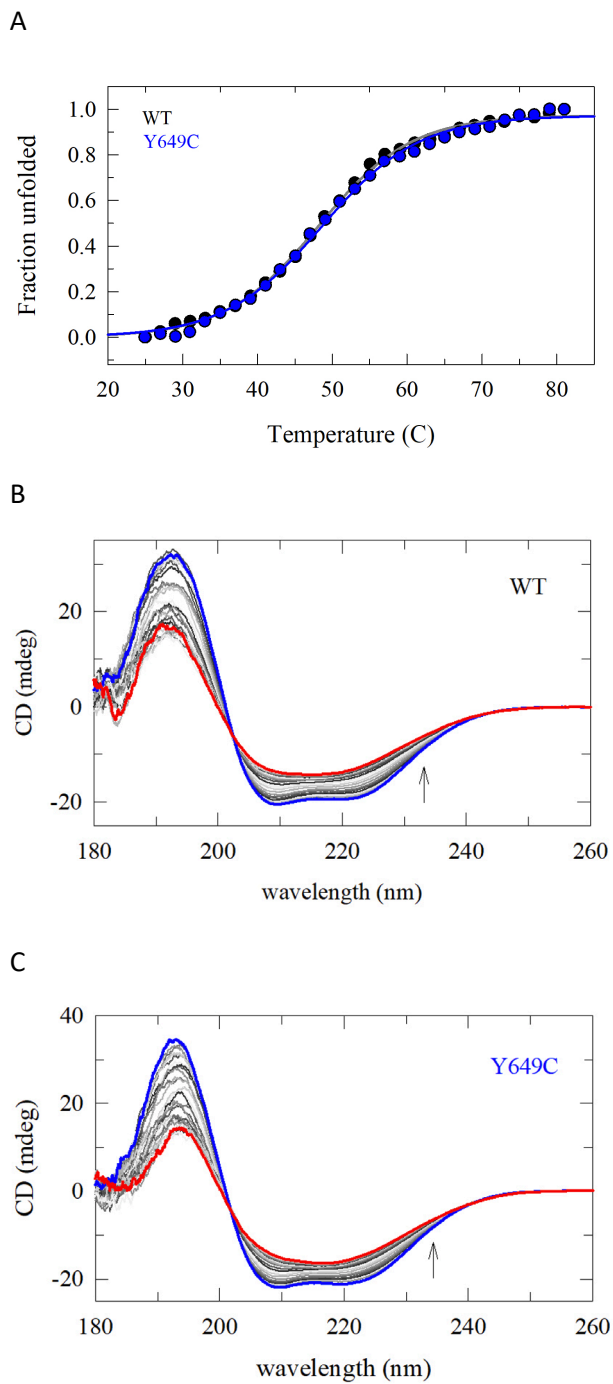
Figure S3. **A**. Thermal unfolding of h12-LOX WT (black) and Y649C (blue) as a function of temperature. These unfolding data were obtained by averaging the measured spectral data from 205 to 225 nm (Figure SZ). Fitting the data to sigmoidal functions gives T_m's of 48 ± 0.5 ° C and 48 ± 1 °C for the WT and Y649C proteins, respectively. **B**. CD spectra for h12-LOX WT. **C**. CD spectra for h12-LOX Y649C.

[1] Robless, P., Mikhailidis, D. P., and Stansby, G. (2001) Systematic review of antiplatelet therapy for the prevention of myocardial infarction, stroke or vascular death in patients with peripheral vascular disease, *The British journal of surgery 88*, 787-800.

[2] Thachil, J. (2016) Antiplatelet therapy - a summary for the general physicians, *Clin Med (Lond) 16*, 152-160.

[3] Beer, J. H., Pederiva, S., and Pontiggia, L. (2000) Genetics of platelet receptor single-nucleotide polymorphisms: clinical implications in thrombosis, *Ann Med 32 Suppl 1*, 10-14.

[4] Xiang, Q., Ji, S. D., Zhang, Z., Zhao, X., and Cui, Y. M. (2016) Identification of ITGA2B and ITGB3 Single-Nucleotide Polymorphisms and Their Influences on the Platelet Function, *Biomed Res Int 2016*, 5675084.

[5] Stierlin, F. B., Molica, F., Reny, J. L., Kwak, B. R., and Fontana, P. (2017) Pannexin1 Single Nucleotide Polymorphism and Platelet Reactivity in a Cohort of Cardiovascular Patients, *Cell Commun Adhes 23*, 11-15.

[6] Hurd, C. M., Cavanagh, G., Schuh, A., Ouwehand, W. H., and Metcalfe, P. (2002) Genotyping for platelet-specific antigens: techniques for the detection of single nucleotide polymorphisms, *Vox Sang 83*, 1-12.

[7] Aleem, A. M., Wells, L., Jankun, J., Walther, M., Kuhn, H., Reinartz, J., and Skrzypczak-Jankun, E. (2009) Human platelet 12-lipoxygenase: naturally occurring Q261/R261 variants and N544L mutant show altered activity but unaffected substrate binding and membrane association behavior, *Int J Mol Med 24*, 759-764.

[8] Zheng, Z., Li, Y., Jin, G., Huang, T., Zou, M., and Duan, S. (2020) The biological role of arachidonic acid 12-lipoxygenase (ALOX12) in various human diseases, *Biomed Pharmacother 129*, 110354.

[9] Walther, M., Wiesner, R., and Kuhn, H. (2004) Investigations into calcium-dependent membrane association of 15-lipoxygenase-1. Mechanistic roles of surface-exposed hydrophobic amino acids and calcium, *J Biol Chem 279*, 3717-3725.

[10] Brinckmann, R., Schnurr, K., Heydeck, D., Rosenbach, T., Kolde, G., and Kuhn, H. (1998) Membrane translocation of 15-lipoxygenase in hematopoietic cells is calcium-dependent and activates the oxygenase activity of the enzyme, *Blood 91*, 64-74.

[11] Baba, A., Sakuma, S., Okamoto, H., Inoue, T., and Iwata, H. (1989) Calcium induces membrane translocation of 12-lipoxygenase in rat platelets, *J Biol Chem 264*, 15790-15795.

[12] Deschamps, J. D., Ogunsola, A. F., Jameson, J. B., 2nd, Yasgar, A., Flitter, B. A., Freedman, C. J., Melvin, J. A., Nguyen, J. V., Maloney, D. J., Jadhav, A., Simeonov, A., Bomberger, J. M., and Holman, T. R. (2016) Biochemical and Cellular Characterization and Inhibitor Discovery of Pseudomonas aeruginosa 15-Lipoxygenase, *Biochemistry 55*, 3329-3340

[13] Nardi, M., Feinmark, S. J., Hu, L., Li, Z., and Karpatkin, S. (2004) Complement-independent Ab-induced peroxide lysis of platelets requires 12-lipoxygenase and a platelet NADPH oxidase pathway, *J Clin Invest 113*, 973-980.

[14] Guo, Y., Zhang, W., Giroux, C., Cai, Y., Ekambaram, P., Dilly, A. K., Hsu, A., Zhou, S., Maddipati, K. R., Liu, J., Joshi, S., Tucker, S. C., Lee, M. J., and Honn, K. V. (2011) Identification of the orphan G protein-coupled receptor GPR31 as a receptor for 12-(S)-hydroxyeicosatetraenoic acid, *J Biol Chem 286*, 33832-33840.

[15] Tourdot, B. E., and Holinstat, M. (2017) Targeting 12-Lipoxygenase as a Potential Novel Antiplatelet Therapy, *Trends Pharmacol Sci 38*, 1006-1015.

[16] Thomas, C. P., Morgan, L. T., Maskrey, B. H., Murphy, R. C., Kühn, H., Hazen, S. L., Goodall, A. H., Hamali, H. A., Collins, P. W., and O'Donnell, V. B. (2010) Phospholipid-esterified eicosanoids are generated in agonist-activated

human platelets and enhance tissue factor-dependent thrombin generation, *J Biol Chem 285*, 6891-6903.

[17] O'Donnell, V. B., Murphy, R. C., and Watson, S. P. (2014) Platelet lipidomics: modern day perspective on lipid discovery and characterization in platelets, *Circ Res 114*, 1185-1203.

[18] Yeung, J., Tourdot, B. E., Fernandez-Perez, P., Vesci, J., Ren, J., Smyrniotis, C. J., Luci, D. K., Jadhav, A., Simeonov, A., Maloney, D. J., Holman, T. R., McKenzie, S. E., and Holinstat, M. (2014) Platelet 12-LOX is essential for FcγRIIa-mediated platelet activation, *Blood 124*, 2271-2279.

[19] Tsai, W. C., Aleem, A. M., Whittington, C., Cortopassi, W. A., Kalyanaraman, C., Baroz, A., Iavarone, A. T., Skrzypczak-Jankun, E., Jacobson, M. P., Offenbacher, A. R., and Holman, T. (2021) Mutagenesis, Hydrogen-Deuterium Exchange, and Molecular Docking Investigations Establish the Dimeric Interface of Human Platelet-Type 12-Lipoxygenase, *Biochemistry 60*, 802-812.

[20] Witola, W. H., Liu, S. R., Montpetit, A., Welti, R., Hypolite, M., Roth, M., Zhou, Y., Mui, E., Cesbron-Delauw, M. F., Fournie, G. J., Cavailles, P., Bisanz, C., Boyer, K., Withers, S., Noble, A. G., Swisher, C. N., Heydemann,

P. T., Rabiah, P., Muench, S. P., and McLeod, R. (2014) ALOX12 in human

    toxoplasmosis, *Infect Immun 82*, 2670-2679.

[21] Prasad, V. V., Kolli, P., and Moganti, D. (2011) Association of a functional

    polymorphism (Gln261Arg) in 12-lipoxygenase with breast cancer, *Exp Ther*

    Med 2, 317-323.

[22] Kim, T., Kim, H. J., Park, J. K., Kim, J. W., and Chung, J. H. (2010) Association

    between polymorphisms of arachidonate 12-lipoxygenase (ALOX12) and

    schizophrenia in a Korean population, *Behav Brain Funct 6*, 44.

[23] Harslof, T., Husted, L. B., Nyegaard, M., Carstens, M., Stenkjaer, L., Brixen, K.,

    Eiken, P., Jensen, J. E., Borglum, A. D., Mosekilde, L., Rejnmark, L., and

    Langdahl, B. L. (2011) Polymorphisms in the ALOX12 gene and

    osteoporosis, *Osteoporos Int 22*, 2249-2259.

[24] Liu, P., Lu, Y., Recker, R. R., Deng, H. W., and Dvornyk, V. (2010) ALOX12

    gene is associated with the onset of natural menopause in white women,

    Menopause 17, 152-156.

[25] Horn, T., Reddy Kakularam, K., Anton, M., Richter, C., Reddanna, P., and

    Kuhn, H. (2013) Functional characterization of genetic enzyme variations in

    human lipoxygenases, *Redox Biol 1*, 566-577.

[26] Mitsui, T., Makino, S., Tamiya, G., Sato, H., Kawakami, Y., Takahashi, Y., Meguro, T., Izumino, H., Sudo, Y., Norota, I., Ishii, K., and Hayasaka, K. (2021) ALOX12 mutation in a family with dominantly inherited bleeding diathesis, *Journal of human genetics 66*, 753-759.

[27] Amagata, T. W., S.; Johnson, T.A.; Stessman, C.C.; Loo, C.P.; Lobkovsky, E.; Clardy, J.; Crews, P.; Holman, T.R. (2003) Exploring Sponge-Derived Terpenoids for Their Potency and Selectivity Against 12-Human, 15-Human, and 15-Soybean Lipoxygenases, *J. Nat. Prod 66*, 230-235.

[28] Voss, O. H., Lee, H. N., Tian, L., Krzewski, K., and Coligan, J. E. (2018) Liposome Preparation for the Analysis of Lipid-Receptor Interaction and Efferocytosis, *Current protocols in immunology 120*, 14 44 11-14 44 21.

[29] Tsai, W. C., Gilbert, N. C., Ohler, A., Armstrong, M., Perry, S., Kalyanaraman, C., Yasgar, A., Rai, G., Simeonov, A., Jadhav, A., Standley, M., Lee, H. W., Crews, P., Iavarone, A. T., Jacobson, M. P., Neau, D. B., Offenbacher, A. R., Newcomer, M., and Holman, T. R. (2021) Kinetic and structural investigations of novel inhibitors of human epithelial 15-lipoxygenase-2, *Bioorg Med Chem 46*, 116349.

[30] Pascal, B. D., Willis, S., Lauer, J. L., Landgraf, R. R., West, G. M., Marciano, D., Novick, S., Goswami, D., Chalmers, M. J., and Griffin, P. R. (2012) HDX

Workbench: software for the analysis of H/D exchange MS data, *J. Am. Soc. Mass Spectrom. 23*, 1512-1521.

[31] Hoofnagle, A. N., Resing, K. A., and Ahn, N. G. (2003) Protein analysis by hydrogen exchange mass spectrometry, *Annu Rev Biophys Biomol Struct 32*, 1-25.

[32] Ikei, K. N., Yeung, J., Apopa, P. L., Ceja, J., Vesci, J., Holman, T. R., and Holinstat, M. (2012) Investigations of human platelet-type 12-lipoxygenase: role of lipoxygenase products in platelet activation, *J Lipid Res 53*, 2546-2559.

[33] Tsai, W. C., Kalyanaraman, C., Yamaguchi, A., Holinstat, M., Jacobson, M. P., and Holman, T. R. (2021) In Vitro Biosynthetic Pathway Investigations of Neuroprotectin D1 (NPD1) and Protectin DX (PDX) by Human 12-Lipoxygenase, 15-Lipoxygenase-1, and 15-Lipoxygenase-2, *Biochemistry 60*, 1741-1754.

[34] Perry, S. C., Kalyanaraman, C., Tourdot, B. E., Conrad, W. S., Akinkugbe, O., Freedman, J. C., Holinstat, M., Jacobson, M. P., and Holman, T. R. (2020) 15-Lipoxygenase-1 biosynthesis of 7S,14S-diHDHA implicates 15-lipoxygenase-2 in biosynthesis of resolvin D5, *J Lipid Res 61*, 1087-1103.

[35] Freedman, C., Tran, A., Tourdot, B. E., Kalyanaraman, C., Perry, S., Holinstat, M., Jacobson, M. P., and Holman, T. R. (2020) Biosynthesis of the Maresin Intermediate, 13S,14S-Epoxy-DHA, by Human 15-Lipoxygenase and 12-Lipoxygenase and Its Regulation through Negative Allosteric Modulators, *Biochemistry 59*, 1832-1844.

[36] Aleem, A. M., Tsai, W. C., Tena, J., Alvarez, G., Deschamps, J., Kalyanaraman, C., Jacobson, M. P., and Holman, T. (2019) Probing the Electrostatic and Steric Requirements for Substrate Binding in Human Platelet-Type 12-Lipoxygenase, *Biochemistry 58*, 848-857.

[37] Green, A. R., Freedman, C., Tena, J., Tourdot, B. E., Liu, B., Holinstat, M., and Holman, T. R. (2018) 5 S,15 S-Dihydroperoxyeicosatetraenoic Acid (5,15-diHpETE) as a Lipoxin Intermediate: Reactivity and Kinetics with Human Leukocyte 5-Lipoxygenase, Platelet 12-Lipoxygenase, and Reticulocyte 15-Lipoxygenase-1, *Biochemistry 57*, 6726-6734.

[38] Yeung, J., Hawley, M., and Holinstat, M. (2017) The expansive role of oxylipins on platelet biology, *J Mol Med 95*, 575-588.

[39] Luci, D. K., Jameson, J. B., Yasgar, A., Diaz, G., Joshi, N., Kantz, A., Markham, K., Perry, S., Kuhn, N., Yeung, J., Kerns, E. H., Schultz, L., Holinstat, M., Nadler, J. L., Taylor-Fishwick, D. A., Jadhav, A., Simeonov, A., Holman, T.

R., and Maloney, D. J. (2014) Synthesis and Structure-Activity Relationship
Studies of 4-((2-Hydroxy-3-methoxybenzyl)amino)benzenesulfonamide
Derivatives as Potent and Selective Inhibitors of 12-Lipoxygenase, *J Med
Chem 57*, 495-506.

[40] Adili, R., Tourdot, B. E., Mast, K., Yeung, J., Freedman, J. C., Green, A., Luci,
D. K., Jadhav, A., Simeonov, A., Maloney, D. J., Holman, T. R., and
Holinstat, M. (2017) First Selective 12-LOX Inhibitor, ML355, Impairs
Thrombus Formation and Vessel Occlusion In Vivo With Minimal Effects on
Hemostasis, *Arteriosclerosis, thrombosis, and vascular biology 37*, 1828-
1839.

[41] He, W., Zhang, H. M., Chong, Y. E., Guo, M., Marshall, A. G., and Yang, X. L.
(2011) Dispersed disease-causing neomorphic mutations on a single protein
promote the same localized conformational opening, *Proc Natl Acad Sci U S
A 108*, 12307-12312.

[42] Illes-Toth, E., Meisl, G., Rempel, D. L., Knowles, T. P. J., and Gross, M. L.
(2021) Pulsed Hydrogen-Deuterium Exchange Reveals Altered Structures and
Mechanisms in the Aggregation of Familial Alzheimer's Disease Mutants,
ACS Chem Neurosci 12, 1972-1982.

[43] Das, M., Wilson, C. J., Mei, X., Wales, T. E., Engen, J. R., and Gursky, O. (2016) Structural Stability and Local Dynamics in Disease-Causing Mutants of Human Apolipoprotein A-I: What Makes the Protein Amyloidogenic?, *J Mol Biol 428*, 449-462.

[44] Ambrus, A., Wang, J., Mizsei, R., Zambo, Z., Torocsik, B., Jordan, F., and Adam-Vizi, V. (2016) Structural alterations induced by ten disease-causing mutations of human dihydrolipoamide dehydrogenase analyzed by hydrogen/deuterium-exchange mass spectrometry: Implications for the structural basis of E3 deficiency, *Biochim Biophys Acta 1862*, 2098-2109.

[45] Tajoddin, N. N., and Konermann, L. (2020) Analysis of Temperature-Dependent H/D Exchange Mass Spectrometry Experiments, *Anal Chem 92*, 10058-10067.

[46] Englander, S. W. (2006) Hydrogen exchange and mass spectrometry: A historical perspective, *J Am Soc Mass Spectrom 17*, 1481-1489.

[47] Offenbacher, A. R., Hu, S., Poss, E. M., Carr, C. A. M., Scouras, A. D., Prigozhin, D. M., Iavarone, A. T., Palla, A., Alber, T., Fraser, J. S., and Klinman, J. P. (2017) Hydrogen-deuterium exchange of lipoxygenase uncovers a relationship between distal, solvent exposed protein motions and

the thermal activation barrier for catalytic proton-coupled electron tunneling, *ACS Cent. Sci. 3*, 570-579.

[48] Gao, S., Thompson, E. J., Barrow, S. L., Zhang, W., Iavarone, A. T., and Klinman, J. P. (2020) Hydrogen-Deuterium Exchange within Adenosine Deaminase, a TIM Barrel Hydrolase, Identifies Networks for Thermal Activation of Catalysis, *J Am Chem Soc 142*, 19936-19949.

[49] Zhang, J., Balsbaugh, J. L., Gao, S., Ahn, N. G., and Klinman, J. P. (2020) Hydrogen deuterium exchange defines catalytically linked regions of protein flexibility in the catechol O-methyltransferase reaction, *Proc Natl Acad Sci U S A 117*, 10797-10805.

[50] Seelig, J., and Schonfeld, H. J. (2016) Thermal protein unfolding by differential scanning calorimetry and circular dichroism spectroscopy
Two-state model versus sequential unfolding, *Q Rev Biophys 49*, e9.

[51] Eriksson, A. E., Baase, W. A., and Matthews, B. W. (1993) Similar hydrophobic replacements of Leu99 and Phe153 within the core of T4 lysozyme have different
structural and thermodynamic consequences, *J Mol Biol 229*, 747-769.

[52] Eriksson, A. E., Baase, W. A., Zhang, X. J., Heinz, D. W., Blaber, M., Baldwin, E. P., and Matthews, B. W. (1992) Response of a protein structure to cavity-

creating mutations and its relation to the hydrophobic effect, *Science 255*,
178-183.

[53] Takano, K., Ogasahara, K., Kaneda, H., Yamagata, Y., Fujii, S., Kanaya, E.,
Kikuchi, M., Oobatake, M., and Yutani, K. (1995) Contribution of
hydrophobic residues to the stability of human lysozyme: calorimetric studies
and X-ray structural analysis of the five isoleucine to valine mutants, *J Mol
Biol 254*, 62-76.

[54] Kraut, D. A., Sigala, P. A., Fenn, T. D., and Herschlag, D. (2010) Dissecting the
paradoxical effects of hydrogen bond mutations in the ketosteroid isomerase
oxyanion hole, *Proc Natl Acad Sci U S A 107*, 1960-1965.

[55] Masterson, L. R., Mascioni, A., Traaseth, N. J., Taylor, S. S., and Veglia, G.
(2008) Allosteric cooperativity in protein kinase A, *Proc Natl Acad Sci U S A
105*, 506-511.

[56] Yang, J., Garrod, S. M., Deal, M. S., Anand, G. S., Woods, V. L., Jr., and
Taylor, S. (2005) Allosteric network of cAMP-dependent protein kinase
revealed by mutation of Tyr204 in the P+1 loop, *J Mol Biol 346*, 191-201.

[57] Yang, J., Ten Eyck, L. F., Xuong, N. H., and Taylor, S. S. (2004) Crystal structure of a cAMP-dependent protein kinase mutant at 1.26A: new insights into the catalytic mechanism, *J Mol Biol 336*, 473-487.

[58] Kornev, A. P., and Taylor, S. S. (2015) Dynamics-Driven Allostery in Protein Kinases, *Trends Biochem Sci 40*, 628-647.

[59] Cooper, A., and Dryden, D. T. (1984) Allostery without conformational change. A plausible model, *Eur Biophys J 11*, 103-109.

[60] Frederick, K. K., Marlow, M. S., Valentine, K. G., and Wand, A. J. (2007) Conformational entropy in molecular recognition by proteins, *Nature 448*, 325-329.

[61] Torkamani, A., Kannan, N., Taylor, S. S., and Schork, N. J. (2008) Congenital disease SNPs target lineage specific structural elements in protein kinases, *Proc Natl Acad Sci U S A 105*, 9011-9016.

[62] Offenbacher, A. R., and Holman, T. R. (2020) Fatty Acid Allosteric Regulation of C-H Activation in Plant and Animal Lipoxygenases, *Molecules 25*.

[63] Offenbacher, A. R., Iavarone, A. T., and Klinman, J. P. (2018) Hydrogen-deuterium exchange reveals long-range dynamical allostery in soybean lipoxygenase, *J Biol Chem 293*, 1138-1148.

[64] Roberts, D. E., Benton, A. M., Fabian-Bayola, C., Spuches, A. M., and Offenbacher, A. R. (2022) Thermodynamic and biophysical study of fatty acid effector binding to soybean lipoxygenase: implications for allostery driven by helix alpha2 dynamics, *Febs Lett 596*, 350-359.

[65] Gilbert, N. C., Gerstmeier, J., Schexnaydre, E. E., Borner, F., Garscha, U., Neau, D. B., Werz, O., and Newcomer, M. E. (2020) Structural and mechanistic insights into 5-lipoxygenase inhibition by natural products, *Nat. Chem. Biol. 16*, 783-790.

[66] Mogul, R., Johansen, E., and Holman, T. R. (2000) Oleyl sulfate reveals allosteric inhibition of Soybean Lipoxygenase-1 and Human 15-Lipoxygenase, *Biochemistry 39*, 4801-4807.

[67] Peacock, R. B., and Komives, E. A. (2021) Hydrogen/Deuterium Exchange and Nuclear Magnetic Resonance Spectroscopy Reveal Dynamic Allostery on Multiple Time Scales in the Serine Protease Thrombin, *Biochemistry 60*, 3441-3448.

[68] Thompson, E. J., Paul, A., Iavarone, A. T., and Klinman, J. P. (2021) Identification of Thermal Conduits That Link the Protein-Water Interface to the Active Site Loop and Catalytic Base in Enolase, *J Am Chem Soc 143*, 785-797.

[69] Shi, Z., Resing, K. A., and Ahn, N. G. (2006) Networks for the allosteric control of protein kinases, *Curr Opin Struct Biol 16*, 686-692.

[70] Koeppe, J. R., Beach, M. A., Baerga-Ortiz, A., Kerns, S. J., and Komives, E. A. (2008) Mutations in the fourth EGF-like domain affect thrombomodulin-induced changes in the active site of thrombin, *Biochemistry 47*, 10933-10939.

[71] Xu, X., Shi, Y., Zhang, H. M., Swindell, E. C., Marshall, A. G., Guo, M., Kishi, S., and Yang, X. L. (2012) Unique domain appended to vertebrate tRNA synthetase is essential for vascular development, *Nat Commun 3*, 681.

Chapter 3:

Inhibitory Investigations of Acyl-CoA Derivatives against Human Lipoxygenase Isozymes

[This chapter has been adapted from publication, Inhibitory Investigations of Acyl-CoA Derivatives against Human Lipoxygenase Isozymes. (Tran et al. 2023, International Journal of Molecular Sciences)

Michelle Tran,[1] Kevin Yang[1], Alisa Glukhova,[2] Michael Holinstat,[3] Theodore Holman[1]*

[1]Department of Chemistry and Biochemistry, University of California Santa Cruz, Santa Cruz, CA 95064, United States

[2] Department of Biochemistry and Pharmacology, University of Melbourne, Melbourne, Victoria, Australia

[3] Department of Pharmacology, University of Michigan Medical School, Ann Arbor, MI, 48109

*Corresponding Author:

TRH: Tel.: +1-831-459-5884, holman@ucsc.edu

Abbreviations:

LOX, lipoxygenase; h12-LOX, human platelet 12S-LOX; h15-LOX-1, human reticulocyte 15S-LOX-1; WT h5-LOX, human 5S-LOX; h15-LOX-2, human epithelial 15S-LOX-2; r15-LOX-1 or r12/15-LOX or rALOX15, rabbit 15S-LOX-1; c11-LOX, coral 11R-LOX; SLO-1, soybean lipoxygense-1; AA, arachidonic acid; DHA, docosahexaenoic acid; 12(S)-HpETE, 12(S)-hydroperoxyeicosatetraenoic acid; 12(S)-HETE, 12(S)-hydroxyeicosatetraenoic acid; COX, cyclooxygenase; ML355, h12-LOX specific inhibitor; NSAIDs, nonsteroidal anti-inflammatory drugs; coxib, COX-2 selective inhibitor; ICP-MS, inductively coupled plasma mass spectroscopy; SEC, size exclusion chromatography; BSA, bovine serum albumin; DCM, dichloromethane; DMF, Dimethylformamide; SDS-PAGE, sodium dodecyl sulfate-polyacrylamide gel electrophoresis; EDTA, Ethylenediaminetetraacetic acid; HEPES, N-2-hydroxyethylpiperazine-N'-2-ethanesulfonic acid; PMSF, phenylmethylsulfonyl fluoride; Palmitoyl-CoA(16:0), Palmitoyl-Coenzyme A (16:0); Palmitoleoyl-CoA(16:1), Palmitoleoyl- Coenzyme A (16:1); Stearoyl-CoA(18:0), Stearoyl-Coenzyme A (18:0); Oleoyl-CoA(18:1), Oleoyl-Coenzyme A (18:1); Linoleoyl-CoA(18:2), Linolenoyl-Coenzyme A (18:2); ɣ-Linolenoyl-CoA(18:3), ɣ-Linolenoyl-Coenzyme A (18:3); Arachidonoyl-CoA(20:4), Arachidonoyl-Coenzyme A (20:4); Docosahexaenoyl-CoA (22:6). Docosahexaenoyl-Coenzyme A(22:6); Methyl-13Z,16Z-docosadienoic, Methyl-13Z,16Z-docosadienoic (22:2); Methyl-13(Z),16(Z),19(Z)-Docosatrienoate, Methyl-13(Z),16(Z),19(Z)-Docosatrienoate (22:3); Methyl-9(Z),13(Z),16(Z),19(Z)-docosatetraenoate, Methyl-9(Z),13(Z),16(Z),19(Z)-docosatetraenoate (22:4)

Abstract:

Lipid metabolism is a complex process crucial for energy production, resulting in high levels of acyl-coenzyme A (acyl-CoA) molecules in the cell. Acyl-CoAs have also been implicated in inflammation which was possibly linked to lipoxygenase (LOX) biochemistry by the observation that an acyl-CoA was bound to human platelet 12-lipoxygenase via cryo-EM.[1] Given that LOX isozymes play a pivotal role in inflammation, a more thorough investigation into the inhibitory effects of acyl-CoAs on lipoxygenase isozymes was warranted. Subsequently, it was determined that C18 acyl-CoA derivatives were the most potent against h12-LOX, human reticulocyte 15-LOX-1 (h15-LOX-1) and human endothelial 15-LOX-2 (h15-LOX-2), while C16 acyl-CoAs were more potent against human 5-LOX. Specifically, oleoyl-CoA (18:1) was most potent against h12-LOX (IC_{50} = 32 mM) and h15-LOX-2 (IC_{50} = 0.62 mM), stearoyl-CoA against h15-LOX-1 (IC_{50} = 32 mM), and palmitoleoyl-CoA against h5-LOX (IC_{50} = 2 mM). The inhibition of h15-LOX-2 by oleoyl-CoA was further determined to be an allosteric inhibitor with a K_i of 82 +/- 70 nM, an a of 3.2 +/- 1, a b of 0.30 +/- 0.07, and a β/α = 0.09. Interestingly, linoleoyl-CoA (18:2) was a weak inhibitor against h5-LOX, h12-LOX and h15-LOX-1, but a rapid substrate for h15-LOX-1, with comparable kinetic rates to free linoleic acid (k_{cat} = 7.8 +/- 1 s^{-1}, k_{cat}/K_M = 2.5 +/- 0.2 $\mu M^{-1}s^{-1}$). Additionally, it was determined that methylated fatty acids were not substrates but rather weak inhibitors. These findings implicate a greater role of acyl-CoAs in the regulation of LOX activity in the cell, either through inhibition of novel oxylipin species or a novel source of oxylipin-CoAs.

Introduction:

Fat and lipid metabolism is a complex process that involves the synthesis, breakdown, and transport of lipids throughout the body.[2] Lipids not only play a vital role in providing energy for the body but also help in the formation of cell membranes,[3] hormone synthesis,[4, 5] and storage of fat-soluble vitamins.[6] Dysregulation of lipid metabolism has been associated with a range of diseases, including obesity,[7, 8] type 2 diabetes,[9, 10] and cardiovascular disease.[11, 12] One important aspect of lipid metabolism is the synthesis and breakdown of fatty acids, the building blocks of triglycerides, phospholipids, and cholesterol esters.[13, 14] Fatty acid metabolism involves a series of enzymatic reactions that convert fatty acids into acetyl-CoA, which can then enter the citric acid cycle for energy production.[15-17] In addition to their role in energy production, fatty acid-CoA esters have been shown to act as signaling molecules,[18, 19] regulating the activity of enzymes involved in lipid metabolism and other cellular processes.[20, 21] Some studies have suggested that acyl-CoA synthase can even modulate the activity of cyclooxygenase (COX) and lipoxygenase (LOX) isozymes, which are involved in the production of pro-inflammatory lipid mediators.[22] For example, it has been observed that COX can be inhibited by palmitoyl-CoA, which can have concentrations as high as 10µM in platelets.[23] Since COX reacts with fatty acids, such as arachidonic acid (AA), to produce specialized pro-resolving lipid mediators (SPMs),[24, 25] this mechanism of inhibition could have significant biological effects. Lipoxygenase is also involved in the production of SPMs and uses the same substrate profile to produce potent pro- and anti-inflammatory mediators involved in allergic reactions and other immune

responses;[26, 27] therefore, inhibition of LOX isozyme by acyl-CoAs could have significant biological effects.

Lipoxygenases are a class of non-heme iron-containing dioxygenases that catalyze the oxygenation of polyunsaturated fatty acids, resulting in the formation of lipid mediators such as leukotrienes and lipoxins.[28-30] The high-resolution cryo-EM structures of human 12S-Lipoxygenase (h12-LOX) was determined for the first time in a recent study, providing valuable insights into its oligomeric states, but equally interesting was the discovery that an acyl-CoA was bound to its active site.[1] The resolution of the h12-LOX structure was not high enough to identify the acyl-CoA; however, by screening a family of acyl-CoAs, oleoyl-CoA was the most likely candidate due to its potency (IC_{50} = 32 µM). The current work expands on this result, screening a larger family of acyl-CoAs against h5-LOX, h12-LOX, h15-LOX-1, and h15-LOX-2. This work provides new insights into the inhibitory mechanism of acyl-CoAs against LOX isozymes, potentially indicating an endogenous role for acyl-CoAs as LOX inhibitors, which could lead to the development of novel therapeutics targeting these enzymes.

Methods

2.1 Chemicals

Fatty acids used in this study were purchased from Nu Chek Prep, Inc. (MN, USA). All other solvents and chemicals were reagent grade or better and were used as purchased without further purification.

Scheme 1: Synthesis of DHA-CoA
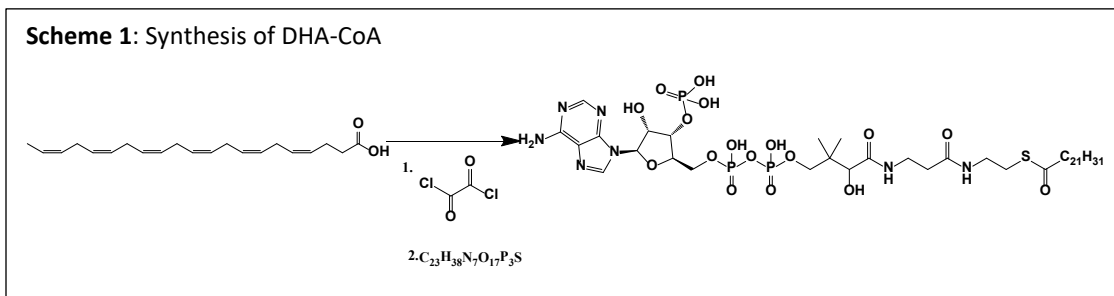
2.2 Synthesis of DHA-CoA

Reactions were done in an oxygen-deficient environment. DHA was added to an equimolar amount of butylated hydroxytoluene. Oxalyl chloride along with 1 drop of dry dimethylformamide (DMF) was then added, stirred for 1 hour at 37 °C and dried under vacuum. CoA was then added to a solution of tetrahydrofuran and 150 mM sodium bicarbonate in ratio of 2.2/1.0. This solution was combined with the DHA solution for 30 minutes at 37 °C. The solution was dried to remove the tetrahydrofuran. Dichloromethane, with 1.3% perchloric acid, was used to extract the desired product away from the unreacted DHA acid. The water layer was retained and mixed with an equal volume of acetonitrile and lyophilized. The solid was washed with dry acetone and ether (**Scheme 1**). The synthesis is based on published protocols.[31, 32]

2.3 Expression and Purification of h5-LOX, h12-LOX, h15-LOX-1, and h15-LOX-2.

Overexpression and purification of his-tagged wild-type h12-LOX (Uniprot entry P18054),[33] h15-LOX-1 (Uniprot entry P16050)[33] and h15-LOX-2 (Uniprot entry O15296)[34] was performed using nickel-affinity chromatography. The purity of h12-LOX, h15-LOX-1 and h15-LOX-2 were assessed by SDS gel to be greater than 85%, and metal content was assessed on a Finnigan inductively-coupled plasma-mass spectrometer (ICP-MS), via comparison with iron standard solution. Cobalt-EDTA was used as an internal standard. WT h5-LOX (UniProt entry P09917) was expressed in Rosetta 2 cells (Novagen) transformed with the pET14b-Stable-5-LOX plasmid (a gift from Marcia Newcomer of Louisiana State University) and grown in Terrific Broth containing 34 μg/ml chloramphenicol and 100 μg/ml ampicillin at 37°C for 3.5 h and then placed at 20°C for an additional 26 h. Cells were pelleted and resuspended in 50 mM Tris (pH 8.0), 500 mM NaCl, 20 mM imidazole with 1 μM pepstatin, 100 μM PMSF, and DNaseI (Sigma). The cells were lysed in a French pressure cell and centrifuged at 40,000 g for 20 minutes at 4°C. Saturated ammonium sulfate was added to have a final solution of 10% and inverted several times. The lysate was centrifuged at 40,000g for 10 minutes at 4°C. The pellet was discarded, and the supernatant was increased to a final concentration of 50% ammonium sulfate. The supernatant was rotated for 10 minutes at 4°C then centrifuged at 40,000g for 10 minutes at 4°C. The pellet was split into 150 mg aliquots. The WT h5-LOX used in the kinetics of this work was not purified due to a dramatic loss in activity and was therefore prepared as an ammonium-sulfate precipitate.

2.4 IC$_{50}$ Determination

IC_{50} values for each acyl-CoA was measured against h5-LOX, h12-LOX, h15-LOX-1, and h15-LOX-2. The reactions were carried out in 25 mM HEPES buffer (pH 8.00), 0.01% Triton X-100, 10 μM AA for h12-LOX, 25 mM HEPES buffer (pH 7.5), 0.01% Triton X-100, 10 μM AA for h15-LOX-1 and h15-LOX-2, and 50 mM HEPES buffer (pH 7.5), 100 μM EDTA, 50mM NaCl, 200μM ATP, 10 μM AA for h5-LOX. IC_{50} reactions were reacted with h15-LOX-1 (0.125 μM), h12-LOX (0.300 μM), h15-LOX-2 (0.5 μM), and h5-LOX (~600 nM ammonium sulfate salt) at 22°C in a 1 cm^2 quartz cuvette containing 2 mL of the according buffer and 10 μM AA for no longer than 2 minutes to avoid any cleavage of the acyl coenzyme As. Inhibitor concentrations ranging from 50 μM to 0.01 μM were used. All reactions were conducted using a Cary-UV Vis spectrophotometer, The fastest rates over 15-second intervals were recorded. IC_{50} values were obtained by determining the percent of inhibition of the enzymatic rate at ten inhibitor concentrations and plotting rate against their inhibitor concentration, followed by a hyperbolic saturation curve fit. The data used for the saturation curve fits were performed in duplicate or triplicate, depending on the quality of the data. It should be noted that stability measurements of the acyl-CoAs indicated that there was no appreciable hydrolysis in the short timeframe of the kinetic measurements; approximately one minute. Through HPLC monitoring, we were able to determine a lack of degradation of the fatty acyl-coAs over the first hour.

2.5 Enzymatic Products Determination

h15-LOX-2 (0.200 µM), h15-LOX-1 (0.125µM), h5-LOX (0.300 µM) and h12-LOX (0.300 µM) were reacted with 30µM of acyl-CoAs in 2 mL of 25mM HEPES (pH 7.5 for h15-LOX-1 and h15-LOX-2 , pH 8.0 for h12-LOX) at room temperature and ambient oxygen. The same buffer to determine IC_{50} values of h5-LOX was used for product determination. Turnover was monitored by absorbance at 234 nm.

2.6 Kinetic investigation of oleoyl-CoA (18:1) inhibition of h15-LOX-2

The reactions were carried out in 25 mM HEPES buffer (pH 7.5), 0.01% Triton X-100. Varying amount of substrates from AA ranging from 50 µM to 0.01 µM and the 0, 150, 300, 450, and 600 nM of 18:2 acyl-coA were used. Reactions were performed at 22°C in a 1 cm² quartz cuvette containing 2 mL of the according buffer and for no longer than 2 minutes to avoid any cleavage of the acyl coenzyme As. Using a Cary-UV Vis spectrophotometer, the fastest rates over 15-second intervals were recorded. Kinetic values were obtained by plotting rate against their substrate concentration, followed by a hyperbolic saturation curve fit. The data used for the saturation curve fits were performed in triplicate and on separate days to ensure there was no bias. The equations used to find kinetic values were from previous literature.[35]

3. Results and Discussion

3.1 IC_{50} determination of unsaturated fatty acyl CoAs

For h12-LOX, the IC_{50} values of palmitoyl-CoA(16:0), palmitoleoyl-CoA(16:1), stearoyl-CoA(18:0), linoleoyl-CoA(18:2), γ-linolenoyl-CoA(18:3) and docosahexaenoyl-CoA (22:6) indicated weak inhibition, with values greater than 200 μM (**Table 1**). Oleoyl-CoA (18:1) and arachidonoyl-CoA (20:4) had slightly greater inhibition potency, with IC_{50} values of 110 ± 20 μM and 32 ± 4 μM, respectively (**Table 1**). This data was published previously.[1]

For h15-LOX-1, the IC_{50} values of palmitoyl-CoA(16:0), palmitoleoyl-CoA(16:1), linoleoyl-CoA(18:2), γ-linolenoyl-CoA(18:3), arachidonoyl-CoA(20:4), and docosahexaenoyl CoA(22:6) indicated weak inhibition, with all values being greater than 50 μM (**Table 1**). However, oleoyl-CoA (18:1) and stearoyl-CoA (18:0) had relatively stronger inhibition with values of 39 ± 1.9 μM and 4.2 ± 0.6 μM, respectively. The data indicate C18 acyl-CoAs have the greatest potency, however, since γ-linolenoyl-CoA(18:3) is not inhibitory, the degree of saturation also affects potency.

For h15-LOX-2, the IC_{50} values of palmitoyl-CoA (16:0), palmitoleoyl-CoA(16:1), linoleoyl-CoA (18:2), γ-linolenoyl-CoA (18:3), arachidonoyl-CoA(20:4), and docosahexaenoyl CoA(22:6), indicated weak inhibition, with values greater than 100 mM (**Table 1**). Stearoyl-CoA (18:0) had relatively strong inhibition with a value of 7.6 ± 1 μM; however, oleoyl-CoA(18:1) had exceptionally strong inhibition with an IC_{50} of 620 ± 60 nM. Similar to that seen for h15-LOX-1, the C18 acyl-CoAs had the greatest potency; however, with the presence of three double bonds, as with γ-linolenoyl-CoA (18:3), all inhibitor potency was lost.

For h5-LOX, the IC_{50} values of γ-linolenoyl-CoA (18:3) and docosahexaenoyl CoA (22:6) indicated weak inhibition, with values greater than 200 μM. Stearoyl-CoA (18:0), oleoyl-CoA (18:1), and linoleoyl-CoA (18:2) had slightly stronger inhibition with IC_{50} values greater than 50 μM (**Table 1**). However, palmitoyl-CoA (16:0) and palmitoleoyl-CoA (16:1) had low micromolar inhibition with values of 3.3 ± 0.3 μM and 2.0 ± 0.4 μM. The fact that the C16 acyl-CoAs are potent against h5-LOX contrasts with the other LOX isozymes, possibly due to the active site requirement for the reverse binding of the substrate of h5-LOX relative to the other isozymes.

Table 1: IC$_{50}$ values with lipoxygenase isozymes.[#]

Acyl-Coenzyme A	h12-LOX* (µM)	h15-LOX-1 (µM)	h15-LOX-2 (µM)	h5-LOX (µM)
Palmitoyl-CoA(16:0)	> 200	> 500	> 200	*__3.3 ± 0.3__*
Palmitoleoyl-CoA(16:1)	> 500	> 500	> 200	*__2.0 ± 0.4__*
Stearoyl-CoA(18:0)	> 200	*__4.2 ± 0.6__*	*__7.6 ± 1__*	>50
Oleoyl-CoA(18:1)	*__32 ± 4__*	*__39 ± 2__*	*__0.62 ± 0.060__*	> 50
Linoleoyl-CoA(18:2)	> 200	(Substrate)	> 100	> 100
ɣ-Linolenoyl-CoA(18:3)	> 200	> 500	> 500	> 500
Arachidonoyl-CoA(20:4)	*__110 ± 20__*	> 500	> 500	> 200
Docosahexaenoyl CoA(22:6)	>500	>500	>500	> 200

[#]See Supporting Information for data analysis. * The h12-LOX data was published previously.[1]

In summary, the majority of the acyl-CoAs were not inhibitors against LOX isozymes, however, certain acyl-CoAs displayed micromolar potency. For h5-LOX, the C16 acyl-CoAs displayed the most promising inhibitory properties, with low micromolar potencies. However, with all the other isozymes, h15-LOX-1, h15-LOX-2, and h12-LOX, the C18 acyl-CoAs had the most potent inhibitory properties. Interestingly, adding double bonds to the acyl chain, such as from oleoyl-coA (18:1) to linoleoyl-CoA (18:2), eliminated significant inhibition potency and complete loss of inhibitory activity was observed with g-linolenoyl-CoA(18:3). This effect is most

likely due to the added restriction in structural freedom with the additional double

bonds, which would decrease flexibility and lower binding affinity, thus reducing the

availability of the proper orientation. With respect to biological relevancy, the most

potent acyl-CoA interaction was that between oleoyl-CoA and h15-LOX-2, which

displayed submicromolar potency. This level of potency drew us to do a more

detailed kinetic analysis (*vide infra*).

3.2 Acyl-CoA substrate activity

Considering that some of these acyl-CoAs could potentially be substrates for

LOX isozymes, each acyl-CoA was tested at 70 µM against each LOX isozyme to

establish the possibility of catalysis. These measurements revealed that none of the

acyl-CoAs were substrates against the LOX isozymes, except for linoleoyl-CoA

(18:2) and h15-LOX-1, as monitored by a change in 234 nm absorbance (**Table 2**).

The kinetic parameters were determined to be 7.5 ± 0.4 s^{-1} for k_{cat}, 12 ± 0.8 µM for

K_M, and 0.62 ± 0.1 µM^{-1} s^{-1} for k_{cat}/K_M, at 22 °C. These values are comparable to that

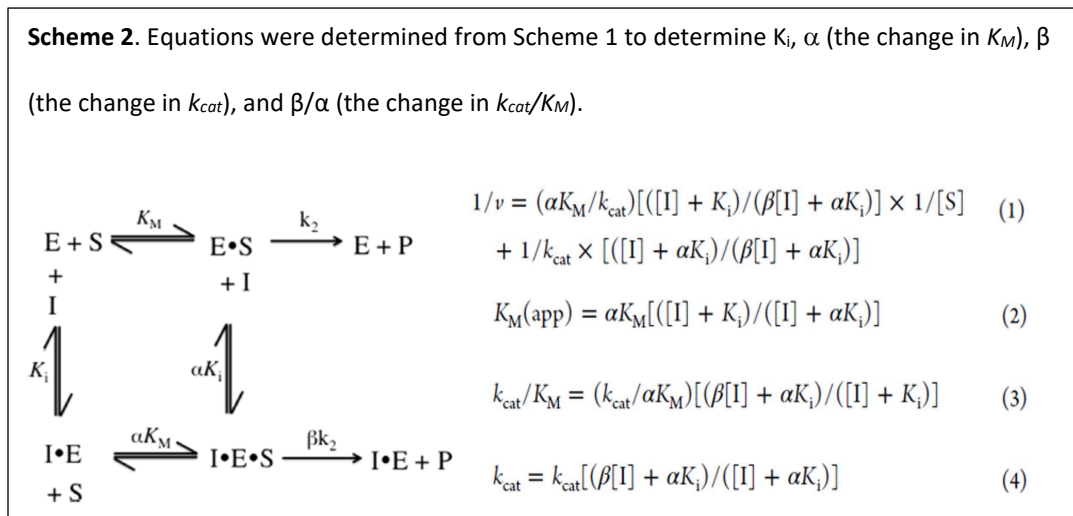of the free linoleic acid,[36] suggesting it as a biological substrate for h15-LOX-1.

Table 2: Kinetic parameters for h15-LOX-1 with linoleoyl-CoA.	
k_{cat}	7.5 (0.4) s^{-1}
K_M	12 (0.8) µM

3.3 IC$_{50}$ determination and substrate activity of methyl ester unsaturated fatty acids

The acyl-CoAs are large ester derivatives of fatty acids and given this fact, it was deemed appropriate to determine if simpler esters could also inhibit the LOX isozymes. In this respect, methyl-13Z,16Z-docosadienoic, methyl 13(Z),16(Z),19(Z)-docosatrienoate, and methyl docosatetraenoate were investigated and determined to be weak inhibitors, with IC$_{50}$ values greater than 200 μM for h12-LOX, h-15LOX-1, h15-LOX-2. It should be noted that none of the methyl ester unsaturated fatty acids were substrates, except for methyl ester arachidonic acid and h15-LOX-1, as previously observed. However, the rate of this activity was low enough to still allow for IC$_{50}$ measurements.
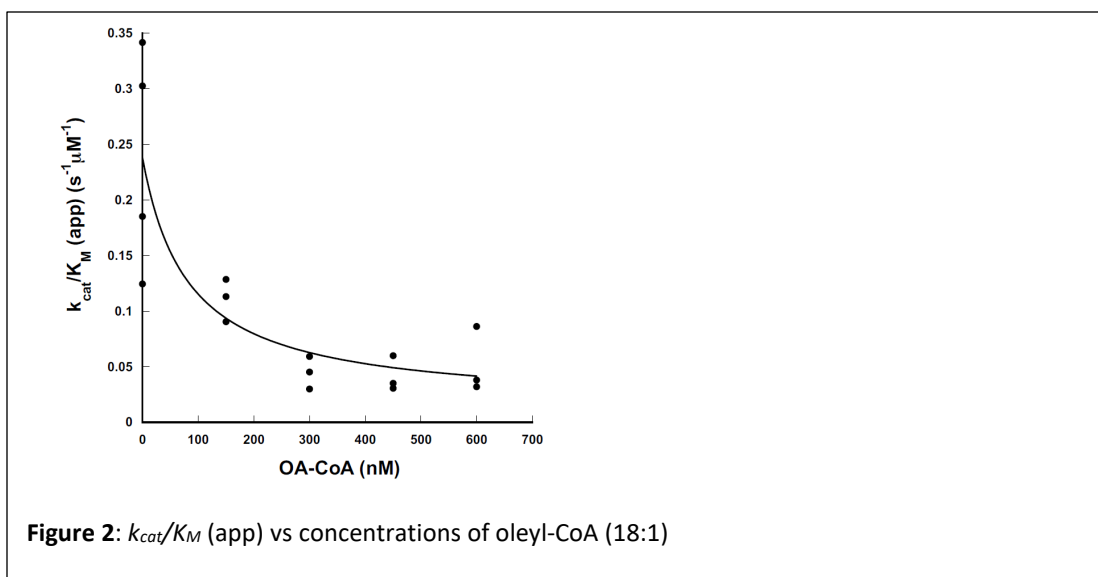
3.3 Kinetic investigation of oleoyl-CoA(18:1) inhibition of h15-LOX-2

Oleoyl-CoA displayed nanomolar IC$_{50}$ potency against h15-LOX-2 (620 ± 60 nM), which led to further kinetic investigations at varying inhibitor concentrations.

<div>

Scheme 2. Equations were determined from Scheme 1 to determine K$_i$, α (the change in K_M), β (the change in k_{cat}), and β/α (the change in k_{cat}/K_M).

$$1/v = (\alpha K_M/k_{cat})[([I] + K_i)/(\beta[I] + \alpha K_i)] \times 1/[S] \quad (1)$$
$$+ 1/k_{cat} \times [([I] + \alpha K_i)/(\beta[I] + \alpha K_i)]$$

$$K_M(\text{app}) = \alpha K_M[([I] + K_i)/([I] + \alpha K_i)] \quad (2)$$

$$k_{cat}/K_M = (k_{cat}/\alpha K_M)[(\beta[I] + \alpha K_i)/([I] + K_i)] \quad (3)$$

$$k_{cat} = k_{cat}[(\beta[I] + \alpha K_i)/([I] + \alpha K_i)] \quad (4)$$

Scheme:

E + S $\underset{}{\overset{K_M}{\rightleftharpoons}}$ E•S $\xrightarrow{k_2}$ E + P

$+$ I (downward K_i) and E•S $+$ I (downward αK_i)

I•E $\underset{+ S}{\overset{\alpha K_M}{\rightleftharpoons}}$ I•E•S $\xrightarrow{\beta k_2}$ I•E + P

</div>

The replot of the apparent K_M versus concentration oleoyl-CoA exhibited a

hyperbolic response with increasing amounts of the acyl-CoA, from 624 nM to 3.6

μM (**Figure 1**). This hyperbolic response is representative of allosteric inhibition (i.e.

partial inhibition), which was previously observed with 13-(S)-HOTrE(γ) and h15-

LOX-2, as described by **Scheme 2** (eqs. 1-4).[35]

Figure 1: K_M (app) vs concentrations of oleyl-CoA (18:1)

Figure 2: k_{cat}/K_M (app) vs concentrations of oleyl-CoA (18:1)
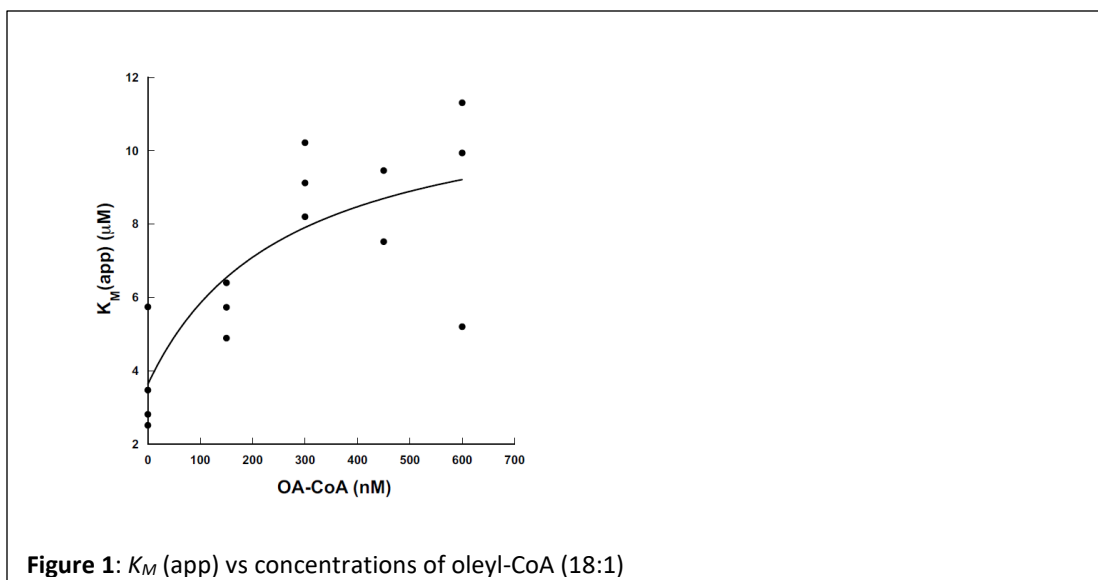
Utilizing the equations derived from **Scheme 2**, the K_M(app) values were fitted with equation 2 to yield a value of α to be 3.2 +/- 1 and a value of K_i to be 82 +/- 70 nM (**Figure 1**). These two parameters were then utilized to fit equation 3 relative to k_{cat}/K_M (app), which yielded a β value of 0.26 +/- 0.23 (**Figure 2**). Given the high

117

error for the β value, β was also determined by applying the values for α and K_i from

the K_M (app) plot to equation 4 and fitted to the k_{cat} data (**Figure 3**). This fit yielded a

β value of 0.30 +/- 0.07, consistent with the equation 3 fit but with a lower error

value. These kinetic values indicate hyperbolic allostery, a > 1 (K-type inhibition) and

b < 1 (V-type inhibition), with the kinetic change being equally observed in both K_M

(a = 3.2 +/- 1) and k_{cat} (b = 0.30 +/- 0.07). This combined effect is emphasized in the

β/α value, the

allosteric effect on k_{cat}/K_M, which is significantly less than 1 (β/α = 0.09) and

indicates k_{cat}/K_M allosteric inhibition. These allosteric kinetic data indicate the

formation of a catalytically active ternary complex (I·E·S) between h15-LOX-2 and

oleoyl-CoA and are consistent with our previous finding of an allosteric site for 13-

(S)-HODE with 15-LOX-2.[35] It should be noted that the K_i value from our hyperbolic

fits (82 +/- 70 nM) are dramatically lower than that determined from IC_{50}

measurements (620 ± 60 nM), which is consistent with the more accurate nature of

the hyperbolic fits relative to the IC_{50} fits, due to the oversimplification of the IC_{50}

analysis.

Interestingly, in our recently published structure,[1] oleoyl-CoA was bound in the active site of 12-LOX with its head group occupying the entrance to the binding site and the fatty acid tail extending deep into the U-shaped catalytic cavity. Similar
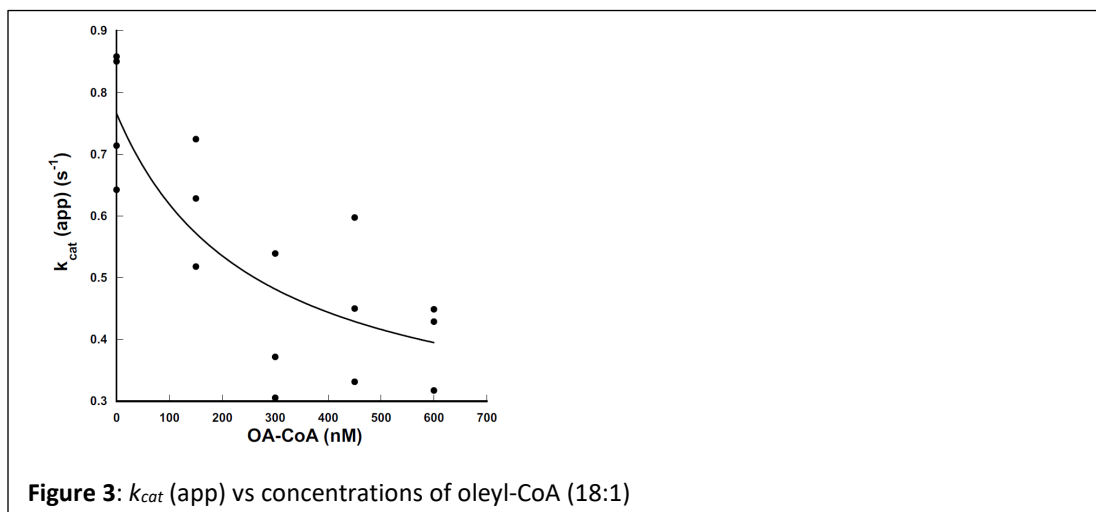

Figure 3: k_{cat} (app) vs concentrations of oleyl-CoA (18:1)

to the previously predicted pose of AA bound to h12-LOX,[37] H596 forms hydrogen bonds with the carbonyl group of the thioester bond. Also consistent with the predicted pose of AA bound to h12-LOX, L407, F414, A417, and V418 form Van der Waals interactions with the oleic acid tail. The h12-LOX binding site is quite narrow, consisting of two mostly linear segments connected by a single kink near the C9 position of the oleic acid (equivalent to C11 of AA). The shape of the binding cavity likely restricts the binding of other acyl-CoAs tested in this study due to the strict requirements imposed on the position and saturation state of the fatty acid. With respect to the allosteric inhibition observed for h15-LOX-2, its binding site and that of h5-LOX and h15-LOX-1, appear to be wider and shorter, providing a possible explanation for their slightly better tolerance of different fatty acid saturation states.

Conclusion:

In conclusion, our previously reported cryo-EM structure of h12-LOX indicated that an acyl-CoA bound to its active site, most likely oleoyl-CoA.[1] Based on this discovery, we investigated the inhibitory potency of acyl-CoAs against lipoxygenase isozymes and were able to determine that acyl-CoAs can be micromolar inhibitors against LOX isozymes, with oleoyl-CoA(18:1) being the most potent, having nanomolar allosteric potency against h15-LOX-2. Considering that acyl-CoAs exist in the cell at micromolar concentrations,[38] it is reasonable to assume that acyl-CoAs could have a significant effect on the cellular activity of LOX isozymes, especially h15-LOX-2. We are currently investigating whether the cellular concentration of acyl-CoAs affect LOX activity ex vivo and if this inhibition affects LOX signaling.

Supplementary Information

Biochemical and hydrogen-deuterium exchange studies of the single nucleotide polymorphism Y649C in human platelet 12-lipoxygenase linked to a bleeding disorder

[This chapter has been adapted from publication, Inhibitory Investigations of Acyl-CoA Derivatives against Human Lipoxygenase Isozymes. (Tran et al. 2023, International Journal of Molecular Sciences)

Michelle Tran,[1] Kevin Yang[1], Alisa Glukhova,[2] Michael Holinstat,[3] Theodore Holman[1]*

[1]Department of Chemistry and Biochemistry, University of California Santa Cruz, Santa Cruz, CA 95064, United States

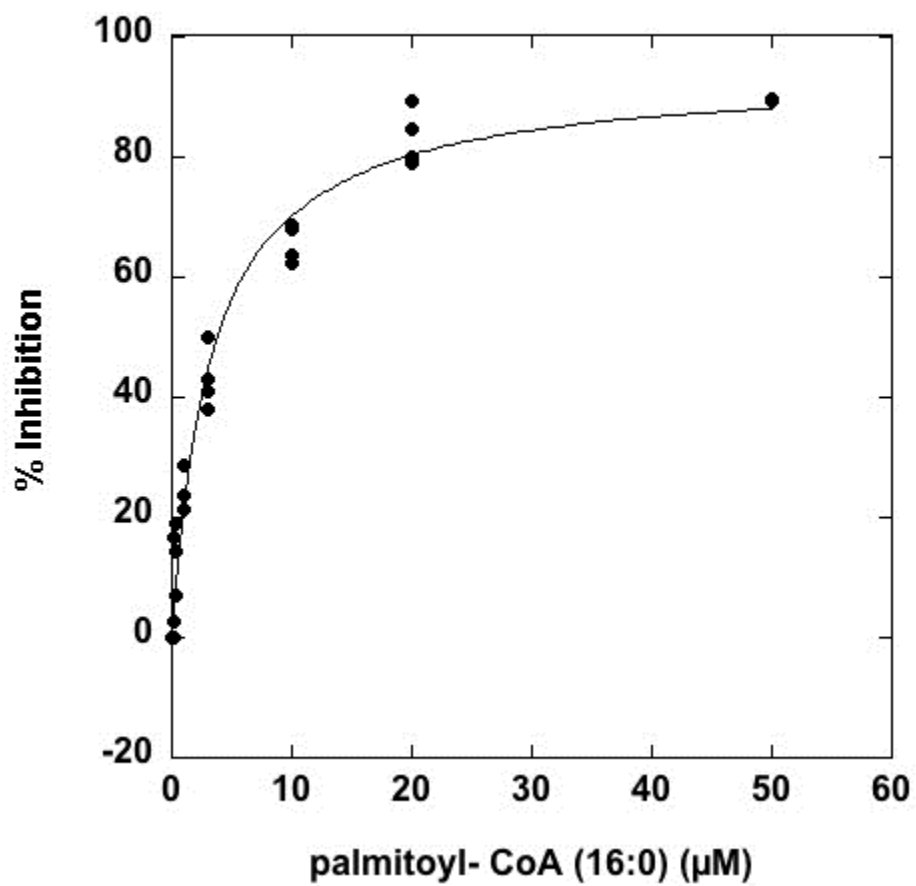[2] Department of Biochemistry and Pharmacology, University of Melbourne, Melbourne, Victoria, Australia

[3] Department of Pharmacology, University of Michigan Medical School, Ann Arbor, MI, 48109

*Corresponding Author:

TRH: Tel.: +1-831-459-5884, holman@ucsc.edu

Supplemental Figure 1S. IC$_{50}$ of Palmitoyl-CoA (16:0) with h5-LOX
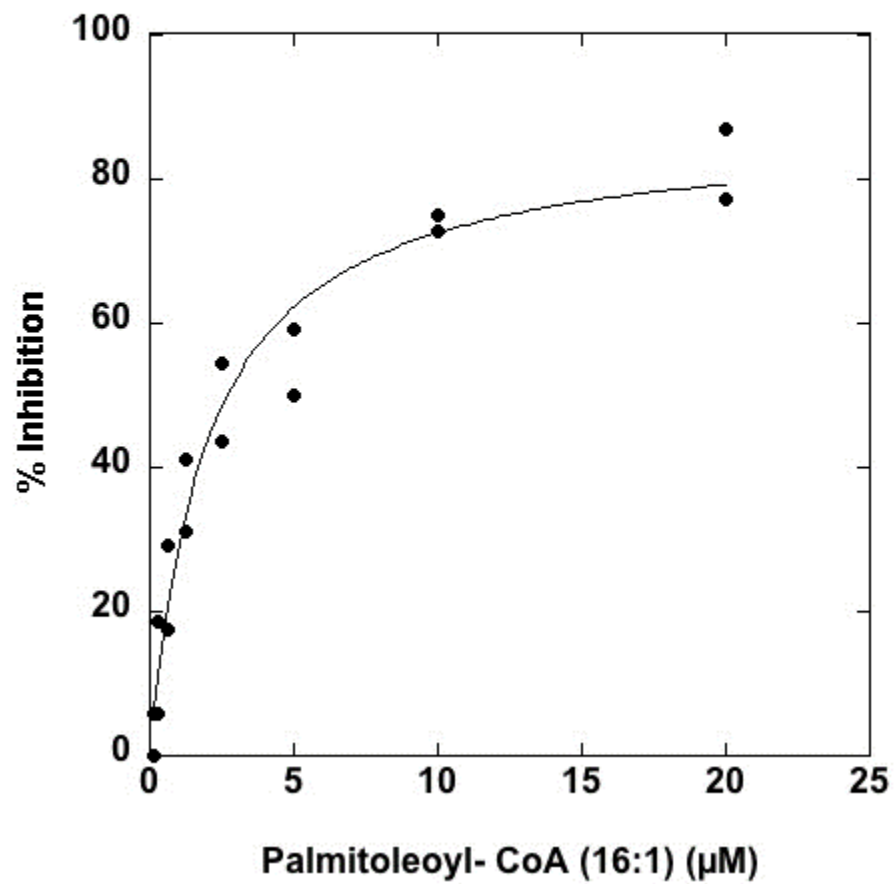
Supplemental Figure 2S. IC$_{50}$ of Palmitoleoyl-CoA (16:1) with h5-LOX
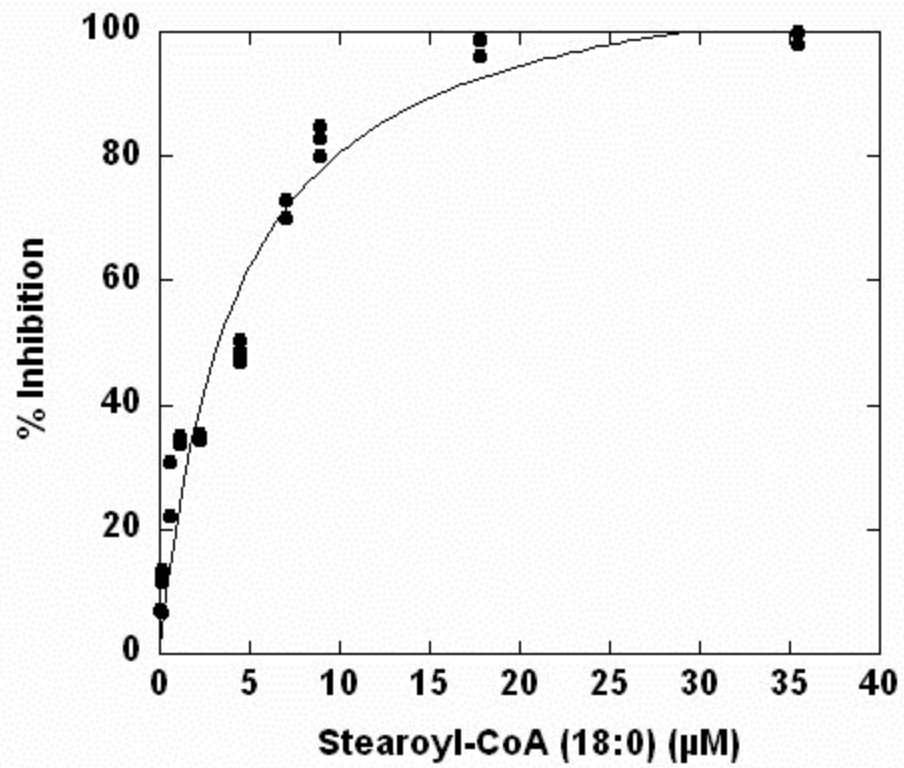
Supplemental Figure 3S. IC$_{50}$ of the h15-LOX-1 with Stearoyl-CoA (18:0)
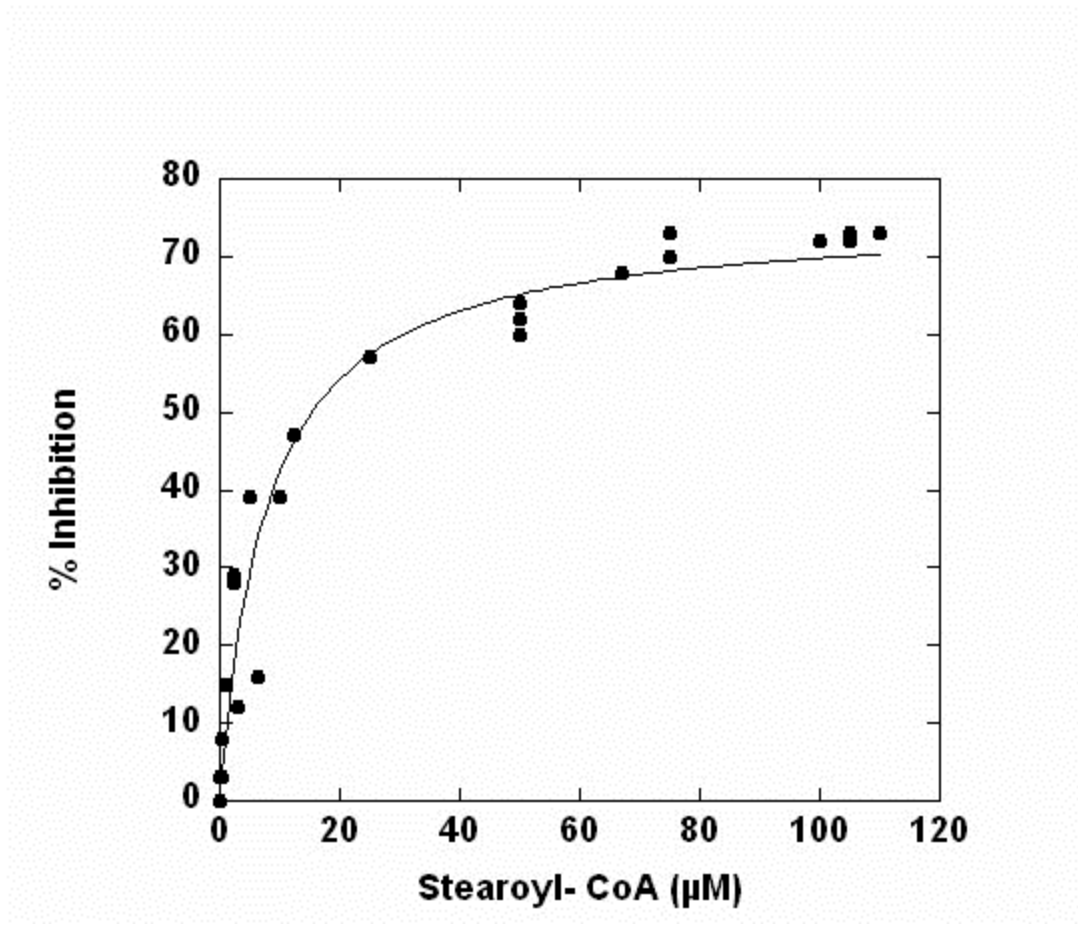
Supplemental Figure 4S. IC$_{50}$ of h15-LOX-2 with Stearoyl-CoA(18:0)
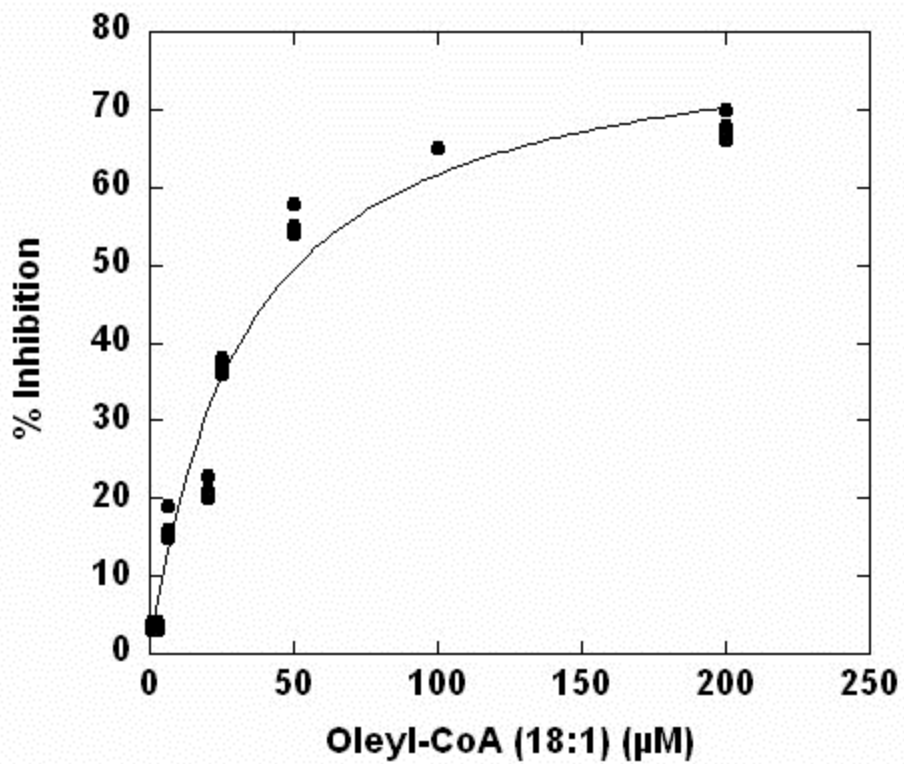
Supplemental Figure 5S. IC$_{50}$ of the Oleoyl-CoA (18:1) with h12-LOX
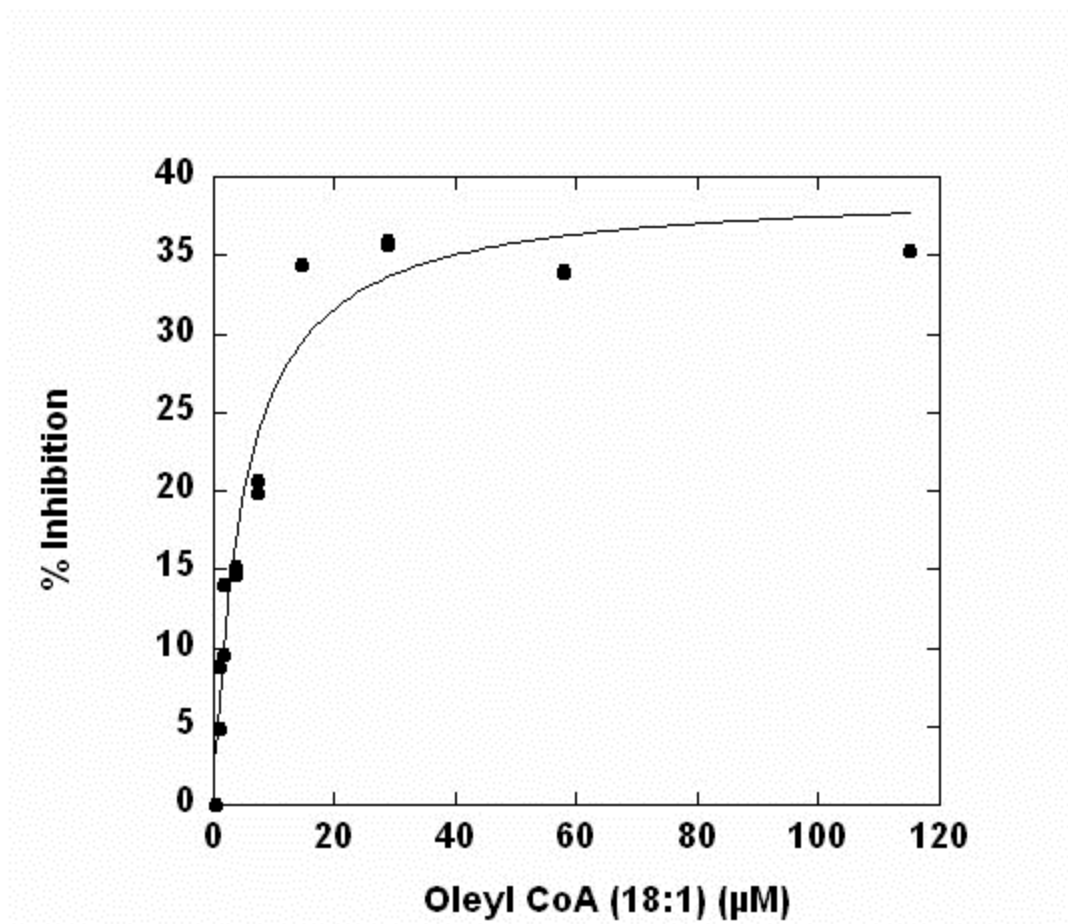
Supplemental Figure 6S. IC$_{50}$ of Oleoyl-CoA (18:1) with h15-LOX-1

Supplemental Figure 7S. IC$_{50}$ of Oleoyl-CoA (18:1) with h15-LOX-2
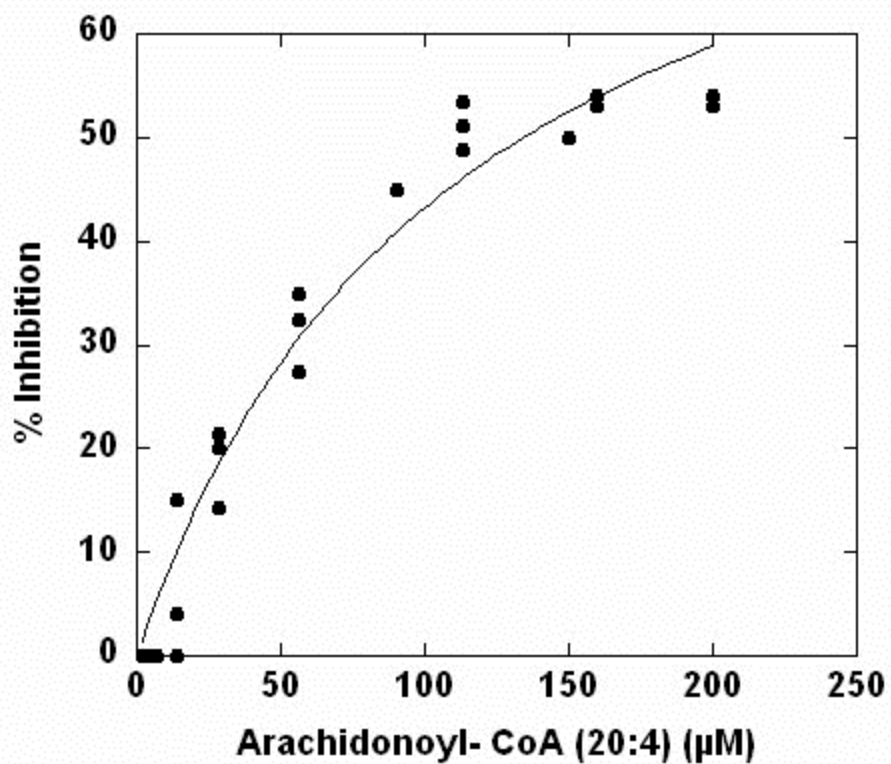
Supplemental Figure 8S. IC$_{50}$ of Arachidonoyl-CoA (20:4) with h12-LOX

References

[1] Mobbs, J. I., Black, K. A., Tran, M., Venugopal, H., Holman, T. R., Holinstat, M., Thal, D. M., and Glukhova, A. (2023) Cryo-EM structures of human arachidonate 12S-Lipoxygenase (12-LOX) bound to endogenous and exogenous inhibitors, *BioRxiv*.
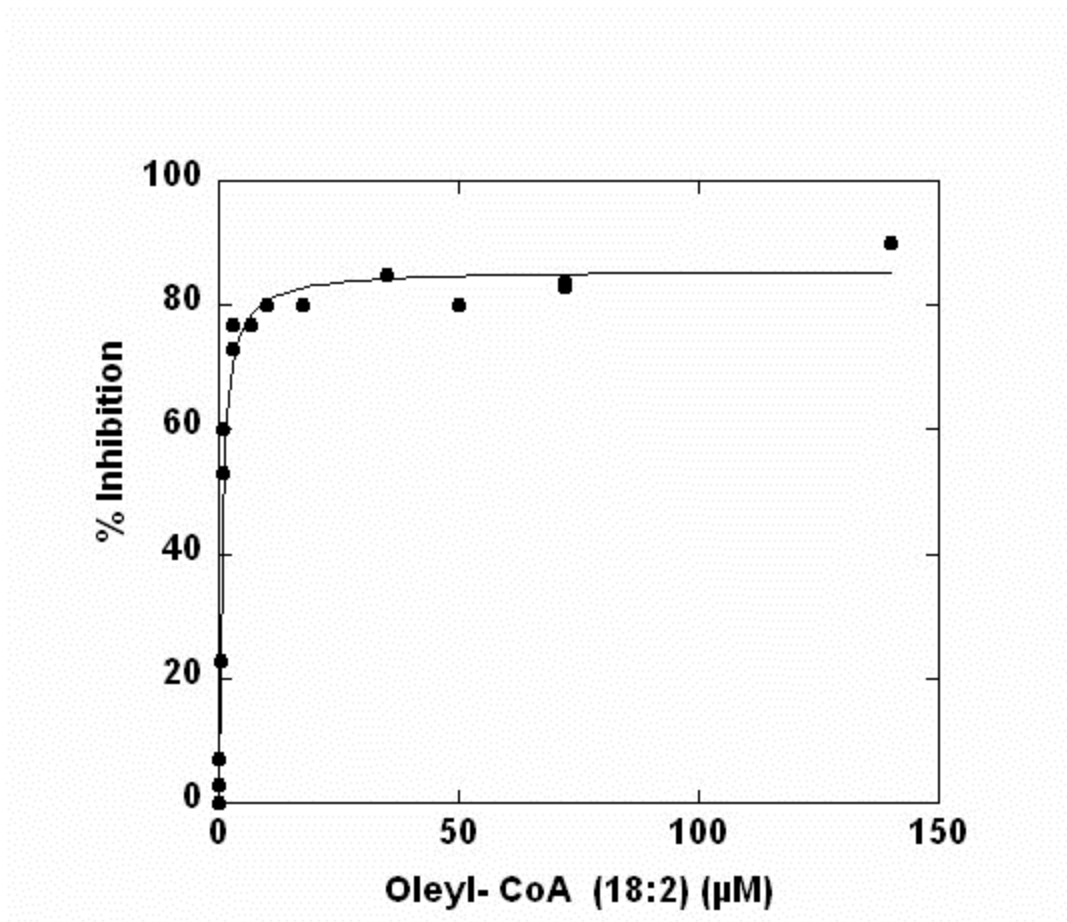
[2] Feingold, K. R. (2000) The Effect of Endocrine Disorders on Lipids and Lipoproteins, In *Endotext* (Feingold, K. R., Anawalt, B., Blackman, M. R., Boyce, A., Chrousos, G., Corpas, E., de Herder, W. W., Dhatariya, K., Dungan, K., Hofland, J., Kalra, S., Kaltsas, G., Kapoor, N., Koch, C., Kopp, P., Korbonits, M., Kovacs, C. S., Kuohung, W., Laferrere, B., Levy, M., McGee, E. A., McLachlan, R., New, M., Purnell, J., Sahay, R., Shah, A. S., Singer, F., Sperling, M. A., Stratakis, C. A., Trence, D. L., and Wilson, D. P., Eds.), South Dartmouth (MA).

[3] Horn, A., and Jaiswal, J. K. (2019) Structural and signaling role of lipids in plasma membrane repair, *Curr Top Membr 84*, 67-98.

[4] Markovic, M., Ben-Shabat, S., Aponick, A., Zimmermann, E. M., and Dahan, A. (2020) Lipids and Lipid-Processing Pathways in Drug Delivery and Therapeutics, *Int J Mol Sci 21*.

[5] Zhang, D., Wei, Y., Huang, Q., Chen, Y., Zeng, K., Yang, W., Chen, J., and Chen, J. (2022) Important Hormones Regulating Lipid Metabolism, *Molecules 27*.

[6] Reddy, P., and Jialal, I. (2023) Biochemistry, Fat Soluble Vitamins, In *StatPearls*, Treasure Island (FL).

[7] Feingold, K. R. (2000) Obesity and Dyslipidemia, In *Endotext* (Feingold, K. R., Anawalt, B., Blackman, M. R., Boyce, A., Chrousos, G., Corpas, E., de Herder, W. W., Dhatariya, K., Dungan, K., Hofland, J., Kalra, S., Kaltsas, G., Kapoor, N., Koch, C., Kopp, P., Korbonits, M., Kovacs, C. S., Kuohung, W., Laferrere, B., Levy, M., McGee, E. A., McLachlan, R., New, M., Purnell, J., Sahay, R., Shah, A. S., Singer, F., Sperling, M. A., Stratakis, C. A., Trence, D. L., and Wilson, D. P., Eds.), South Dartmouth (MA).

[8] Singla, P., Bardoloi, A., and Parkash, A. A. (2010) Metabolic effects of obesity: A review, *World J Diabetes 1*, 76-88.

[9] Parhofer, K. G. (2015) Interaction between Glucose and Lipid Metabolism: More than Diabetic Dyslipidemia, *Diabetes Metab J 39*, 353-362.

[10] Athyros, V. G., Doumas, M., Imprialos, K. P., Stavropoulos, K., Georgianou, E., Katsimardou, A., and Karagiannis, A. (2018) Diabetes and lipid metabolism, *Hormones (Athens) 17*, 61-67.

[11] Bhargava, S., de la Puente-Secades, S., Schurgers, L., and Jankowski, J. (2022) Lipids and lipoproteins in cardiovascular diseases: a classification, *Trends Endocrinol Metab 33*, 409-423.

[12] Yan, A., Xie, G., Ding, X., Wang, Y., and Guo, L. (2021) Effects of Lipid Overload on Heart in Metabolic Diseases, *Horm Metab Res 53*, 771-778.

[13] Craig, M., Yarrarapu, S. N. S., and Dimri, M. (2023) Biochemistry, Cholesterol, In *StatPearls*, Treasure Island (FL).

[14] Ahmed, S., Shah, P., and Ahmed, O. (2023) Biochemistry, Lipids, In *StatPearls*, Treasure Island (FL).

[15] Wakil, S. J., and Abu-Elheiga, L. A. (2009) Fatty acid metabolism: target for metabolic syndrome, *J Lipid Res 50 Suppl*, S138-143.

[16] Kelly, D. J., and Hughes, N. J. (2001) The Citric Acid Cycle and Fatty Acid Biosynthesis, In *Helicobacter pylori: Physiology and Genetics* (Mobley, H. L. T., Mendz, G. L., and Hazell, S. L., Eds.), Washington (DC).

[17] Haddad, A., and Mohiuddin, S. S. (2023) Biochemistry, Citric Acid Cycle, In *StatPearls*, Treasure Island (FL).

[18] Shi, L., and Tu, B. P. (2015) Acetyl-CoA and the regulation of metabolism: mechanisms and consequences, *Curr Opin Cell Biol 33*, 125-131.

[19] Martinez-Reyes, I., and Chandel, N. S. (2018) Acetyl-CoA-directed gene transcription in cancer cells, *Genes Dev 32*, 463-465.

[20] Felix, J. B., Cox, A. R., and Hartig, S. M. (2021) Acetyl-CoA and Metabolite Fluxes Regulate White Adipose Tissue Expansion, *Trends Endocrinol Metab 32*, 320-332.

[21] Wang, Y., Yu, W., Li, S., Guo, D., He, J., and Wang, Y. (2022) Acetyl-CoA Carboxylases and Diseases, *Front Oncol 12*, 836058.

[22] Maloberti, P. M., Duarte, A. B., Orlando, U. D., Pasqualini, M. E., Solano, A. R., Lopez-Otin, C., and Podesta, E. J. (2010) Functional interaction between acyl-CoA synthetase 4, lipooxygenases and cyclooxygenase-2 in the aggressive phenotype of breast cancer cells, *PLoS One 5*, e15540.

[23] Sakuma, S., Fujimoto, Y., Katoh, Y., Kitao, A., and Fujita, T. (2001) The effects of fatty acyl CoA esters on the formation of prostaglandin and arachidonoyl-CoA formed from arachidonic acid in rabbit kidney medulla microsomes, *Prostaglandins Leukot Essent Fatty Acids 64*, 61-65.

133

[24] Bannenberg, G., and Serhan, C. N. (2010) Specialized pro-resolving lipid mediators in the inflammatory response: An update, *Biochim Biophys Acta 1801*, 1260-1273.

[25] Basil, M. C., and Levy, B. D. (2016) Specialized pro-resolving mediators: endogenous regulators of infection and inflammation, *Nat Rev Immunol 16*, 51-67.

[26] Yang, A., Wu, Y., Yu, G., and Wang, H. (2021) Role of specialized pro-resolving lipid mediators in pulmonary inflammation diseases: mechanisms and development, *Respir Res 22*, 204.

[27] Schebb, N. H., Kuhn, H., Kahnt, A. S., Rund, K. M., O'Donnell, V. B., Flamand, N., Peters-Golden, M., Jakobsson, P. J., Weylandt, K. H., Rohwer, N., Murphy, R. C., Geisslinger, G., FitzGerald, G. A., Hanson, J., Dahlgren, C., Alnouri, M. W., Offermanns, S., and Steinhilber, D. (2022) Formation, Signaling and Occurrence of Specialized Pro-Resolving Lipid Mediators-What is the Evidence so far?, *Front Pharmacol 13*, 838782.

[28] Haeggstrom, J. Z., and Funk, C. D. (2011) Lipoxygenase and leukotriene pathways: biochemistry, biology, and roles in disease, *Chem Rev 111*, 5866-5898.

[29] Mashima, R., and Okuyama, T. (2015) The role of lipoxygenases in pathophysiology; new insights and future perspectives, *Redox Biol 6*, 297-310.

[30] Kuhn, H., Banthiya, S., and van Leyen, K. (2015) Mammalian lipoxygenases and their biological relevance, *Biochim Biophys Acta 1851*, 308-330.

[31] Bishop, J. E., and Hajra, A. K. (1980) A method for the chemical synthesis of 14C-labeled fatty acyl coenzyme A's of high specific activity, *Anal Biochem 106*, 344-350.

[32] Blecher, M. (1981) Synthesis of long-chain fatty acyl-coa thioesters using N-hydroxysuccinimide esters, *Methods Enzymol 72*, 404-408.

[33] Amagata, T., Whitman, S., Johnson, T. A., Stessman, C. C., Loo, C. P., Lobkovsky, E., Clardy, J., Crews, P., and Holman, T. R. (2003) Exploring sponge-derived terpenoids for their potency and selectivity against 12-human, 15-human, and 15-soybean lipoxygenases, *J Nat Prod 66*, 230-235.

[34] Vasquez-Martinez, Y., Ohri, R. V., Kenyon, V., Holman, T. R., and Sepulveda-Boza, S. (2007) Structure-activity relationship studies of flavonoids as potent inhibitors of human platelet 12-hLO, reticulocyte 15-hLO-1, and prostate epithelial 15-hLO-2, *Bioorganic & Medicinal Chemistry 15*, 7408-7425.

[35] Joshi, N., Hoobler, E. K., Perry, S., Diaz, G., Fox, B., and Holman, T. R. (2013) Kinetic and structural investigations into the allosteric and pH effect on the substrate specificity of human epithelial 15-lipoxygenase-2, *Biochemistry 52*, 8026-8035.

[36] Schwarz, K., Borngraber, S., Anton, M., and Kuhn, H. (1998) Probing the substrate alignment at the active site of 15-lipoxygenases by targeted substrate modification and site-directed mutagenesis. Evidence for an inverse substrate orientation, *Biochemistry 37*, 15327-15335.

[37] Aleem, A. M., Tsai, W. C., Tena, J., Alvarez, G., Deschamps, J., Kalyanaraman, C., Jacobson, M. P., and Holman, T. (2019) Probing the Electrostatic and Steric Requirements for Substrate Binding in Human Platelet-Type 12-Lipoxygenase, *Biochemistry 58*, 848-857.

[38] Ronowska, A., Szutowicz, A., Bielarczyk, H., Gul-Hinc, S., Klimaszewska-Lata, J., Dys, A., Zysk, M., and Jankowska-Kulawy, A. (2018) The Regulatory Effects of Acetyl-CoA Distribution in the Healthy and Diseased Brain, *Front Cell Neurosci 12*, 169.

Chapter 4

Cryo-EM structures of human arachidonate 12S-Lipoxygenase (12-LOX) bound to endogenous and exogenous inhibitors

[This chapter has been adapted from publication, **Cryo-EM structures of human arachidonate 12S-Lipoxygenase (12-LOX) bound to endogenous and exogenous inhibitors.** (Glukhova et al. 2023, _____)

Jesse I. Mobbs[1,2,*], Katrina A. Black[3,4,5,*], Michelle Tran[6], Wessel A. C. Burger[2,3,4,5], Hariprasad Venugopal[7], Theodore R. Holman[6], Michael Holinstat[8,9], David M. Thal[1,2,#], and Alisa Glukhova[1,2,3,4,5,#]

[1]Drug Discovery Biology and [2]ARC Centre for Cryo-Electron Microscopy of Membrane Proteins, Monash Institute of Pharmaceutical Sciences, Monash University, Parkville, Vic, Australia; [3]Walter and Eliza Hall Institute of Medical Research, Parkville, Victoria, Australia; [4]Department of Medical Biology and [5]Department of Biochemistry and Pharmacology, University of Melbourne, Melbourne, Victoria, Australia; [6]Department of Chemistry and Biochemistry, University of California, Santa Cruz, Santa Cruz, CA, USA; [7]Ramaciotti Centre for Cryo-Electron Microscopy, Monash University, Clayton, Vic, Australia;[8]Department of Pharmacology, University of Michigan, Ann Arbor, MI, USA; Department of Internal Medicine[9], Division of Cardiovascular Medicine, University of Michigan, Ann Arbor, MI, USA;

*These authors made equal contributions
#Correspondence: david.thal@monash.edu and glukhova.a@wehi.edu.au

Key Points

1) The first full-length structures of human arachidonate 12S-Lipoxygenase (12-LOX) reveal mechanisms of oligomeric and conformational states

2) The structures uncover natural inhibitor of 12S-Lipoxygenase (12-lox) and reveal a binding site of inhibitor ML355

Abstract

Human 12-lipoxygenase (12-LOX) is a key enzyme involved in platelet activation and regulation of its activity has been targeted for treatment of heparin-induced thrombocytopenia. Despite the clinical importance of 12-LOX, the exact mechanisms of how it affects platelet activation are not fully understood, and the lack of structural information has limited drug discovery efforts. In this study, we used single-particle cryo-electron microscopy to determine the high-resolution structures (1.7 Å - 2.8 Å) of human 12-LOX for the first time. Our results showed that 12-LOX can exist in multiple oligomeric states, from monomer to hexamer, which may impact its catalytic activity and membrane association. We also identified different conformations within a 12-LOX dimer, likely representing different time points in its catalytic cycle. Furthermore, we were able to identify small molecules bound to the 12-LOX structures. The active site of the 12-LOX tetramer is occupied by an endogenous 12-LOX inhibitor, a long-chain acyl-Coenzyme A. Additionally, we found that the 12-LOX hexamer can simultaneously bind to arachidonic acid and ML355, a selective 12-LOX inhibitor that has passed a phase I clinical trial for treating heparin-induced

138

thrombocytopenia and has received fast-track designation by the FDA. Overall, our findings provide novel insights into the assembly of 12-LOX oligomers, its catalytic mechanism, and small molecule binding, paving the way for further drug development targeting the 12-LOX enzyme.

Introduction

Platelet activation is essential for maintaining haemostasis. However, uncontrolled platelet activation leads to abnormal clot formation and an increased risk of thrombosis and cardiovascular disease [1,2]. Inhibition of platelet activation has been shown as an effective treatment that reduces the morbidity and mortality of cardiovascular ischemic events, such as myocardial infarction and stroke. Despite the use of antiplatelet therapies such as aspirin and $P2Y_{12}$ receptor antagonists to reduce thrombotic risk, a high prevalence of ischemic events leading to unacceptable levels of morbidity and mortality remain. Due to this continued risk for thrombosis, the development of alternative therapies to further limit occlusive thrombotic events is warranted.

The enzyme, human 12-lipoxygenase (12-LOX, ALOX12), is highly expressed in platelets [3], and its activation leads to the production of 12-hydroperoxyeicosatetraenoic acid (12-HpETE), a prothrombotic oxylipin [4,5]. The inhibition of 12-LOX prevents platelet activation [6,7], has a minimal effect on haemostasis, and does not promote increased bleeding, a common side effect of other antiplatelet therapies [6,8,9]. The selective 12-LOX inhibitor, ML355 [10], has passed phase I clinical trials for the treatment of heparin-induced thrombocytopenia and has received fast-track designation by the FDA. Despite 12-LOX being a promising target for antiplatelet therapies there are no experimentally determined structures of the entire human 12-LOX; thus, limiting our understanding of the mechanism and regulation of 12-LOX activity. Although structures of other LOX isozymes have been determined

by x-ray crystallography [11-15], they do not provide enough information to fully comprehend the mechanism of 12-LOX oligomerization and inhibitor binding.

Here we present the first high-resolution structures (1.7–2.8 Å) of human 12-LOX determined using cryo-electron microscopy (cryo-EM). We show that 12-LOX possesses a similar protein fold compared to other lipoxygenases[11-15]. From a single sample of 12-LOX, we were able to determine cryo-EM structures in multiple oligomeric forms from the monomer up to a hexamer. This observation is consistent with prior studies that demonstrated the existence of multiple oligomeric forms of lipoxygenases, including monomers, dimers and tetramers [16-18]. Similar to human 15-LOX, we also captured 12-LOX in different conformational states that likely reflect the different parts of the catalytic cycle for this enzyme – the "open" and "closed" conformation [11]. Due to the high-resolution features of the cryo-EM map, we were able to identify an endogenous 12-LOX inhibitor, a long-chain acyl-Coenzyme A, that co-purifies with the enzyme from mammalian cells. Finally, we were able to elucidate a putative allosteric binding site for the phase II inhibitor ML355. Collectively, we anticipate these structures guiding further research into the function of 12-LOX for platelet activation and promote further drug discovery efforts at this clinically relevant enzyme.

Materials and Methods

A more detailed methods section is provided in the Supplemental Data.

Expression and purification

The human 12-LOX was expressed in Expi293 cells. Following cell lysis, the protein was purified using Ni-affinity and size-exclusion chromatography (SEC).

Cryo-electron microscopy

Vitrification was performed at 1 mg/ml using UltrAufoil R1.2/1.3 300 mesh holey grids and a Vitrobot Mark IV. Movies were collected at 0.82 Å/pix on a G1 Titan Krios microscope with the K3 detector. Data processing was performed following standard pipelines in RELION v3.1[19,20] and cryoSPARC[21] with the aid of UCSF MotionCor2 [22] and GCTF[23]. The 3D variability analysis (3DVA)[24] was used to assess sample variability. Modelling was performed with the aid of the AlphaFold Protein Structure Database[25,26], UCSF ChimeraX[27], COOT[28], PHENIX[29], MolProbity[30] and the GRADE webserver[31].

Steady-State Kinetics and IC$_{50}$ Determination

The 12-LOX enzyme kinetics was performed as described previously[32].

Liposome binding

A lipid suspension was made with the following molar ratios: 99.9:0.1 DOPC: DSPE-PEG (i.e. DOPC). Liposomes were created using the literature protocol[33] using a 100 nm filter at a final concentration of 10 mg/mL.

Data availability.

Atomic coordinates and the cryo-EM density maps have been deposited in the Protein Data Bank and the Electron Microscopy Data Bank. The accession codes are 8GHB and EMD-40039 for 12-LOX monomers; 8GHC and EMD-40040 for dimers; 8GHE and EMD-40042 for tetramers and 8GHD and EMD-40041 for hexamers.

Results

High-resolution structures of 12S-Lipoxygenase

The purification of 12-LOX from mammalian Expi293 cells yielded an oligomeric mixture of 12-LOX forms that were separated by size using size-exclusion chromatography (SEC) **(Fig. 1** and **Supp. Fig. 1)**. The two main peak fractions primarily corresponded to a dimer and a tetramer based on their size, however, the populations were heterogeneous and contained small amounts of other oligomeric forms **(Supp. Fig. 1E).** Both SEC fractions displayed similar enzyme kinetics with a k_{cat} of 12 ± 0.9 s^{-1} for the dimer and 4.8 ± 0.2 s^{-1} for the tetramer. Both had a k_{cat}/K_M value of 1.4 ± 0.1 s^{-1}mM^{-1}. The enzyme activities of both SEC fractions were inhibited by ML355 with IC_{50}'s of 1.6 ± 0.3 μM and 1.4 ± 0.3 μM, for the dimer and tetramer, respectively **(Supp. Fig. 1C,D and Table S2)**. Prior efforts to determine structures of 12-LOX using x-ray crystallography likely failed due to sample heterogeneity. Thus, we turned to cryo-EM to determine the structure of 12-LOX from each SEC fractions. To understand the binding mechanism of ML355, we added the inhibitor during protein expression and purification used in cryo-EM.

Unexpectedly, the dimer peak from the SEC 12-LOX purification gave rise to multiple high-resolution cryo-EM structures of 12-LOX in different oligomeric forms including monomers (2.8 Å), dimers (2.5 Å), tetramers (2.3 Å), and hexamers (2.6 Å), all from the same imaged grid **(Fig. 1**, **Supp. Fig. 2, 4** and **Table S1)**. In contrast, the tetramer peak yielded a structure of only the 12-LOX tetramer **(Fig. 1**, **Supp. Fig. 3,4** and **Table S1)** with an overall resolution of 1.8 Å. All oligomeric forms of 12-LOX exhibited significant intermolecular flexibility determined by 3D variability analysis (3DVA) in cryoSPARC **(Supp. Movies 1-3)**[24]. Thus, we employed local refinement (cryoSPARC) to improve the map resolution and quality for the individual subunits **(Supp. Fig. 2-5)** within each oligomer. For the tetramer peak

144

sample, this improved the resolution to 1.7 Å allowing for accurate model building of the full-length 12-LOX (residues G2 to I663) **(Fig. 2A-B)**.

The structural architecture of 12-LOX is typical of lipoxygenases with the N-terminal β-barrel PLAT (polycystin-1-lipoxygenase α-toxin) domain and a C-terminal α-helical catalytic domain **(Fig. 2A)**. Structural alignments with other LOX structures **(Supp. Fig. 6A)** revealed markedly similar folds with root mean square deviations (RMSDs) <1Å with the largest variations occurring in the PLAT domain **(Supp. Fig. 6B)**. The active site of 12-LOX is located in the catalytic domain, where a catalytic iron atom is coordinated by three conserved histidine residues (H360, H365 and H540) as well as N544 and the carboxyl C-terminus of I663 **(Supp. Fig. 6C-D)**. Next to the catalytic iron is the typical LOX U-shaped lipid-binding pocket that is lined with hydrophobic residues. The entrance to the active site is bordered by an arched helix and an α2-helix in an extended conformation (**Fig. 2A** and **Supp. Fig. 6C-D**).

Oligomeric states of 12S-lipoxygenase

The biological unit of the 12-LOX oligomers appears to be a dimer arranged "head-to-toe". The tetramer and hexamer are made of a dimer of dimers and a trimer of dimers, respectively **(Fig. 1** and **2)**. The overall dimer substructure in each oligomeric form is maintained mainly through Van der Waals interactions between the α2-α4 helixes and the α3-α4 loop **(Fig. 2B-D)**. The dimer substructures of the 12-LOX tetramer and hexamer were virtually identical (RMSDs 0.78Å), while the individual subunits of the dimer were rotated by 30°, due to change in the conformation of the α2-helix (described below) **(Supp.Fig. 7)**. Higher-level oligomerisation in 12-LOX tetramers was maintained through additional Van der Waals interactions of the α2-helix and hydrogen bond interactions of the arched helix and β9-β10 loop between neighbouring subunits (**Fig. 2C**). The architecture of the hexamers was

145

supported by an additional hydrogen bonding network and a disulphide bond (C89-C89) between neighbouring PLAT domains (**Fig. 2D).**

The oligomerisation of 12-LOX affects the accessibility of the active site to bulk solvent. The entrance to the 12-LOX catalytic site is defined by the α2- and arched helixes and is in the same plane as the predicted membrane-binding residues W70/L71/A180[34]. The entrance is accessible to solvent in the 12-LOX monomer, dimer (the "open" subunit, see below), and hexamer, but is obscured when the two dimers associate to form a tetramer due to the adjacent subunit. (**Supp. Fig. 8)**. Conversely, in the "closed" subunit of a 12-LOX dimer, the occlusion is a result of a conformational change (explained further below).

To investigate whether the oligomerisation affects 12-LOX membrane binding we tested the dimer and the tetramer SEC fractions **(Fig. 1)** for their ability to bind artificial DOPC liposomes. Both 12-LOX preparations bind liposomes to a similar extent (21+/-6% and 36+/-6% for dimers and tetramer peak, respectively) **(Supp Fig. 1B)**.

Conformational changes of 12S-Lipoxygenase

The structure of the 12-LOX monomer in all oligomeric forms was similar, except for the 12-LOX dimer. Similar to the arrangement within the 12-LOX tetramer and the hexamer, the monomers in the dimer are arranged "head-to-toe", with most of the contacts mediated via hydrophobic interactions between the α2-helixes (**Fig. 2B**), previously determined by HDX-MS[35]. However, contrary to the protein chains in the tetramer and hexamer, the individual subunits in a dimer are not equivalent. Instead, they adopt either an "open" conformation (as observed in the 12-LOX monomer, tetramer, and a hexamer) or a "closed" conformation, predominantly facilitated by a large-scale motion of the α2-helix and corresponding rearrangements of the neighbouring loops **(Fig. 3)**. In the open conformation, the α2-helix forms a long single helix that lies at the edge of the active site. Conversely, in the closed

conformation, the α2-helix undergoes a rigid 23° pivot and rotation that blocks the entrance to the active site reducing its internal volume **(Fig. 3B)**. The conformational change of the α2-helix also leads to a 30° rotation of the two monomers relative to each other and relative to the dimer substructure observed in the 12-LOX tetramers and hexamers **(Supp. Fig. 7)**.

Natural inhibition of 12S-Lipoxygenase by long chain fatty acid acyl-CoAs

In all of our 12-LOX structures the active site of the 12-LOX subunits in the open conformation was occupied by extra density in the cryo-EM maps **(Supp. Fig. 9)**, suggesting the presence of a bound ligand. The shape of the density varied between oligomeric forms suggesting different ligands. The high-resolution of the tetramer (1.7 Å) and the hexamer (2.3 Å) cryo-EM maps allowed us to model ligands into these densities with high confidence. However, due to the lower resolution of the monomer and dimer cryo-EM maps, we were not able to confidently identify the bound molecules. We hypothesized the observed densities were either ML355 or an endogenous lipid(s) co-purified from Expi293 cells.

The 12-LOX tetramer is made of a dimer of dimers. The subunits at the inter-dimer interface face each other with their lipid binding sites **(Fig. 4A)**. Within each of the U-shaped pockets, we observed a density that resembled a lipid tail. The lipid density extended out of the binding site, spanning the gap between two neighbouring subunits **(Supp. Fig. 10A)**. This density was also present in the apo 12-LOX tetramer samples that were expressed and purified in the absence of ML355 suggesting the ligand was co-purified from the HEK293 cells (data not shown). To improve the resolution of the cryo-EM maps further, we performed a 3D variability analysis (3DVA) on individual subunits within a tetramer **(Sup Fig. 10B, Supp. Movie 2)**. Using the cluster mode of the 3DVA, we were able to separate the protein chains that were fully occupied with the molecule and reconstruct the corresponding 12-LOX subunits and a full tetramer to a resolution of 1.9 Å and 2.05 Å, respectively **(Fig. 4A-C)**. Furthermore,

the 3DVA revealed that the lipid is only bound to one of the subunits at the inter-dimer interface at a time (thus averaging to ½ lipid occupancy in the entire 12-LOX tetramer) **(Supp. Fig. 10C, Supp. Movie 4)**. In contrast, the opposite subunit was mostly empty with some weak non-continuous density in the active site that could represent another unidentified lipid or incomplete separation of the occupied vs. unoccupied subunits during 3DVA.

Because of the high resolution and quality of the density map, we were able to identify the lipid as a fatty acid acyl-CoA ester with a tail approximately 18 carbons long and unknown saturation (oleoyl-CoA was used for modelling purposes) **(Fig. 4B)**. The CoA headgroup is positioned at the inter-dimer interface at the entrance to the catalytic site, between the α2-helix and the arched helix with the fatty acid tail extending into the U-shaped hydrophobic cavity **(Fig. 4C)**. The purine group of CoA forms CH-p interactions with I413, a hydrogen bond with Q406 of the arched helix, and cation-p interactions with the neighbouring molecule's R290 **(Fig. 4D)**. The carbonyl of the oleic acid forms a hydrogen bond with H596. The three phosphate groups form electrostatic interactions with R189, R290, and R585 of the bound 12-LOX, as well as R189, R290, K416 and R585 of the neighbouring 12-LOX subunit. Overlay of these two subunits reveals that the polar residues at the dimeric interface undergo significant rearrangement to better accommodate the interaction with oleoyl-CoA **(Fig. 4F).** The fatty acid tail extends into the catalytic site, forming extensive hydrophobic contacts **(Fig. 4E)**.

Due to the chemical lability of the acyl-CoA's thioester and hence difficulty in detection by mass spectrometry, we set out to confirm our structural findings by determining whether fatty acid acyl-CoAs inhibit 12-LOX. We tested a panel of long chain acyl-CoAs with different lipid tail length and saturation to determine their ability to inhibit 12-LOX catalysis **(Table S3)**. The 12-LOX inhibition by acyl-CoAs depends on both their length and saturation status, with oleoyl-CoA (18:1) being the most potent inhibitor with an IC_{50} of $32 \pm 4 \ \mu$M. None

of the tested acyl-CoAs were substrates for 12-LOX. These data confirm that oleyl-CoA is the most potent inhibitor of 12-LOX, although the exact nature of the bound acyl-CoA in the structure is unconfirmed.

ML355 binding of 12-LOX

In contrast to the tetramer structure, cryo-EM density within the active site of the 12-LOX hexamer was identical across subunits and was distinct from the acyl-CoA. Moreover, the density was of two independent molecules that could be perfectly fit with AA and ML355 (**Fig. 5A-C**). The AA molecule occupies the U-shaped hydrophobic cavity that was occupied by the fatty acid tail of the acyl-CoA in the 12-LOX tetramer. The carboxyl group of AA interacts with 12-LOX via a H-bond with H596, as predicted [36], positioning the C11-C12 double bond in the vicinity of the catalytic iron. The remainder of the contacts are from Van der Waals interactions with hydrophobic residues lining the channel of the active site (**Fig. 5E**). The position of AA is nearly identical to that of the anaerobic structure of coral 8R-LOX [37].

Docking and mutagenesis studies predicted ML355 to bind deep in the 12-LOX active site [32], but our cryo-EM density maps showed no evidence of ML355 occupying that region. Unexpectedly, however, a molecule of ML355 perfectly fit into the EM density found at the entrance to the active site in the hexamer. Interactions of ML355 with 12-LOX include the hydroxyl group of the 2-hydroxy-3-methoxyphenyl moiety forming H-bonds with the backbone carbonyl of L178 and amide of A182 (**Fig. 5D**). The sulphur of benzothiazole ring forms a H-bond with R189 with the sulphonyl group within H-bonding distance to R290 and R585. The sulphonyl interactions of ML355 mimic the interactions observed with the phosphates from oleoyl-CoA and residues R189, R290, and R585. The rest of the molecule forms Van der Waals interactions with M185, I413, L589 and I 5993 (**Fig. 5D**). To validate the ML355 binding pose, we generated four 12-LOX mutants: L589A, L589F, 4A

(R189A/R290A/R585A/K416A), and DLQN (R189D/R290L/K416Q/R585H) **(Fig. 5D)**. Although all mutants folded correctly (based on their thermal unfolding profiles), L589F, 4A, and DLQN were catalytically inactive. Notably, the L589A mutation decoupled catalytic activity from ML355 inhibition **(Supp. Fig. 11 And B)**. This mutant displayed similar kinetics as the wt 12-LOX but remained unresponsive to ML355 inhibition. Mass photometry demonstrated that L589A also impaired the formation of higher-order oligomers associated with ML355 or acyl-CoA binding **(Supp. Fig. 11C)**. While these results support the identified ML355 binding site, a more rigorous investigation into the mechanism of ML355 binding and inhibition is required in the future.

Discussion

To our knowledge, this is the first study to use cryo-EM to determine high-resolution structures of lipoxygenases. Compared to x-ray crystallography, the ability of cryo-EM to separate heterogeneous samples into discrete populations revealed distinct 12-LOX oligomeric states. Human LOXs display oligomeric diversity: while 5-LOX and 15-LOX primarily function as monomers, they dimerize under high protein and salt concentrations[17]. On the contrary, 12-LOX is primarily dimeric[38], but can form larger aggregates[16]. Other studies suggested that most human LOXs can form high-order oligomers in solution[39]. Our structures provide the first high-resolution insights into the diversity of 12-LOX oligomeric forms that can likely be extended to other LOXs.

SAXS experiments predicted that all LOX dimers (12-LOX[16], 15-LOX[18] and 5-LOX[17]) have a similar organisation, including the "head-to-toe" arrangement of individual monomers that are interacting through their α2-helixes. Prior to our structures, such an arrangement was only directly observed in x-ray structures of rabbit 15-LOX-1[11,13] and human

15-LOX-2[40]. While the overall dimer organisation is similar between all 3 enzymes, the relative position of individual subunits varies, owing to differences in specific interacting residues.

Cryo-EM allowed us for the first time to observe structures of 12-LOX tetramers and hexamers. Interestingly, both are made from the dimer building blocks that further oligomerise either into the dimer of dimers or trimer of dimers. Prior studies suggested that reducing agents might prevent the oligomerisation of 12-LOX [16], proposing that higher-order oligomers form through intramolecular disulphide bonds upon protein oxidation. Our 12-LOX hexamer structure is consistent with this observation as it is stabilised by an intermolecular disulphide bond (C89-C89). Other interactions in the dimer, tetramer and hexamer included an extensive network of hydrophobic interactions and hydrogen bonds. As such, the assembly of 12-LOX into dimers and tetramers is independent of the oxidation state of the enzyme, while higher-molecular oligomers could represent a change to the oxidative environment of the cell.

The oligomerisation of 12-LOX might be a regulatory mechanism for enzyme activity and/or membrane binding as the accessibility of the active site varies between different oligomeric forms. The predicted membrane-binding residues for the 12-LOX are located in the same plane as the entrance to its binding site. Interestingly, the membrane binding surface within the 12-LOX dimer building block (present in dimers, tetramers and hexamers) is located within the same surface plane. However, in the tetramer the membrane-binding surface and active site entrance are further sequestered by interdimer contacts. As such, they might represent inactive states or storage pools for the enzyme. While we did not observe significant differences in AA oxidation rates or DOPC liposome binding between the dimer and tetramer SEC peaks used for cryo-EM data collection, the data could possibly be explained by our heterogeneous preparations containing a mixture of the 12-LOX oligomeric forms. Thus,

further analysis using isolated 12-LOX oligomeric forms is necessary to better understand their role in membrane binding and catalysis.

Intriguingly, the higher-order oligomers of 15-LOX-1 were found to induce pore formation in the lead to organelle clearance during erythrocyte maturation[41]. The two-ring arrangement of the 12-LOX hexamer creates a channel with a diameter of ~30 Å. While the physiological role of this oligomeric species of 12-LOX requires further investigation, it is tempting to speculate that similar conformations might exist in other LOXs.

The protein chains in the 12-LOX monomer, tetramer, and hexamer adopt "open" conformation characterised by an extended α2-helix that pack along the entrance to the active site. Such an α2 conformation is seen in many of the LOX structures, including coral 8R-LOX [37], human 15-LOX-2 [14] and porcine 12-LOX (ALOX15)[15]. In the 12-LOX dimer, one subunit adopts an "open" conformation while another undergoes significant conformational change involving a large-scale α2 movement. The alterations to the extended α2 conformation were observed previously in crystal structures of stable 5-LOX [12,42-44] (broken or disordered α2) and 15-LOX-1 [11,13] (large-scale α2 movement). The 15-LOX-1 and now the 12-LOX are the only LOXs that were captured forming non-symmetrical dimers with one subunit in the "open" and one in the "closed" conformations. While the conformational change leading to the formation of the "closed" conformation differs in the degree of the α2 movement and the subunit rotation relative to each other, both result in the closure of the entrance to the active site.

The conformational change between the "open" and "closed" subunits in LOX dimers might be linked to their catalytic cycle[18] or be involved in inhibitor binding[11]. Similar to the 15-LOX-1 structure[11], some of our 12-LOX oligomers demonstrate half occupancy of their active sites. In the 12-LOX dimer, only the active site of the "open" subunit is occupied by what appears to be a lipid density. This suggests that only half of the oligomeric subunits may

be active at any given time, while the other subunit serves a regulatory role. This mechanism could be responsible for differences in inhibitor binding observed previously between the dimeric and monomeric 12-LOX (converted by introducing L183E/L187E mutations). Only the dimer showed inhibition by ML355 (Ki = 0.43 μM), while monomeric 12-LOX was unaffected[35]. Unfortunately, our dimer 12-LOX structure cannot distinguish between part-of-the-site reactivity mechanism, where only one subunit is capable of catalysis, as described for cyclooxygenases (COX)[45,46], and the flip-flop mechanism, where the subunits are taking turns at the catalysis as is the case for biotin carboxylase and transketolase [47,48,49]. Additional analysis is needed to understand the 12-LOX catalytic mechanism further.

One of the unexpected findings was the presence of the fatty acid acyl-CoA molecule in the 12-LOX tetramer that co-purified with our enzyme from Expi293 cells. Fatty acid acyl-CoA derivatives have long been known to inhibit platelet aggregation[50,51] in a chain, length, and saturation-dependent manner. Specifically, the medium-chain acyl-CoA (palmitoyl, stearoyl, oleoyl and linoleoyl) inhibit lipoxygenase activity in platelets at concentrations ranging from 10 to 50 μM[52]. We have confirmed that oleoyl-CoA inhibits 12-LOX at micromolar concentrations. Thus, the presence of acyl-CoA in the binding site is intriguing, particularly as the purified enzyme remains catalytically active. This paradox may relate to the 12-LOX reactivity mechanism and potential half-occupancy of active sites (described above). However, the cause for the half-site occupancy of the tetramer is different from that of a dimer, as the neighbouring subunits create steric hindrance preventing acyl-CoA binding to opposing subunit. Considering that the levels of acyl-CoAs within the cell could reach micromolar concentration [53], the long chain acyl-CoAs could be physiologically important regulators of 12-LOX function in the cell. The effect of acyl-CoA on platelet aggregation is thought to be mediated through P2Y1 and P2Y12 receptors [54]. However, with the discovery that fatty acid

acyl-CoA directly binds and inhibits 12-LOX, it might be possible that the inhibition of 12-LOX could also contribute to this process.

Despite the presence of ML355 during the expression and purification of 12-LOX, ML355 was only bound in the hexameric form of 12-LOX. It is likely, that ML355 was competed out in the other oligomeric forms due to the presence of endogenous lipids. The observed pose of ML355 is in contradiction to previously published docking/ mutagenesis studies that predicted ML355 binding deep in the 12-LOX active site [32]. However, the simultaneous binding of ML355 and AA observed in our structure could explain the "mixed" mode of ML355 inhibition described previously[55]. Nevertheless, future studies are needed to delineate the mechanism of ML355 inhibition with respect to different oligomeric forms of the enzyme along with the role of endogenous inhibitors that may or may not be present in platelets.

In conclusion, this study presents the first high-resolution cryo-EM structures of 12-LOX in multiple oligomeric forms, provides the first structural information on the clinically relevant 12-LOX inhibitor ML355, shows evidence for conformational changes that might accompany the 12-LOX catalytic cycle, and demonstrates that acyl-CoA can serve as endogenous 12-LOX inhibitor. This structural information will aid future studies of 12-LOX biology and its contribution to platelet activity, regulation of hemostasis and thrombosis, and facilitate structure-based drug discovery efforts on a therapeutically validated enzyme for regulation of immune thrombotic diseases such as heparin-induced thrombocytopenia and thrombosis.

Author contributions A.G. developed protein purification strategy, performed protein expression and negative stain transmission EM. A.G. and J.I.M purified the protein. H.V. vitrified the sample and performed image acquisition within the Monash EM facility. J.I.M., K.A.B and A.G. performed cloning, cryo-EM data processing, model building, refinement and validation. M.T. performed enzyme kinetics, inhibition and liposome binding. W.A.C.B. performed mass photometry and 12-LOX mutant purification, characterization, and kinetics. M.H., T.D., participated in experimental design and result interpretation. A.G., D.M.T, J.I.M. and K.A.B wrote the manuscript with contributions from all authors. A.G. and D.M.T. supervised the project.

Competing interests. M. Holinstat is an equity holder and serves on the scientific advisory board for Veralox Therapeutics and Cereno Scientific. M. Holinstat and T. R. Holman are co-inventors for the patented compound ML355.

References:

1. Lebas H, Yahiaoui K, Martos R, Boulaftali Y. Platelets Are at the Nexus of Vascular Diseases. *Front Cardiovasc Med*. 2019;6:132.

2. Willoughby S. Platelets and cardiovascular disease. *European Journal of Cardiovascular Nursing*. 2002;1(4):273-288.

3. Burkhart JM, Vaudel M, Gambaryan S, et al. The first comprehensive and quantitative analysis of human platelet protein composition allows the comparative analysis of structural and functional pathways. *Blood*. 2012;120(15):e73-82.

4. Hamberg M, Samuelsson B. Prostaglandin endoperoxides. Novel transformations of arachidonic acid in human platelets. *Proc Natl Acad Sci U S A*. 1974;71(9):3400-3404.

5. Ikei KN, Yeung J, Apopa PL, et al. Investigations of human platelet-type 12-lipoxygenase: role of lipoxygenase products in platelet activation. *Journal of lipid research*. 2012;53(12):2546-2559.

6. Adili R, Tourdot BE, Mast K, et al. First Selective 12-LOX Inhibitor, ML355, Impairs Thrombus Formation and Vessel Occ

lusion In Vivo With Minimal Effects on Hemostasis. *Arterioscler Thromb Vasc Biol*. 2017;37(10):1828-1839.

7. Yeung J, Tourdot BE, Fernandez-Perez P, et al. Platelet 12-LOX is essential for FcgammaRIIa-mediated platelet activation. *Blood*. 2014;124(14):2271-2279.

8. Svensson Holm AC, Grenegard M, Ollinger K, Lindstrom EG. Inhibition of 12-lipoxygenase reduces platelet activation and prevents their mitogenic function. *Platelets*. 2014;25(2):111-117.

9. Yeung J, Li W, Holinstat M. Platelet Signaling and Disease: Targeted Therapy for Thrombosis and Other Related Diseases. *Pharmacol Rev*. 2018;70(3):526-548.

10. Luci D, Jameson JB, Yasgar A, et al. Discovery of ML355, a Potent and Selective Inhibitor of Human 12-Lipoxygenase. *Probe Reports from the NIH Molecular Libraries Program*. 2010.

11. Choi J, Chon JK, Kim S, Shin W. Conformational flexibility in mammalian 15S-lipoxygenase: Reinterpretation of the crystallographic data. *Proteins: Structure, Function, and Bioinformatics*. 2008;70(3):1023-1032.

12. Gilbert NC, Bartlett SG, Waight MT, et al. The Structure of Human 5-Lipoxygenase. *Science (New York, NY)*. 2011;331(6014):217-219.

13. Gillmor SA, Villasenor A, Fletterick R, Sigal E, Browner MF. The structure of mammalian 15-lipoxygenase reveals similarity to the lipases and the determinants of substrate specificity. *Nature Structural Biology*. 1997;4(12):1003-1009.

14. Kobe MJ, Neau DB, Mitchell CE, Bartlett SG, Newcomer ME. The Structure of Human 15-Lipoxygenase-2 with a Substrate Mimic. *Journal of Biological Chemistry*. 2014;289(12):8562-8569.

15. Xu S, Mueser TC, Marnett LJ, Funk Jr MO. Crystal Structure of 12-Lipoxygenase Catalytic-Domain-Inhibitor Complex Identifies a Substrate-Binding Channel for Catalysis. *Structure*. 2012;20(9):1490-1497.

16. Aleem AM, Jankun J, Dignam JD, et al. Human platelet 12-lipoxygenase, new findings about its activity, membrane binding and low-resolution structure. *J Mol Biol*. 2008;376(1):193-209.

17. Hafner AK, Cernescu M, Hofmann B, et al. Dimerization of human 5-lipoxygenase. *Biol Chem*. 2011;392(12):1097-1111.

18. Ivanov I, Shang W, Toledo L, et al. Ligand-induced formation of transient dimers of mammalian 12/15-lipoxygenase: a key to allosteric behavior of this class of enzymes? *Proteins*. 2012;80(3):703-712.

19. Zivanov J, Nakane T, Forsberg BO, et al. New tools for automated high-resolution cryo-EM structure determination in RELION-3. *Elife*. 2018;7:163.

20. Scheres SHW. A Bayesian View on Cryo-EM Structure Determination. *Journal of molecular biology*. 2012;415(2):406-418.

21. Punjani A, Rubinstein JL, Fleet DJ, Brubaker MA. cryoSPARC: algorithms for rapid unsupervised cryo-EM structure determination. *Nat Methods*. 2017;14(3):290-296.

22. Zheng SQ, Palovcak E, Armache J-P, Verba KA, Cheng Y, Agard DA. MotionCor2: anisotropic correction of beam-induced motion for improved cryo-electron microscopy. *Cell Research*. 2017;14(4):331-332.

23. Zhang K. Gctf: Real-time CTF determination and correction. *Journal of Structural Biology*. 2016;193(1):1-12.

24. Punjani A, Fleet DJ. 3D variability analysis: Resolving continuous flexibility and discrete heterogeneity from single particle cryo-EM. *J Struct Biol*. 2021;213(2):107702.

25. Varadi M, Anyango S, Deshpande M, et al. AlphaFold Protein Structure Database: massively expanding the structural coverage of protein-sequence space with high-accuracy models. *Nucleic Acids Res*. 2022;50(D1):D439-D444.

26. Jumper J, Evans R, Pritzel A, et al. Highly accurate protein structure prediction with AlphaFold. *Nature*. 2021;596(7873):583-589.

27. Pettersen EF, Goddard TD, Huang CC, et al. UCSF ChimeraX: Structure visualization for researchers, educators, and developers. *Protein Sci*. 2021;30(1):70-82.

28. Emsley P, Lohkamp B, Scott WG, Cowtan K. Features and development of Coot. *Acta Crystallographica Section D*. 2010;66(Pt 4):486-501.

29. Adams PD, Afonine PV, Bunkóczi G, et al. PHENIX: a comprehensive Python-based system for macromolecular structure solution. *Acta Crystallographica Section D*. 2010;66(Pt 2):213-221.

30. Chen VB, Arendall WB, 3rd, Headd JJ, et al. MolProbity: all-atom structure validation for macromolecular crystallography. *Acta Crystallogr D Biol Crystallogr*. 2010;66(Pt 1):12-21.

31. Smart OS, Womack TO, Sharff A, et al. grade v.1.2.13. *wwwglobalphasingcom*. 2011

.

32. Tsai WC, Aleem AM, Tena J, et al. Docking and mutagenesis studies lead to improved inhibitor development of ML355 for human platelet 12-lipoxygenase. *Bioorg Med Chem*. 2021;46:116347.

33. Voss OH, Lee HN, Tian L, Krzewski K, Coligan JE. Liposome Preparation for the Analysis of Lipid-Receptor Interaction and Efferocytosis. *Curr Protoc Immunol*. 2018;120:14 44 11-14 44 21.

34. Walther M, Anton M, Wiedmann M, Fletterick R, Kuhn H. The N-terminal domain of the reticulocyte-type 15-lipoxygenase is not essential for enzymatic activity but contains determinants for membrane binding. *J Biol Chem*. 2002;277(30):27360-27366.

35. Tsai WC, Aleem AM, Whittington C, et al. Mutagenesis, Hydrogen-Deuterium Exchange, and Molecular Docking Investigations Establish the Dimeric Interface of Human Platelet-Type 12-Lipoxygenase. *Biochemistry*. 2021;60(10):802-812.

36. Aleem AM, Tsai WC, Tena J, et al. Probing the Electrostatic and Steric Requirements for Substrate Binding in Human Platelet-Type 12-Lipoxygenase. *Biochemistry*. 2019;58(6):848-857.

37. Neau DB, Bender G, Boeglin WE, Bartlett SG, Brash AR, Newcomer ME. Crystal Structure of a Lipoxygenase in Complex with Substrate. *Journal of Biological Chemistry*. 2014;289(46):31905-31913.

38. Shang W, Ivanov I, Svergun DI, et al. Probing dimerization and structural flexibility of mammalian lipoxygenases by small-angle X-ray scattering. *J Mol Biol*. 2011;409(4):654-668.

39. Aleem AM, Wells L, Jankun J, et al. Human platelet 12-lipoxygenase: naturally occurring Q261/R261 variants and N544L mutant show altered activity but unaffected substrate binding and membrane association behavior. *Int J Mol Med*. 2009;24(6):759-764

40. Tsai WC, Gilbert NC, Ohler A, et al. Kinetic and structural investigations of novel inhibitors of human epithelial 15-lipoxygenase-2. *Bioorg Med Chem*. 2021;46:116349

41. van Leyen K, Duvoisin RM, Engelhardt H, Wiedmann M. A function for lipoxygenase in programmed organelle degradation. *Nature*. 1998;395(6700):392-395.

42. Gallegos EM, Reed TD, Mathes FA, et al. Helical remodeling augments 5-lipoxygenase activity in the synthesis of proinflammatory mediators. *J Biol Chem*. 2022;298(9):102282.

43. Gilbert NC, Gerstmeier J, Schexnaydre EE, et al. Structural and mechanistic insights into 5-lipoxygenase inhibition by natural products. *Nat Chem Biol*. 2020;16(7):783-790.

44. Gilbert NC, Rui Z, Neau DB, et al. Conversion of human 5-lipoxygenase to a 15-lipoxygenase by a point mutation to mimic phosphorylation at Serine-663. *FASEB journal : official publication of the Federation of American Societies for Experimental Biology*. 2012;26(8):3222-3229.

45. Yuan C, Rieke CJ, Rimon G, Wingerd BA, Smith WL. Partnering between monomers of cyclooxygenase-2 homodimers. *Proc Natl Acad Sci U S A*. 2006;103(16):6142-6147.

46. Yuan C, Sidhu RS, Kuklev DV, et al. Cyclooxygenase Allosterism, Fatty Acid-mediated Cross-talk between Monomers of Cyclooxygenase Homodimers. *J Biol Chem*. 2009;284(15):10046-10055.

47. Sevostyanova I, Solovjeva O, Selivanov V, Kochetov G. Half-of-the-sites reactivity of transketolase from Saccharomyces cerevisiae. *Biochem Biophys Res Commun*. 2009;379(4):851-854.

48. Janiyani K, Bordelon T, Waldrop GL, Cronan JE, Jr. Function of Escherichia coli biotin carboxylase requires catalytic activity of both subunits of the homodimer. *J Biol Chem*. 2001;276(32):29864-29870.

49. Wielgus-Kutrowska B, Grycuk T, Bzowska A. Part-of-the-sites binding and reactivity in the homooligomeric enzymes - facts and artifacts. *Arch Biochem Biophys*. 2018;642:31-45.

50. Lin C, Lubin B, Smith S. Inhibition of platelet aggregation by acyl-CoA thioesters. *Biochimica et Biophysica Acta (BBA) - General Subjects*. 1976;428(1):45-55.

51. Lascu I, Edwards B, Cucuianu MP, Deamer DW. Platelet aggregation is inhibited by long chain acyl-CoA. *Biochemical and Biophysical Research Communications*. 1988;156(2):1020-1025.

52. Fujimoto Y, Tsunomori M, Sumiya T, Nishida H, Sakuma S, Fujita T. Effects of fatty acyl coenzyme a esters on lipoxygenase and cyclooxygenase metabolism of arachidonic acid in rabbit platelets. *Prostaglandins, Leukotrienes and Essential Fatty Acids*. 1995;52(4):255-258.

53. Abranko L, Williamson G, Gardner S, Kerimi A. Comprehensive quantitative analysis of fatty-acyl-Coenzyme A species in biological samples by ultra-high performance liquid chromatography-tandem mass spectrometry harmonizing hydrophilic interaction and reversed phase chromatography. *J Chromatogr A*. 2018;1534:111-122

54. Manolopoulos P, Glenn JR, Fox SC, et al. Acyl derivatives of coenzyme A inhibit platelet function via antagonism at P2Y1 and P2Y12 receptors: a new finding that may influence the design of anti-thrombotic agents. *Platelets*. 2008;19(2):134-145.

55. Luci DK, Jameson JB, 2nd, Yasgar A, et al. Synthesis and structure-activity relationship studies of 4-((2-hydroxy-3-methoxybenzyl)amino)benzenesulfonamide derivatives as potent and selective inhibitors of 12-lipoxygenase. *J Med Chem*. 2014;57(2):495-506.

Figure Legends

Figure 1. Different oligomeric forms of 12-LOX. (A) Size exclusion chromatography (SEC) UV absorbance trace (280 nm absorbance) from 12-LOX purification. 12-LOX separated as two distinct peaks, one corresponding to a tetramer (red box) and the other a dimer (blue box). (B) Cryo-EM map of a 12-LOX tetramer from "tetrameric" SEC peak. (C) Cryo-EM maps of different 12-LOX oligomers resolved from "dimeric" SEC peak.

Figure 2. Oligomeric structures of 12-LOX. Models of 12-LOX as a (A) monomer, (B) dimer, (C) tetramer and (D) hexamer. Each subunit represented in a different colour and the α2-helix coloured in pink and arched helix in cyan. Graphical representation of each oligomeric state in bottom left and insets details the oligomeric interface. Interacting amino acids are shown as sticks. (D) Cys39 (in red) contributes a disulphide bridge to the interface of the hexamer. Fe atom is shown as a red sphere.

Figure 3. Conformational changes in the 12-LOX dimer. (A) Surface representation of 12-LOX in the "open" (left) and "closed" states (right) showing the active site cavity of the dimer 12-LOX subunits. In the open conformation this cavity is occupied by a small molecule. (B) An alignment of "open" and "closed" states shows a 23°C rotation and unwinding of the N-terminal residues of the α2-helix. The inset shows zoomed-in view of the active site entrance. The α2-helix is in cyan.

Figure 4. Acyl-CoA binding site in the 12-LOX tetramer. (A) Model of a 12-LOX tetramer, with density in the catalytic site shown as cyan volume. Graphical representation is in right corner. (B) Acyl-CoA model and the density. Density is shown as wire mesh, the model is in sticks coloured by heteroatoms. (C) Model of acyl-CoA within the catalytic site of 12-LOX. (D-E) 12-LOX residues that contact the acyl-CoA (orange) shown as sticks. (D) Contacts of the adenosine tri-phosphate group. (E) Contacts of the acyl tail. (F) Conformational change of

residues in contact with the acyl-CoA. Acyl-CoA bound subunit in purple and unbound in pink. Fe atom is shown as a red sphere.

Figure 5. ML355 and arachidonic acid (AA) binding sites in the 12-LOX hexamer. (A) Model of the 12-LOX hexamer with density in the catalytic site shown as grey volume. Graphical representation in the bottom left. (B) Density for AA and ML355. Density is shown as wire mesh, the models is in sticks (orange for ML355 and pink for AA) coloured by heteroatoms. (C) Model of 12-LOX bound to ML355 and AA. (D-E) 12-LOX residues that contact (D) ML355 (orange) and (E) AA (pink) shown as sticks. Fe atom is shown as a red sphere.

Figure 1
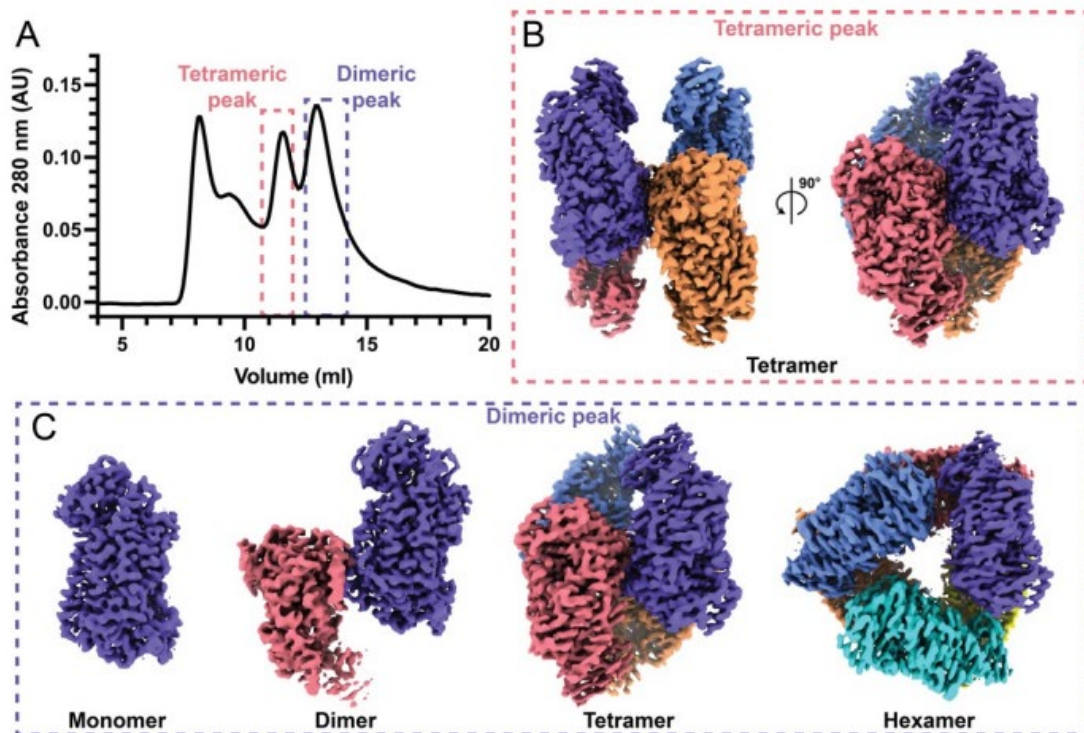
Figure 1. Different oligomeric forms of 12-LOX. (A) Size exclusion chromatography (SEC) UV absorbance trace (280 nM absorbance) from 12-LOX purification. 12-LOX separated as two distinct peaks, one corresponding to a tetramer (red box) and the other a dimer (blue box). (B) Cryo-EM map of a 12-LOX tetramer from "tetrameric" SEC peak. (C) Cryo-EM maps of different 12-LOX oligomers resolved from "dimeric" SEC peak.
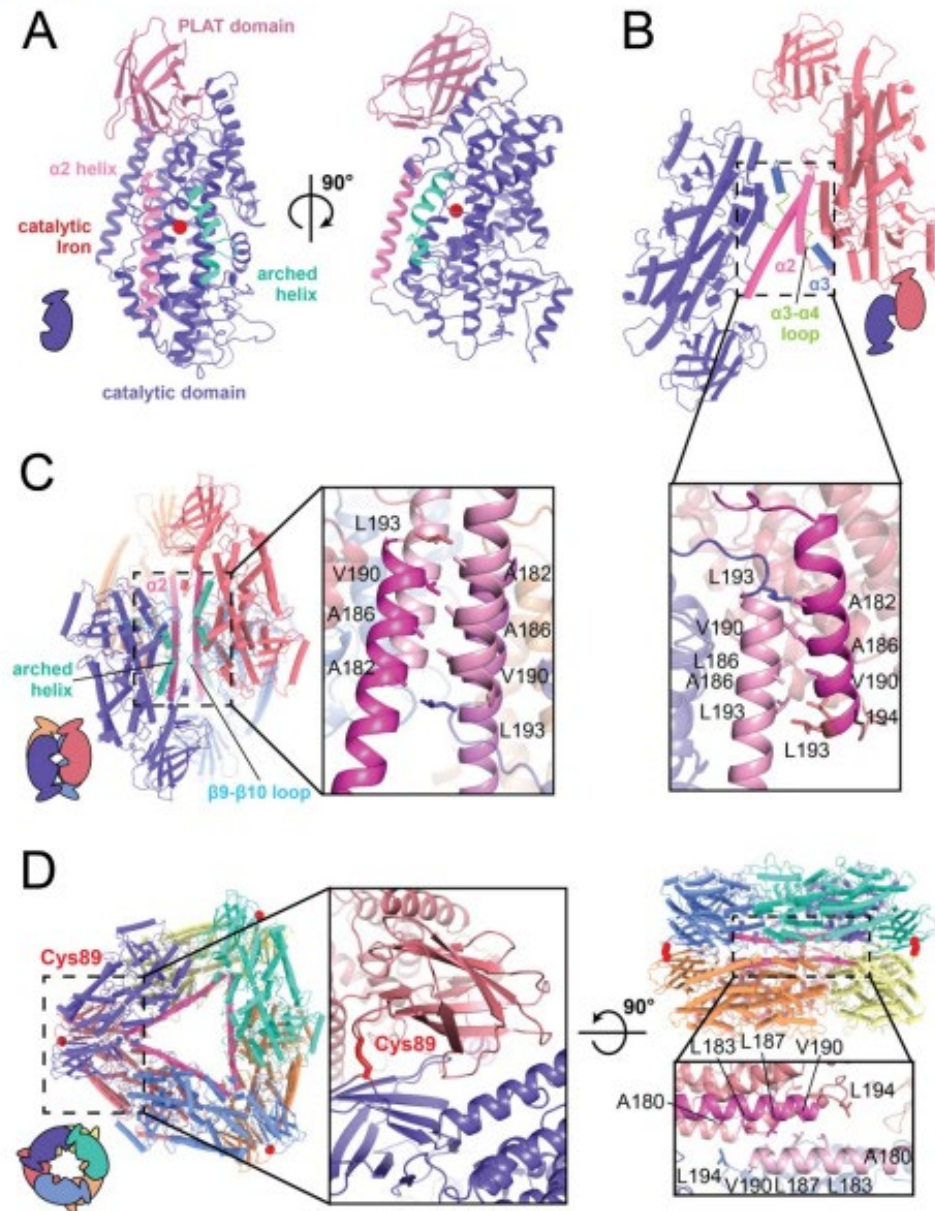
Figure 2

Figure 2. Oligomeric structures of 12-LOX. Models of 12-LOX as (A) monomer, (B) dimer, (C) Tetramer and (D) hexamer. Each subunit represented in a different colour and the α2-helix coloured in pink. Graphical representation of each oligomeric state in bottom left and insets details the oligomeric interface. Interacting amino acids are shown as sticks. (D) Cys39 (in red) contributes a disulphide bridge to the interface of the hexamer. Fe atom is shown as a red sphere.
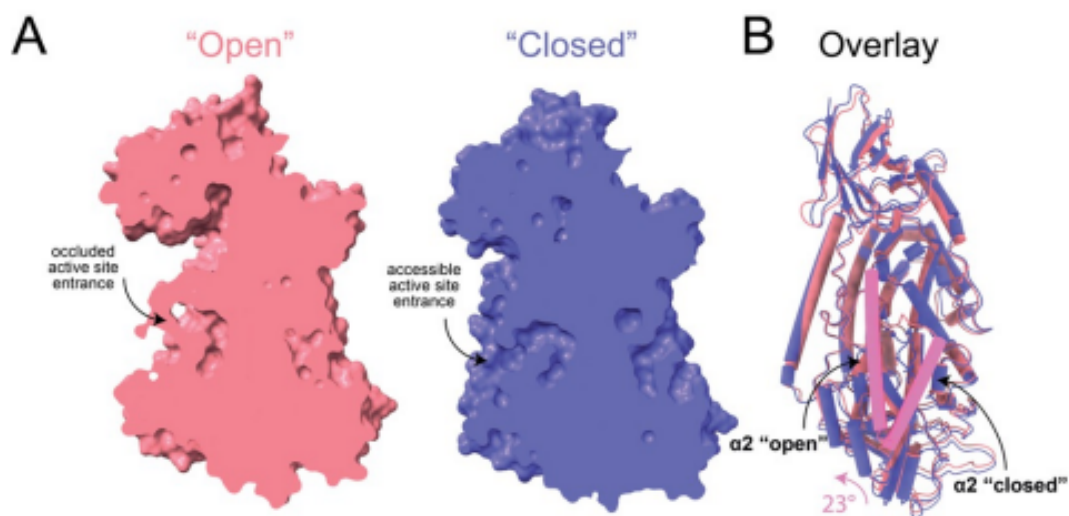
Figure 3

Figure 3. Conformational changes in the 12-LOX dimer. (A) Surface representation of 12-LOX in the "closed" (left) and "open" states (right) showing the active site cavity of the dimer 12-LOX subunits. In the open conformation this cavity is occupied by a small molecule. (B) An alignment of "open" and "closed" states shows a 23°C rotation and unwinding of the N-terminal residues of the α2-helix. The structures are shown as cartoons with cylindrical helixes, the α2-helix is in pink.

Figure 4
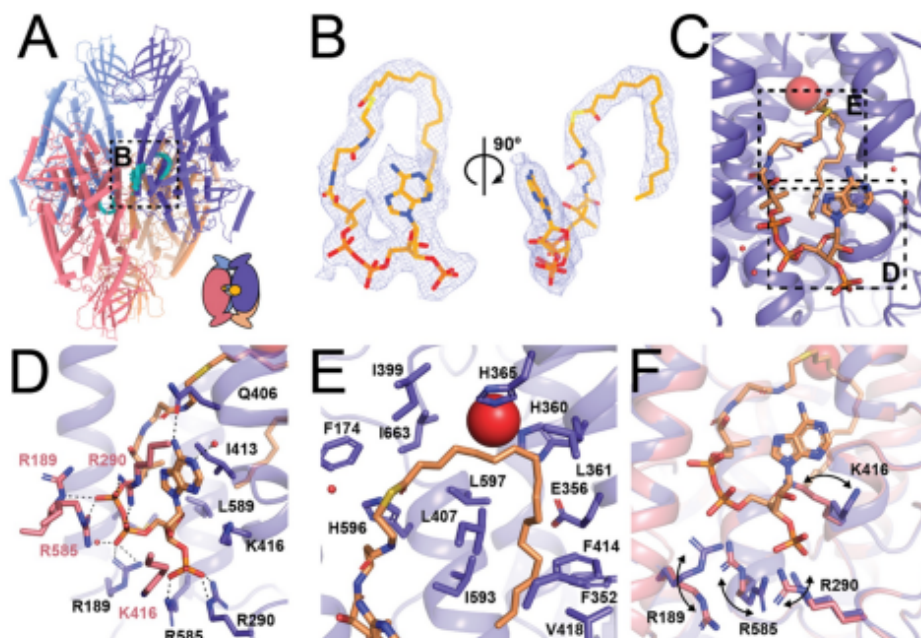
Figure 4. Acetyl-CoA binding site in the 12-LOX tetramer. (A) Model of tetrameric 12-LOX, with density in the catalytic site shown as cyan volume. Graphical representation is in right corner. (B) Acyl-CoA model and the density. Density is shown as wire mesh, the model is in sticks coloured by heteroatoms. (C) Model of acetyl-CoA within the catalytic site of 12-LOX. (D-E) 12-LOX residues that contact the acetyl-CoA (orange) shown as sticks. (D) Contacts of the adenosine tri-phosphate group. (E) Contacts of the acetyl tail. (F) Conformational change of residues in contact with the acetyl-CoA. Acetyl-CoA bound subunit in purple and unbound in pink. Fe atom is shown as a red sphere.
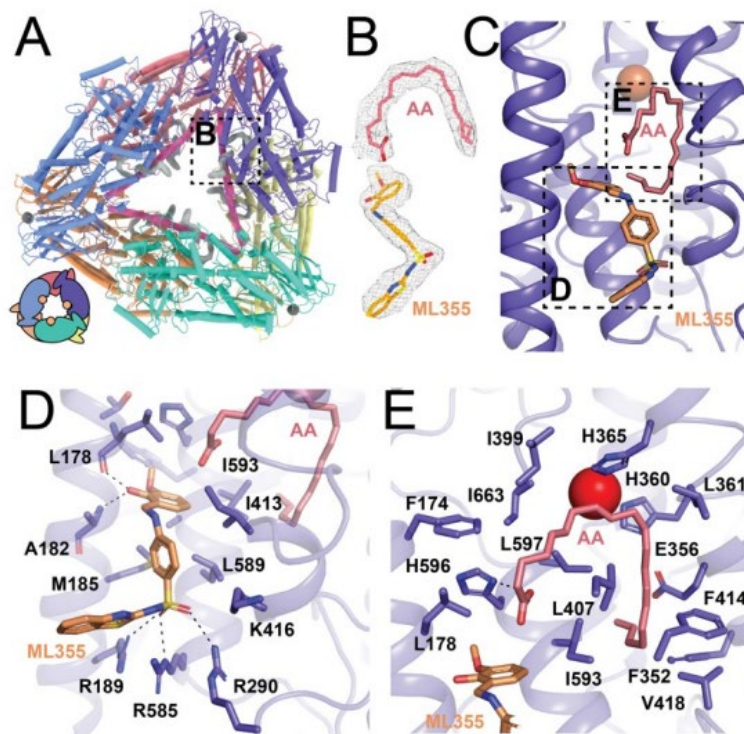
Figure 5

Figure 5. ML355 and arachidonic acid (AA) binding sites in the 12-LOX hexamer. (A) Model of hexameric 12-LOX with density in the catalytic site shown as grey volume. Graphical representation in the bottom left. (B) Density for AA and ML355. Density is shown as wire mesh, the models is in sticks (orange for ML355 and pink for AA) coloured by heteroatoms. (C) Model of 12-LOX bound to ML355 and AA. (D-E) 12-LOX residues that contact (D) ML355 (orange) and (E) AA (pink) shown as sticks. Fe atom is shown as a red sphere.

Chapter 4

Investigating the Catalytic Efficiency of C22-Fatty Acids with LOX Human Isozymes and the Platelet Response of the C22-Oxylipin Products

[This chapter has been adapted from publication, **Investigating the Catalytic Efficiency of C22-Fatty Acids with LOX Human Isozymes and the Platelet Response of the C22-Oxylipin Products** (Tran et al. 2023, Archives of biochemistry and biophysics)

Michelle Tran,1 Livia Stanger,2 Srihari Narendra,1 Michael Holinstat,2 Theodore Holman1*

1Department of Chemistry and Biochemistry, University of California Santa Cruz, Santa Cruz,
CA 95064, United States

2 Department of Pharmacology, University of Michigan Medical School, Ann Arbor, MI, 48109

*Corresponding Authors:

TRH: Tel.: +1-831-459-5884, holman@ucsc.edu

Abbreviations:

LOX, lipoxygenase; h12-LOX, human platelet 12S-lipoxygenase; h15-LOX-1, human reticulocyte 15-lipoxygenase-1; h15-LOX-2, human epithelial 15-lipoxygenase-2; r15-LOX-1 or r12/15-LOX or rALOX15, rabbit 15S-LOX-1; c11-LOX, coral 11R-LOX; COX, cyclooxygenase; WT h12-LOX, wild-type human platelet 12S-lipoxygenase; SLO-1, soybean lipoxygense-1; ML355, h12-LOX specific inhibitor; NSAIDs, nonsteroidal anti-inflammatory drugs; coxibs, COX-2 selective inhibitors; ICP-MS, inductively coupled plasma mass spectroscopy; SEC, size exclusion chromatography; BSA, bovine serum albumin; DCM, dichloromethane; EDTA, Ethylenediaminetetraacetic acid; HEPES, N-2-hydroxyethylpiperazine-N'-2-ethanesulfonic acid; SDS-PAGE, sodium dodecyl sulfate-polyacrylamide gel electrophoresis; PDB, Protein Data Bank; AA, arachidonic acid; 12(S)-HpETE, 12(S)-hydroperoxyeicosatetraenoic acid; 12(S)-HETE, 12(S)-hydroxyeicosatetraenoic acid; 12(S)-HETrE, 12(S)-hydroxyeicosatrienoic acid; d8-12HETE, 12(S)-Hydroxyeicosatetraenoic Acid-d8; C22-FAs, 22 carbon long fatty acids; DHA, cis-4,7,10,13,16,19-docosahexaenoic acid; 11-HDHA, 11(S)-hydroxy-4Z,7Z,9E,13Z,16Z,19Z-DHA; 14-HDHA, 14(S)-hydroxy-4Z,7Z,10Z,12E,16Z,19Z-DHA; 17S-HDHA, 17(S)-hydroxy-4Z,7Z,10Z,13Z,15E,19Z-DHA; 20-HDHA, 20(S)-hydroxy-4Z,7Z,10Z,13Z,16Z,18E-DHA; DPAn3, cis-7,10,13,16,19-docosapentaenoic acid; 11-HDPAn3, 11(S)-hydroxy-7Z,9E,13Z,16Z,19Z-DPAn3; 14-HDPAn3, 14(S)-hydroxy-7Z,10Z,12E,16Z,19Z-DPAn3; 17-HDPAn3; 17(S)-hydroxy-7Z,10Z,13Z,15E,19Z -DPAn3; DPAn6, cis-4,7,10,13,16-docosapentaenoic acid; 11-HDPAn6, 11(S)-hydroxy-4Z,7Z,9E,13Z,16Z-DPAn6; 14-HDPAn6, 14(S)-hydroxy-

4Z,7Z,10Z,12E,16Z – DPAn6; 17-HDPAn6, 17(S)-hydroxy-4Z,7Z,10Z,13Z,15E-DPAn6; DTA, cis-7,10,13,16-docosatetraenoic acid; 11-HDTA, 11(S)-hydroxy-7Z,9E,13Z,16Z-DTA; 14-HDTA, 14(S)-hydroxy-7Z,10Z,12E,16Z-DTA; 17-HDTA; 17(S)-hydroxy-7Z,10Z,13Z,15E-DTA; DTrA, cis-13,16,19-docosatrienoic acid; 13-HDTrA, 13(R)-hydroxy-14E,16Z,19Z-DTrA; 17-HDTrA; 17(S)-hydroxy-13Z,15E,19Z-DTrA; DDiA, cis-13,16-docosadienoic acid; 13-HDDiA, 13(R)-hydroxy-14E,16Z-HDDiA; 17-HDDiA; 17(S)-hydroxy-13Z,15E-DDiA.

Abstract:

Omega-3 fatty acids, such as cis-4,7,10,13,16,19-docosahexaenoic acid (DHA) and cis-4,7,10,13,16-docosapentaenoic acid (DPAn6), have been extensively studied for their health benefits because they can be oxidized by lipoxygenases to form bioactive oxylipins. In this study, we investigated the impact of saturation on the kinetic properties and product profiles of human platelet 12-lipoxygenase (h12-LOX), human reticulocyte 15-lipoxygenase-1 (h15-LOX-1), and human endothelial 15-lipoxygenase-2 (h15-LOX-2) by using fatty acid substrates with differing degrees unsaturation, including cis-4,7,10,13,16,19-docosahexaenoic acid (DHA) (22:6), cis-7,10,13,16,19-docosapentaenoic acid (DPAn3) (22:5), cis-4,7,10,13,16-docosapentaenoic acid (DPAn6) (22:5), cis-7,10,13,16-docosatetraenoic acid (DTA) (22:4), cis-13,16,19-docosatrienoic acid (DTrA) (22:3), cis-13,16-docosadienoic acid (DDiA) (22:2). With respect to kinetics, the loss of Δ^4 and Δ^{19} (i.e., DTA) led to an 18-fold loss of kinetic activity of h12-LOX. h15-LOX-1 experienced no change in kinetic capability for all the C22-FAs, but for h15-LOX2, the loss of both Δ^4 and Δ^{19} resulted in significantly lower k_{cat}/K_M values, like that seen for h12-LOX. With respect to the product profiles, h12-LOX produced mainly 14-oxylipins, with slight variations in the 11- and 17-oxylipins. For h15-LOX-1, 14-oxylipin production increased with loss of saturation, however, this trend switched to 17-oxylipins being the major species upon loss of both Δ^4 and Δ^{19} (i.e., DTA). h15-LOX-2 produced mostly the 17-oxylipin products throughout the fatty acid series. This study also investigated the effects of various 17-oxylipins on platelet activation; such as 17(S)-hydroxy-4Z,7Z,10Z,13Z,15E,19Z-DHA (17-HDHA), 17(S)-hydroxy-

7Z,10Z,13Z,15E,19Z -DPAn3 (17-HDPAn3), 17(S)-hydroxy-4Z,7Z,10Z,13Z,15E-DPAn6 (17-HDPAn6), 17(S)-hydroxy-7Z,10Z,13Z,15E-DTA (17-HDTA), 17(S)-hydroxy-13Z,15E,19Z-DTrA (17-HDTrA), and 17(S)-hydroxy-13Z,15E-DDiA (17-HDDiA). The results revealed that both 17-HDHA and 17-HDPAn6 demonstrated anti-aggregation properties against thrombin or thrombin stimulation. 17-HDPAn3 exhibited agonistic properties, and 17-HDTA showed biphasic effects, inhibiting collagen-induced aggregation at lower concentrations but promoting aggregation at higher concentrations. Both 17-HDDiA and 17-HDTrA induced platelet aggregation. Comparison between 17-HDTA and its corresponding 14-oxylipin (14-HDTA) revealed inhibitory properties of 14-HDTA when stimulated with collagen or thrombin. In summary, the degree of saturation and the location of oxidation appear to influence the physiological activity of these oxylipins, with the general trend being that more unsaturated oxylipins generally inhibit aggregation and less unsaturated compounds promote aggregation. These findings enhance our understanding of the role of oxylipins in platelet aggregation and provide insights into the role of fatty acid distribution and specific LOX isozyme activity for cardiovascular health.

Introduction

Omega-3 fatty acids are a group of essential fatty acids (FA) that are important for preventing hypertriglyceridemia*(1)*, hypertension*(2)*, inflammation*(3, 4)*, arrhythmia*(5, 6)*, atherosclerosis*(7, 8)*, and thrombosis*(9, 10)*. cis-4,7,10,13,16,19-docosahexaenoic acid (DHA) is a long-chain polyunsaturated fatty acid with six double bonds (22:6) that is found in high concentrations in salmon, mackerel, and tuna. DHA plays a role in preventing atherothrombosis, which is the formation of blood clots within arteries*(11-13)*. Docosapentaenoic acid (DPA), another essential FA, is a 22 carbon long polyunsaturated fatty acid with five double bonds (22:5)*(14, 15)*, which can be both an omega-3 (DPAn3) and an omega-6 fatty acid (DPAn6) *(15)*. These two DPA fatty acids have been shown to be important in the prevention of atherosclerosis*(16, 17)*. DPAn3 affects colorectal cancer*(18)*, chronic inflammatory diseases*(19, 20)*, myocardial infarct*(21)*, while DPAn6 affects stroke*(22)*. In addition, higher levels of cis-7,10,13,16,19-docosapentaenoic acid (DPAn3) have been shown to be associated with improved cognitive function, specifically memory*(23-25)*. One other essential FA, cis-7,10,13,16-docosatetraenoic acid (DTA), is a 22-carbon long polyunsaturated fatty acid with four double bonds (22:4), it composes 17.5% of all fatty acids found in cerebral grey matter*(26, 27)*, has been shown to have an inverse association with fetal growth*(28)*, and is positively associated with primary open angle glaucoma, a disease that leads to vision loss and blindness*(29-33)*.

The biological benefits of these fatty acids can be attributed to the fact that they can be oxidized into oxylipins by lipoxygenases (LOXs). Lipoxygenases are a family of enzymes that catalyze the oxidation of polyunsaturated fatty acids (PUFAs) to form a variety of biologically active lipid mediators, including leukotrienes and lipoxins*(34-39)*. There is a wide spectrum of substrates that can be catalyzed by lipoxygenase isozymes, with more than 300 fatty acids being cataloged in the human body*(40-42)*. A key chemical property of LOX substrates is the presence of the 1,4-pentadiene moiety, with its position relative to either the carboxylate or methyl end of the fatty acids dictating which LOX isozyme is a competent catalyst*(43-45)*. Arachidonic acid (AA) is the canonical substrate of LOX isozymes due its high levels in the human body and thus the LOX isozymes are named according to their positional specificity with AA*(46-50)*.

In order to understand the positional specificity mechanism of LOX isozymes, the cavity requirements of various LOX isozymes have been investigated through site-directed mutagenesis and docking, identifying critical amino acids required for fatty acid oxidation*(47, 51-56)*. To this end, it has been determined that for human platelet-type 12-lipoxygenase (12-LOX) and human reticulocyte 15-lipoxygenase-1 (h15-LOX-1) the fatty acid substrate enters the active site methyl-end first, with the depth of the cavity determining which carbon is oxidized*(43, 57, 58)*. Specifically, Phe414 pi-pi stacks with substrate double bonds and residues 417 and 418 define the bottom of the cavity in both LOX isozymes *(54, 59, 60)*.

With respect to the biological role of LOX isozymes, platelet activation is highly dependent on LOX products, as seen by the varied aggregation response with the addition of oxylipins*(22, 59, 61-67)*. The 12-oxylipin of AA and eicosapentaenoic acid (EPA, C20:5) do not inhibit platelet aggregation, while the dihomo-γ-linolenic acid (DGLA, C20:3) product does inhibit aggregation, indicating the positional importance of unsaturation with respect to 12-oxylipin activity*(62, 63)*. Interestingly, the 15-oxylipins of all three of these C20 fatty acids inhibit platelet aggregation, indicating that both the level of unsaturation and the position of the oxidation are critical to the selectivity of receptor binding*(61)*. This hypothesis is extended to DHA (C22:6), where its 11-, 14- and 17-oxylipins are all potent aggregation inhibitors, with their potency increasing with the loss of saturation at either end of the C22-oxylipin (i.e., DPAn3 and DPAn6 oxylipins versus DHA oxylipins)*(63, 65, 68, 69)*. These data highlight the biological importance of unsaturation, length, and oxidation position of oxylipins with respect to platelet activation.

In the current work, the kinetics, product profile and platelet activity of a family of C22-FAs against h12-LOX, h15-LOX-, and h15-LOX-2 were performed. This C22 family of fatty acids includes DHA (22:6), DPAn3 (22:5), cis-4,7,10,13,16-docosapentaenoic acid (DPAn6) (22:5), DTA (22:4), cis-13,16,19-docosatrienoic acid (DTrA) (22:3), and cis-13,16-docosadienoic acid (DDiA) (22:2) (**Figure 1**). By quantifying the catalytic efficiency of these C22-FAs and examining the distribution of oxylipins, their biological availability was determined. Finally, the platelet activity was determined of these oxylipins, establishing the effect of double bonds positioning
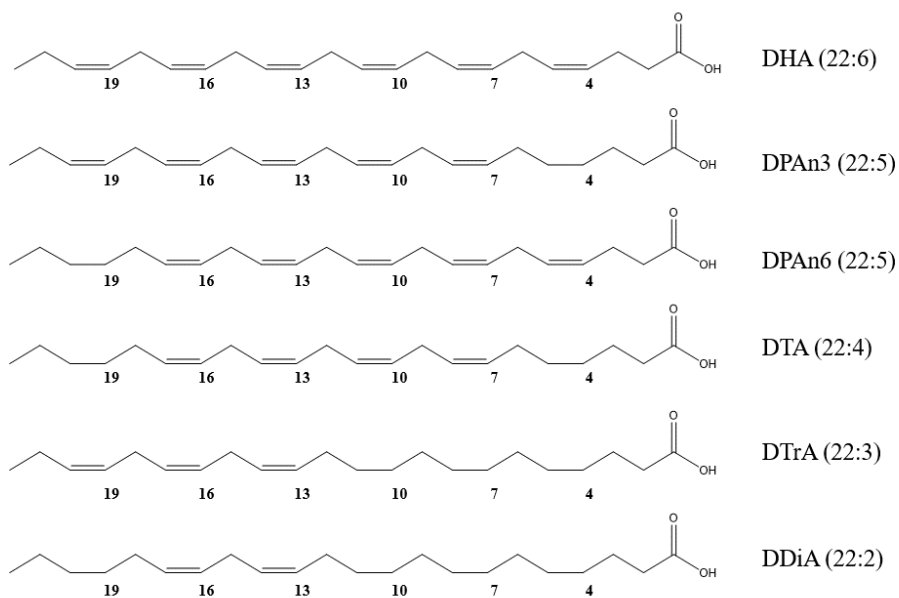
Figure 1. C22-FAs used in this study.

on platelet aggregation.

2.Experimental Procedures

2.1 Chemicals

Fatty acids used in this study were purchased from Nu Chek Prep, Inc. (MN, USA). All other solvents and chemicals were reagent grade or better and were used as purchased without further purification.

2.2 Expression and Purification of 12LOX, h15-LOX-1, and h15-LOX-2.

Recombinant expression and purification of his-tagged h12-LOX (Uniprot entry P18054), h15-LOX-1 (Uniprot entry P16050) and h15-LOX-2 (Uniprot entry O15296) were performed using nickel-affinity chromatography, as previously described *(70, 71)*.The purity of h12LOX, h15-LOX-1 and h15-LOX-2 were assessed by SDS gel to be greater than 85%. The metal content was assessed on a Finnigan inductively-coupled plasma-mass spectrometer (ICP-MS), via comparison with iron standard solution and applied to the kinetic parameters. Cobalt-EDTA was used as an internal standard.

2.3 Product Determination and Isolation

h15-LOX-1 (0.125 μM, pH 7.5), h12-LOX (0.300 μM, pH 8.0), h15-LOX-2 (0.5 μM, pH 7.5 were reacted in 2 mL of 25 mM HEPES at room temperature and ambient oxygen. The enzymatic turnover was monitored by absorbance at 234 nm, with 20 μM fatty acid reacted until 20% turnover occurred (DHA, DPAn3, DPAn6, DTA, DTrA and DDiA). The reactions were quenched with 1% glacial acetic acid

and extracted three times with dichloromethane (DCM). The products were then

reduced with trimethyl phosphite and evaporated under a stream of nitrogen gas. The

reaction products were reconstituted in methanol and analyzed via liquid

chromatography-tandem mass spectrometry (LC-MS/MS). Chromatographic

separation was performed using a C18 column (Phenomenex Kinetex, 4 μm, 150 ×

2.0 mm). Mobile phase solvent A consisted of 99.9% water and 0.1% formic acid,

and solvent B consisted of 99.9% acetonitrile and 0.1% formic acid. Analysis was

carried out over 60 min using isocratic 50:50 A:B for 0–30 min followed by a

gradient from 50:50 A:B to 75:25 A:B from 30 to 60 min. The chromatography

system was coupled to a Thermo-Electron LTQ LC-MS/MS instrument for mass

analysis. All analyses were performed in negative ionization mode at the normal

resolution setting. MS/MS was performed in a targeted manner with a mass list

containing the following m/z ratios containing the following m/z ratios of 343.2 ± 0.5

(HDHAs), 345.2 ± 0.5 (HDPAs), 347.2 ± 0.5 (HDTAs), 349.2 ± 0.5 (HDTrAs), 351.2

± 0.5 (HDDiAs) were used (see Supporting Information, **Figures S1-S5**). All

analyses were performed in negative ionization mode at the normal resolution setting.

Matching retention times, UV spectra, and fragmentation patterns for four common

fragments were used to identify products without standards. To identify the known

standards, at least three common fragments were used to identify the products (listed

in the supporting information). DHA fragmentations used to identify our oxylipins

were from previous literature*(59, 72)*. The commercially obtained standards that were

used were: d8-12-HETE, 17-HDHA, 14-HDHA, 11-HDHA, and 12-HETE. It should

be noted that the enzyme products coeluted with the known standards, so this fact

along with the catalytic nature of LOX isozymes allowed us to assume all products were of the S-configuration, except for the products obtained from reverse substrate insertion.

For product isolation for platelet activity, the same protocol was used except for the high-performance liquid chromatography (HPLC) purification method and amounts of enzyme and fatty acid used. The products were purified isocratically via HPLC on a Higgins Haisil Semi-preparative (5μm, 250 mm x 10 mm) C18 column with 45:55 acetonitrile:water, and 0.1% acetic acid. Oxylipin production reactions required at least 2 hours to complete. 17-HDHA was synthesized from DHA (50 μM) and h15-LOX-1. 17-DPAn3 was synthesized by SLO-1 and DPAn3 (50 μM), and 17-DPAn6 was synthesized by SLO-1 with DPAn6 (50 μM). 17-HDTA and 14-HDTA were synthesized by reaction of DTA (50 μM) with h15-LOX-1 and h12-LOX respectively. 17-HDTrA was synthesized by reaction of DTrA (50 μM) with SLO-1. 17-HDDiA were synthesized by reaction of DDiA (50 μM) with SLO-1.

2.2 Steady-State Kinetics

h12-LOX, h15-LOX-1 and h15LOX-2 reactions were performed at 22°C in a 1 cm^2 quartz cuvette containing 2 mL of 25 mM HEPES (pH 7.5) with substrates (DHA, DPAn3, DPAn6, DTA, DTrA, and DDiA). All substrate concentrations varied from 0.25 to 25 μM. Concentrations of all substrates were determined by measuring the amount of oxylipins produced from complete reaction with SLO-1. Concentrations of oxylipins were determined by measuring the absorbance at 234 nm. Reactions were initiated by the addition of h12-LOX (130 nM), h15-LOX-1 (300 nM)

and h15-LOX-2 (325 nM). Product formation was determined by the increase in absorbance at 234 nm for oxylipin products (ε_{234nm} = 25,000 M^{-1} cm^{-1}) with a Perkin-Elmer Lambda 45 UV/Vis spectrophotometer. KaleidaGraph (Synergy) was used to fit initial rates (at less than 10% turnover), to the Michaelis-Menten equation for the calculation of kinetic parameters.

2.2 Oxylipin titration in human platelet aggregometry

All research involving human subjects was carried out in accordance with the Declaration of Helsinki and approved by the University of Michigan Institutional Review Board (approval number: HUM00100677). Written informed consent was obtained prior to blood collection. Washed platelets were isolated from human whole blood via serial centrifugation and resuspended at a concentration of 3.0×10^8 platelets per milliliter in Tyrode's buffer (10 mM HEPES, 12 mM $NaHCO_3$, 127 mM NaCl, 5 mM KCl, 0.5 mM NaH_2PO_4, 1 mM $MgCl_2$, and 5 mM glucose), as previously published *(65, 73, 74)*. Platelets (250 µl at 3.0×10^8 platelets per milliliter) were dispensed into glass cuvettes and oxylipin at the indicated concentrations (0–40 µM) was added to the platelet solution. The aggregation response to each oxylipin was measured in a Chrono-log Model 700D lumi-aggregometer for 10 min at 37°C. Oxylipins that did not induce platelet aggregation were subsequently added to 250 µl of platelets and incubated for 10 min at 37°C to determine if the oxylipin had an inhibitory effect. Oxylipin-treated platelets were stimulated with an EC_{80} concentration of either collagen (Chrono-log) or thrombin agonist under stirring conditions (1,100 rpm) at 37°C. Platelet aggregation was recorded for 10 min. Bar

185

graphs are shown below (**Figures 2-5**), however, aggregation dose responses are

shown as **Figures S6-S9** in the supporting information.

Results:

h12-LOX kinetics and product profile of fatty acids

The k_{cat} for h12-LOX with DHA, DPAn3, DPAn6, and DTA at 22 °C was 13

± 0.4 s^{-1}, 7.1 ± 0.5 s^{-1}, 11 ± 0.9 s^{-1}, and 0.40 ± 0.05 s^{-1}, respectively; however, DTrA

and DDiA were not substrates (**Table 1**). The k_{cat}/K_M for h12-LOX with DHA,

DPAn3, DPAn6, and DTA at 22 °C was 7.4 ± 0.3 µM^{-1} s^{-1}, 4.0 ± 0.3 µM^{-1} s^{-1}, 5.3 ± 1

µM^{-1} s^{-1}, and 0.30 ± 0.03 µM^{-1} s^{-1}, respectively (**Table 1**). These data indicate that the

loss of either Δ^4 or Δ^{19} double bonds of DHA (i.e., DPAn3 and DPAn6) does not

Table 1: Kinetics values of h12-LOX with various C22-FAs. NA = no
activity

	k_{cat}	k_{cat}/K_M	K_M
DHA	13 (0.4)	7.4 (0.3)	1.7 (0.3)
DPAn3	7.1 (0.5)	4.0 (0.3)	1.8 (0.4)
DPAn6	11 (0.9)	5.3 (1)	2.2 (0.2)
DTA	0.40 (0.05)	0.30 (0.03)	1.1 (0.09)
DTrA	NA	NA	NA
DDiA	NA	NA	NA

significantly affect the k_{cat} or k_{cat}/K_M values. However, losing both Δ^4 and Δ^{19} (i.e.,

DTA) causes more than a 10-fold decrease in the k_{cat} and k_{cat}/K_M values and the loss

of additional double bonds (i.e., DTrA and DDiA) leads to complete loss of catalysis.

186

The latter results can be easily explained due to the lack of a 1,4-diene in the appropriate position relative to the active site iron for DTrA and DDiA, however the 10-fold loss of activity for DTA relative to DPAn3 and DPAn6 is less clear. The loss of both Δ^4 and Δ^{19} would make DTA more flexible and more hydrophobic due to the increase in saturation, which could affect its positioning in the active site. Another possible explanation is the loss of an aromatic interaction. Previously, it was observed that F414 of h12-LOX pi-pi stacked with Δ^{11} of AA*(54)*, therefore it is possible that there is an aromatic residue which could pi-pi stack with both Δ^4 and Δ^{19}, leading to a loss of

catalytic activity for DTA. For example, a loss of activity relative to saturation was previously observed where the k_{cat} value for mead acid (20:3) was ten-fold less than that found for AA (20:4), illustrating how the loss of a double bond could have

Table 2: Product distribution of h12-LOX with various fatty acids. n/d = not detected, NA = no activity

	17-product	**14-product**	**11-product**
DHA	n/d	90± 1	10 ± 1
DPAn6	n/d	100 ±1	n/d
DPAn3	4 ± 1	75 ± 1	21 ± 0.5
DTA	11±0.2	76±3	12±1
DTrA	NA	NA	NA
DDiA	NA	NA	NA

drastic effects to LOX activity*(54)*. It should be noted that the k_{cat} and k_{cat}/K_M values of DHA, DPAn3, DPAn6 with h12-LOX correlated well with our previous work *(54, 61, 65, 72, 75)*.

With respect to product formation, h12-LOX with DHA and DPAn6 produced mostly the 14-oxylipin products, with the 14-oxylipin:11-oxylipin ratios being 90:10 and 100:0, respectively (**Table 2**), consistent with previous work *(64, 67, 73)*. There is an increase in promiscuity in product formation with DPAn3 and DTA, with 17-oxylipins, 14-oxylipins, and 11-oxylipins being made in the ratios of 4:75:21 and 11:76:12, respectively. Nevertheless, h12-LOX still produces mainly the 14-oxylipin product for all the C22-FAs which had activity. Considering that an increase of the 17-oxylipin relative to the 14-oxylipin occurs when the substrate enters the active site less deeply, and the 11-oxylipin occurs when the fatty acid enters more deeply, it appears that loss of either Δ^4 or both Δ^4 and Δ^{19} leads to less precise oxidation. This is consistent

Table 3: Kinetic values of h15-LOX-1 with various C22-FAs.

	k_{cat}	k_{cat}/K_M	K_M
DHA	1.6 (0.1)	0.49 (0.03)	3.3 (0.7)
DPAn3	1.0 (0.1)	0.72 (0.1)	1.4 (0.5)
DPAn6	1.7 (0.2)	0.47 (0.1)	3.7 (0.3)
DTA	2.5 (0.04)	0.35 (0.01)	7.2 (0.1)
DTrA	1.6 (0.06)	0.37 (0.02)	4.3 (0.2)
DDiA	3.3 (0.04)	0.81 (0.06)	4.1 (0.2)

with the substrate not being held as tightly in the active site, possibly due to an increase in flexibility/hydrophobicity and/or a loss of pi-pi stacking (*vide supra*) *(54, 56, 57, 61, 65, 72, 75, 76)*. It is interesting to note that this hypothesis for product formation parallels the lowered rates observed for DTA but not DPAn3. This could indicate that the product ratios are more sensitive to enzyme/substrate interactions, indicating that saturation at Δ^4 is critical for product profiling, while the loss of both

Δ^4 and Δ^{19} is more critical for kinetic efficiency. We are currently investigating

specific active site amino acid interactions with Δ^4 and Δ^{19} through mutagenesis in

order to tease out the specific interactions.

h15-LOX-1 kinetics and product profile of fatty acids

The k_{cat} for h15-LOX-1 with DHA, DPAn3, DPAn6, DTA, DTrA, and DDiA

at 22 °C was 1.6 ± 0.1 s^{-1}, 1.0 ± 0.1 s^{-1}, 1.7 ± 0.2 s^{-1}, and 2.5 ± 0.04 s^{-1}, 1.6 ± 0.06 s^{-1},

and 3.3 ± 0.04 s^{-1} respectively (**Table 3**). The k_{cat}/K_M with DHA, DPAn3, DPAn6,

DTA, DTrA, and DDiA at 22 °C was 0.49 ± 0.03 µM^{-1} s^{-1}, 0.72 ± 0.1 µM^{-1} s^{-1}, $0.47 \pm$

0.1 µM^{-1} s^{-1}, and 0.35 ± 0.01 µM^{-1} s^{-1}, 0.37 ± 0.02 µM^{-1} s^{-1}, and 0.81 ± 0.06 µM^{-1} s^{-1},

respectively (**Table 3**). Surprisingly, there were no significant changes in the k_{cat} or

k_{cat}/K_M values with the loss of multiple double bonds in the C22-FA scaffold,

indicating that the degree and/or placement of unsaturation does not affect h15-LOX-

Table 4: Product distribution of h15-LOX-1 with various C22-FAs. n/d = not detected.

	17 -product	14 -product	13-product	11-product
DHA	48 ± 3	45 ± 2	n/d	7 ± 0.5
DPAn6	37 ± 3	63 ± 3	n/d	n/d
DPAn3	23 ± 3	77 ± 3	n/d	n/d
DTA	68 ± 2	23 ± 1	n/d	5 ± 0.4
DTrA	82 ± 1	n/d	18 ± 1	n/d
DDiA	86 ± 2	n/d	14 ± 2	n/d

1 kinetics appreciably. This is consistent with past literature results which reported that the loss of the Δ^5 double bond in AA did not affect the kinetic values for h5-LOX-1. *(61)*. It should be noted that the k_{cat} and k_{cat}/K_M values of DHA with h15-LOX-1 correlated well with our previous work *(54, 61, 65, 72, 75)*.

With respect to product profiling, h15-LOX-1 reacts with DHA, DPAn6, and DPAn3 producing both the 14-oxylipin and 17-oxylipin products, with a preference for the 14-oxylipin products with DPAn3 and DPAn6 (**Table 4**). With DHA as the substrate, the ratio of 17HDHA:14HDHA:11HDHA was 48:45:7, which is consistent with previous work *(54, 61, 65, 72, 75)*. With DPAn6 as the substrate, the ratio of 17-HDPAn6:14-HDPAn6 was 37:63, with no 11-product being made. With DPAn3 as the substrate, the ratio of 17-HDPAn3:14-HDPAn3 was 23:77. However, with DTA as the substrate, the product preference shifts to the 17-oxylipin product, with the ratio of 17-HDTA:14-HDTA:11-HDTA being 68:23:5. For DTrA and DDiA, the ratio of 17-HDTrA:13-HDTrA is 82:18 and 86:14, respectively. The 17-oxylipin was the majority product because the 14-oxylipin is not catalytically feasible due the position of the 1,4-diene relative to the methyl end of the substrate.

Analyzing the kinetic and product data for h15-LOX-1, it is observed that saturation does not affect enzymatic rates significantly, but the product profile is affected. When both the Δ^4 and Δ^{19} double bonds are removed, there is a novel shift in the product specificity that has not been reported previously. For DHA, DPAn6, and DPAn3, the 14-oxylipin is the majority product, but for DTA, the 17-oxylipin is the majority product, indicating that DTA, slides less deep into the cavity site of h15-LOX-1 than DHA, DPAn6, and DPAn3, thus making more 17-oxylipins. Since DTA is both more flexible and more hydrophobic than either DPAn3 or DPAn6, this effect could be due to a general binding mode change. Another explanation could be that there is a specific residue interacting with the double bonds of

190

DTA, pulling it further into the active site. However, considering that the effect is only observed when both D^4 and D^{19} are removed, it appears there is not one interaction that is important, but rather that there is a synergistic effect between the two double bonds and the

Table 5: Kinetic values of h15-LOX-2 with various C22-FAs.			
	k_{cat}	k_{cat}/K_M	K_M
DHA	3.0 (0.1)	0.78 (0.07)	3.9 (0.3)
DPAn3	1.5 (0.07)	0.38 (0.08)	3.8 (0.4)
DPAn6	2.0 (0.1)	0.76 (0.2)	2.6 (0.5)
DTA	0.13 (0.3)	0.032 (0.004)	4.0 (0.4)
DTrA	0.029 (0.08)	0.022 (0.003)	1.3 (0.2)
DDiA	0.014 (0.02)	0.045 (0.005)	0.31 (0.03)

active site residues. Previously in the literature, a pi-pi interaction between the D^{11} or D^{14} double bond of AA and F414 was observed, but the D^{11} and D^{14} double bonds are in close proximity so in theory F414 could interact with both double bonds *(57, 77)*. The distance between D^4 and D^{19} double bonds of DHA is approximately 4.5 angstroms, greater than that between D^{11} and D^{14} and thus one critical amino acid interaction seems unlikely. Nevertheless, H425 is within 5 angstroms of F414, suggesting the possibility that H425 could be at least partially responsible for the observed kinetic effects. We are currently beginning a mutagenesis campaign to probe the role of H425 and other active site residues that affect C22 substrate catalysis. With respect to DTrA and DDiA, 17-oxylipin is the major product because 14- oxylipin is not catalytically feasible. Due to improper double bond positioning relative to the active site iron, both fatty acids appear to flip and enter the active site in the opposite orientation. This reverse orientation produces the 13-oxylipin from DTrA and DDiA, as is seen for h5-LOX catalysis *(54, 55,71,72)*.

h15-LOX-2 kinetics and product profile of fatty acids

The k_{cat} for h15-LOX-2 with DHA, DPAn3, DPAn6, DTA, DTrA, and DDiA at 22 °C was 3.0 ± 0.1 s^{-1}, 1.5 ± 0.07 s^{-1}, 2.0 ± 0.1 s^{-1}, and 0.13 ± 0.3 s^{-1}, 0.029 ± 0.08 s^{-1}, and 0.014 ± 0.02 s^{-1}, respectively (**Table 5**). The k_{cat}/K_M with DHA, DPAn3, DPAn6, DTA, DTrA, and DDiA at 22 °C was 0.78 ± 0.07 μM^{-1} s^{-1}, 0.38 ± 0.08, 0.76 ± 0.2 μM^{-1} s^{-1}, and 0.032 ± 0.004 μM^{-1} s^{-1}, 0.022 ± 0.003 μM^{-1} s^{-1}, and 0.045 ± 0.005 μM^{-1} s^{-1}, respectively (**Table 5**). There is no significant difference in k_{cat} or k_{cat}/K_M values with the loss of either D^4 or D^{19} from DHA (i.e., DPAn3 and DPAn6). However, the loss of both D^4 and D^{19}, such as for DTA, DTrA and DDiA, leads to more than a greater than 10-fold difference in the k_{cat} and k_{cat}/K_M for h15-LOX-2. As previously proposed for h12-LOX (*vide supra*), this loss of reactivity could be due to an increase in flexibility/hydrophobicity of the fatty acid, or a loss of a specific interaction with an active site residue, such as pi-pi stacking *(76-78)*.

	17-product	14 -product	13-product
Table 6: Product distribution of h15-LOX-2 with various C22-FAs. n/d = not detected.			
DHA	94± 1	6 ± 1	n/d
DPAn6	96 ± 1	4 ± 1	n/d
DPAn3	92 ± 4	8± 4	n/d
DTA	100 ± 1	n/d	n/d
DTrA	88±1	n/d	12±1
DDiA	37±5	n/d	63±5

With all C22-FAs, h15-LOX-2 produced mostly the 17-oxylipins, consistent with its high level of specificity (**Table 6**). With DHA, DPAn6, DPAn3, and DTA, the ratios between the 17-product:14-product were 94:6, 96:4, 92:8, and 100:0, respectively. An exception to this trend is the production of the 13-product with DTrA and DDiA, with the ratio of 17-HDDiA:13-HDDiA being 88:12 and 37:63, respectively. As discussed previously for h15-LOX-1 (*vide supra*), the production of the 14-oxylipin is not possible due to the positions of the double bonds relative to the terminal methyl, and thus 13-oxylipin from h15-LOX-2 and DTrA and DDiA is most likely due to the fatty acid entering the active site carboxylic acid end first, as seen for h5-LOX *(55)*.

Excluding the production of the 13-oxylipin, the degree of unsaturation does not affect the product profile for h15-LOX-2 substantially, which could be due to a lack of pi-pi stacking. Previous literature has shown that F414 is involved in pi-pi stacking with the substrate for h12-LOX and h15-LOX-1, but this residue does not exist in the active site of h15-LOX-2 *(55, 76)*, which could explain the lack of dependence on saturation for product production.

Platelet aggregation effect of C22-oxylipins with variation of oxidation position and degree of unsaturation.

The C22-oxylipins were assessed for their ability to regulate platelet aggregation, either through a stimulatory role, an inhibitory role, or in a biphasic capacity. Previously, it was demonstrated that 17-HDHA was a potent anti-aggregation effector molecule. *(63, 68, 79)* In the current investigation, this family of 17-oxylipins with 22 carbons was investigated further, with 17-HDPAn3, 17-HDPAn6, 17-HDTA, 17-HDTrA, and 17-HDDiA being assessed. In the present investigation, 17-HDHA demonstrated inhibition of collagen-stimulated platelets at low concentrations (24 +/- 10% aggregation at 5 mM), while higher

Figure 2: Inhibition of platelet aggregation with 17-HDHA and 17-HDPAn6.
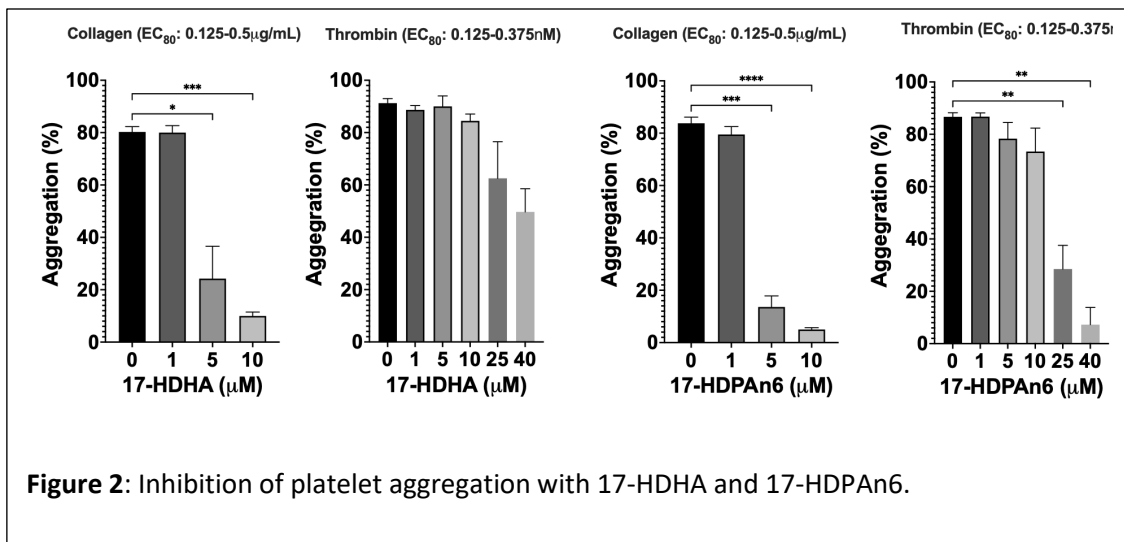
concentrations of 17-HDHA were required to inhibit thrombin-stimulated platelets (63 +/- 10% aggregation at 25 mM) (**Figure 2**). 17-DPAn6 had comparable potency with 14 +/- 4% aggregation at 5 mM when stimulated with collagen and 29 +/- 9% at 25 μM when stimulated with thrombin (**Figure 2**). Interestingly, 17-DPAn3 showed no inhibitory affects but did have agonistic properties with 26 +/- 10% aggregation at 5 μM with no platelet stimulation. 17-HDDiA and 17-HDTrA were also agonists with 55 +/- 10% and 84 +/- 2% at 5 μM, respectively (**Figure 3**). 17-HDTA is the unusual oxylipin of this family of 17-oxylipins. At 0.5 μM of 17-HDTA, 20 +/- 10% platelet aggregation was observed with collagen added, making it a more potent inhibitor than either 17-HDHA or 17-HDPAn6. However, at higher

concentrations, 17-HDTA was an agonist. At 5 μM of 17-HDTA, 41 +/- 10% aggregation

Figure 3. Agonistic effect of platelet aggregation with 17-HDPAn3, 17-HDTrA and 17-HDDiA
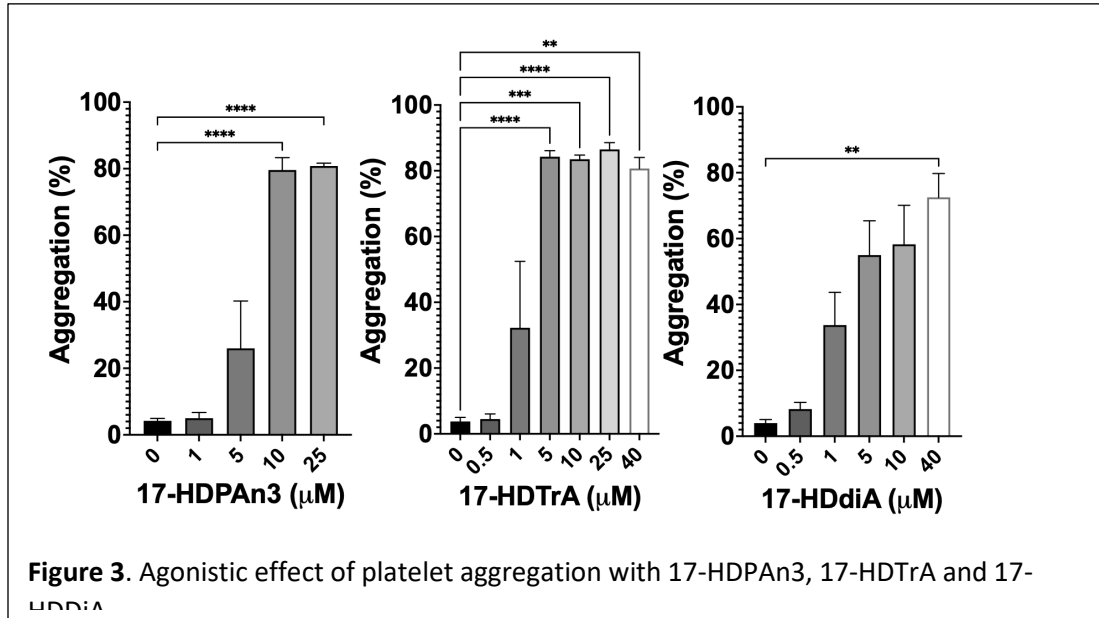
was observed with no platelet stimulation (**Figure 4**).

In general, these data indicate that as the 17-oxylipin loses saturation, it converts from a platelet activation inhibitor to a platelet activation agonist (**Table 7**). The transition point appears to be between 17-HDPAn3 and 17-HDPAn6, with loss of D^{19} maintaining the inhibitory properties of the 17-HDPAn6, but loss of D^4 leads to agnostic properties (i.e., 17-HDPAn3). Interestingly, 17-HDTA, which has lost both D^4 and D^{19}, is both an inhibitor and an agonist. It is tempting to speculate that D^4 and D^{19} on the 17-
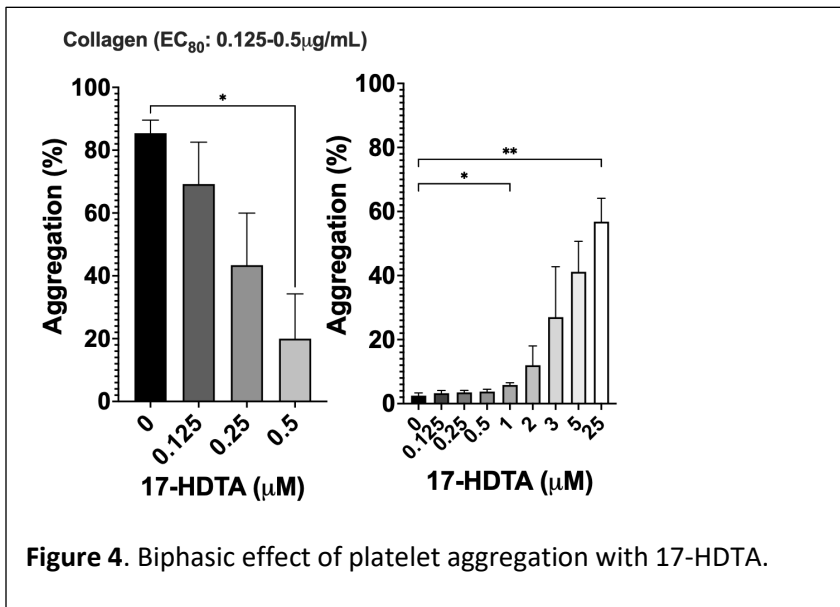
Figure 4. Biphasic effect of platelet aggregation with 17-HDTA.

195

oxylipin regulate two distinct receptor pathways. The mechanism of action of these 17-oxylipins is currently being investigated to better understand these intriguing results.

With respect to the 14-oxylipins, it has previously been observed that 14-HDHA is a potent aggregation inhibitor with 20% aggregation at 5 µM with collagen stimulation[65]. 14-HDPAn6 was also shown to be a potent inhibitor, with 5% at 1 µM when stimulated with collagen and 10% at 1 µM, when stimulated with thrombin [22]. Considering the similar potency between the 14-oxylipins and the 17-oxylipins, the platelet aggregation effect was determined for 14-HDTA to determine if the same transition to agonist as seen for 17-HDTA would also be observed for 14-HDTA. Contrary to the data for 17-HDTA, 14-HDTA was only an inhibitor, with 4.8 +/- 1% aggregation at 5 µM when stimulated with collagen and 49 +/- 10% at 10 µM when stimulated with thrombin (**Figure 5**). These data indicate that the 14-oxylipins do not follow a similar platelet effect mechanism as do the 17-oxylipins and thus, the change in location of oxidation affects their mechanism of actions. This result is like that

Figure 5. Inhibition of platelet aggregation with 14-HDTA.
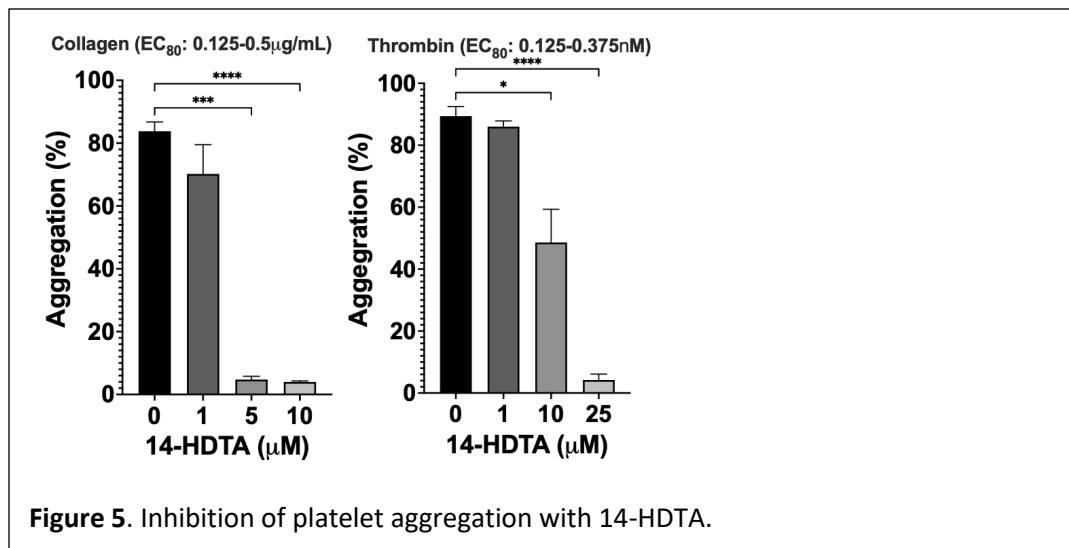
seen for the 12- and 15-oxylipins derived from AA, where 12-HETE induces pro-thrombotic platelet activity, while 15-HETE induces anti-thrombotic activity *(61, 63)*. It should be noted

that due to the lack of activity of h12-LOX against DTrA and DDiA, the isolation of 14-oxylipin products from these fatty acids was not achieved.

CONCLUSION:

Table 7: Effects of oxylipins on platelet aggregation.			
Oxylipin	Inhibition Effect Thrombin Stimulation	Inhibition Effect Collagen Stimulation	Agonistic Effect No Stimulation
17-HDHA	$63 \pm 10\%$ @ 25 µM	$24 \pm 10\%$ @ 5 µM	None
17-DPAn6	$29 \pm 9\%$ @ 25 µM	$14 \pm 4\%$ @ 5 µM	None
17-DPAn3	None	None	$26 \pm 10\%$ @ 5 µM
17-HDTA	None	$20 \pm 10\%$ @ 0.5 µM	$41 \pm 10\%$ @ 5 µM
17-HDTrA	None	None	$84 \pm 2\%$ @ 5 µM
17-HDDiA	None	None	$55 \pm 10\%$ @ 5 µM
14-HDTA	$49 \pm 10\%$ @ 10 µM	$4.8 \pm 1\%$ @ 5 µM	None

In summary, the kinetic rates and product preference of each of the three LOX isozymes, h12-LOX, h15-LOX-1 and h15-LOX-2, is generally not affected if either D^4 or D^{19} is removed from DHA (i.e., DPAn3 or DPAn6). However, if both D^4 and D^{19} are removed, the rate for both h12-LOX and h15-LOX-2 is reduced more than 10-fold, suggesting that the increased flexibility and hydrophobicity, due to the lower saturation state of DTA, leads to a less-productive ES complex. For h15-LOX-2, the rate and product distribution are affected even further with decreased unsaturation (i.e., DTrA and DDiA), indicating the ES complex becomes even more un-productive with additional flexibility and hydrophobicity. In contrast, the kinetic values for h15-LOX-1 do not change appreciably with decreasing degrees of unsaturation, indicating an ES complex that is less dependent on flexibility and hydrophobicity than that for h12-LOX and h15-LOX-2. Interestingly, while the kinetics of h15-LOX-1 are not affected by the unsaturation of the substrate, the product profile is affected. As the C22-FAs become less unsaturated, more of the 17-oxylipin is produced

indicating a reduced penetration of the substrate into the active site. It is unclear why the

C22-FAs have reduced active site penetration as their flexibility and hydrophobicity are

increased, however, it is possible that the loss of a specific pi-pi interaction with an active site

residue is lost, lowering the energetics of active site insertion. We are currently investigating

if a specific active site residue interacts with the fatty acids and accounts for these data

through mutagenesis.

With respect to the effect the 17-oxylipins had on platelet activity, the degree of

unsaturation of C22-FA-derived oxylipins had substantial effects, on both inhibition and

aggregation. The highly saturated 17-oxylipins (i.e., 17-HDHA and 17-HDPAn6) exhibited

inhibitory effects on platelet aggregation, with the effect being larger with collagen

activation. However, as saturation decreases, the effect of the 17-oxylipin switches to

agonistic. The transition occurs with 17-DPAn3, which is purely agonistic and 17-HDTA,

which is mixed inhibitor/agnostic, with the key chemical feature being the loss of D^4.

Surprisingly, the 14-oxylipin of DTA, 14-HDTA, has a different effect on platelet

aggregation. While 14-HDTA inhibits platelet aggregation with both thrombin and collagen,

17-HDTA is inhibitory at low concentrations but agonistic at high concentrations. These

findings highlight the complexity of platelet regulation by oxylipins and may have

implications towards their biological significance. For example, since h15-LOX-1 reacts

equally well with each of these four C22-FAs, but their 17-oxylipin effects on platelet

aggregation are orthogonal to each other, the micro-distribution of these C22-FAs in one's

diet could have distinct consequences with regards to platelet activity and hence

cardiovascular indications. In addition, although platelets do not contain 15-LOX isozymes,

the oxylipins produced by 15-LOXs are highly potent biomolecules towards platelet

activation, suggesting that other cells, such as leukocytes may influence platelet function

significantly. We are currently investigating the inhibitory and agonistic mechanism of action these oxylipins to determine the biochemical requirements for these distinct platelet effects.

References

([1.) Skulas-Ray, A. C., Wilson, P. W. F., Harris, W. S., Brinton, E. A., Kris-
Etherton, P. M., Richter, C. K., Jacobson, T. A., Engler, M. B., Miller, M.,
Robinson, J. G., Blum, C. B., Rodriguez-Leyva, D., de Ferranti, S. D., and
Welty, F. K. (**2019**) Omega-3 Fatty Acids for the Management of
Hypertriglyceridemia: A Science Advisory From the American Heart
Association, *Circulation 140*, e673-e691.

([2.) Cabo, J., Alonso, R., and Mata, P. (**2012**) Omega-3 fatty acids and blood
pressure, *Br J Nutr 107 Suppl 2*, S195-200.

([3.) Simopoulos, A. P. (**2002**) Omega-3 fatty acids in inflammation and autoimmune
diseases, *J Am Coll Nutr 21*, 495-505.

([4.) Calder, P. C. (**2017**) Omega-3 fatty acids and inflammatory processes: from
molecules to man, *Biochem Soc Trans 45*, 1105-1115.

([5.) Cheng, J. W., and Santoni, F. (**2008**) Omega-3 fatty acid: a role in the
management of cardiac arrhythmias?, *J Altern Complement Med 14*, 965-974.

([6.) Curfman, G. (**2021**) Omega-3 Fatty Acids and Atrial Fibrillation, *Jama 325*,
1063.

([7.) Alfaddagh, A., Kapoor, K., Dardari, Z. A., Bhatt, D. L., Budoff, M. J., Nasir, K., Miller, M., Welty, F. K., Miedema, M. D., Shapiro, M. D., Tsai, M. Y., Blumenthal, R. S., and Blaha, M. J. (**2022**) Omega-3 fatty acids, subclinical atherosclerosis, and cardiovascular events: Implications for primary prevention, *Atherosclerosis 353*, 11-19.

([8.) Barry, A. R., and Dixon, D. L. (**2021**) Omega-3 fatty acids for the prevention of atherosclerotic cardiovascular disease, *Pharmacotherapy 41*, 1056-1065.

([9.) Zheng, X., Jia, R., Li, Y., Liu, T., and Wang, Z. (**2020**) Omega-3 fatty acids reduce post-operative risk of deep vein thrombosis and pulmonary embolism after surgery for elderly patients with proximal femoral fractures: a randomized placebo-controlled, double-blind clinical trial, *Int Orthop 44*, 2089-2093.

([10.) McEwen, B. J., Morel-Kopp, M. C., Tofler, G. H., and Ward, C. M. (**2015**) The effect of omega-3 polyunsaturated fatty acids on fibrin and thrombin generation in healthy subjects and subjects with cardiovascular disease, *Semin Thromb Hemost 41*, 315-322.

([11.) Horrocks, L. A., and Yeo, Y. K. (**1999**) Health benefits of docosahexaenoic acid (DHA), *Pharmacol Res 40*, 211-225.

([12.) Calder, P. C. (**2016**) Docosahexaenoic Acid, *Ann Nutr Metab 69 Suppl 1*, 7-21.

([13.) Li, J., Pora, B. L. R., Dong, K., and Hasjim, J. (**2021**) Health benefits of docosahexaenoic acid and its bioavailability: A review, *Food Sci Nutr 9*, 5229-5243.

([14.) Miller, E., Kaur, G., Larsen, A., Loh, S. P., Linderborg, K., Weisinger, H. S., Turchini, G. M., Cameron-Smith, D., and Sinclair, A. J. (**2013**) A short-term n-3 DPA supplementation study in humans, *Eur J Nutr 52*, 895-904.

([15.) Drouin, G., Rioux, V., and Legrand, P. (**2019**) The n-3 docosapentaenoic acid (DPA): A new player in the n-3 long chain polyunsaturated fatty acid family, *Biochimie 159*, 36-48.

([16.) Chen, J., Jiang, Y., Liang, Y., Tian, X., Peng, C., Ma, K. Y., Liu, J., Huang, Y., and Chen, Z. Y. (**2012**) DPA n-3, DPA n-6 and DHA improve lipoprotein profiles and aortic function in hamsters fed a high cholesterol diet, *Atherosclerosis 221*, 397-404.

([17.) de Oliveira Otto, M. C., Wu, J. H., Baylin, A., Vaidya, D., Rich, S. S., Tsai, M. Y., Jacobs, D. R., Jr., and Mozaffarian, D. (**2013**) Circulating and dietary omega-3 and omega-6 polyunsaturated fatty acids and incidence of CVD in the Multi-Ethnic Study of Atherosclerosis, *J Am Heart Assoc 2*, e000506.

([18.) Morin, C., Rousseau, É., and Fortin, S. (**2013**) Anti-proliferative effects of a new docosapentaenoic acid monoacylglyceride in colorectal carcinoma cells, *Prostaglandins Leukot Essent Fatty Acids 89*, 203-213.

([19.) Skulas-Ray, A. C., Flock, M. R., Richter, C. K., Harris, W. S., West, S. G., and Kris-Etherton, P. M. (**2015**) Red Blood Cell Docosapentaenoic Acid (DPA n-3) is Inversely Associated with Triglycerides and C-reactive Protein (CRP) in Healthy Adults and Dose-Dependently Increases Following n-3 Fatty Acid Supplementation, *Nutrients 7*, 6390-6404.

([20.) Gobbetti, T., Dalli, J., Colas, R. A., Federici Canova, D., Aursnes, M., Bonnet, D., Alric, L., Vergnolle, N., Deraison, C., Hansen, T. V., Serhan, C. N., and Perretti, M. (**2017**) Protectin D1(n-3 DPA) and resolvin D5(n-3 DPA) are effectors of intestinal protection, *Proc Natl Acad Sci U S A 114*, 3963-3968.

([21.) Sun, Q., Ma, J., Campos, H., Rexrode, K. M., Albert, C. M., Mozaffarian, D., and Hu, F. B. (**2008**) Blood concentrations of individual long-chain n-3 fatty acids and risk of nonfatal myocardial infarction, *Am J Clin Nutr 88*, 216-223.

([22.) Yeung, J., Adili, R., Yamaguchi, A., Freedman, C. J., Chen, A., Shami, R., Das, A., Holman, T. R., and Holinstat, M. (**2020**) Omega-6 DPA and its 12-lipoxygenase-oxidized lipids regulate platelet reactivity in a nongenomic PPARα-dependent manner, *Blood Adv 4*, 4522-4537.

([23.) Dyall, S. C. (**2015**) Long-chain omega-3 fatty acids and the brain: a review of the independent and shared effects of EPA, DPA and DHA, *Front Aging Neurosci 7*, 52.

([24.) Lim, S. Y., Hoshiba, J., and Salem, N., Jr. (**2005**) An extraordinary degree of structural specificity is required in neural phospholipids for optimal brain function: n-6 docosapentaenoic acid substitution for docosahexaenoic acid leads to a loss in spatial task performance, *J Neurochem 95*, 848-857.

([25.) Welty, F. K. (**2023**) Omega-3 fatty acids and cognitive function, *Curr Opin Lipidol 34*, 12-21.

([26.) Böckmann, K. A., von Stumpff, A., Bernhard, W., Shunova, A., Minarski, M., Frische, B., Warmann, S., Schleicher, E., Poets, C. F., and Franz, A. R. (**2021**) Fatty acid composition of adipose tissue at term indicates deficiency of arachidonic and docosahexaenoic acid and excessive linoleic acid supply in preterm infants, *Eur J Nutr 60*, 861-872.

([27.) Gorusupudi, A., Chang, F. Y., Nelson, K., Hageman, G. S., and Bernstein, P. S. (**2019**) n-3 PUFA Supplementation Alters Retinal Very-Long-Chain-PUFA Levels and Ratios in Diabetic Animal Models, *Mol Nutr Food Res 63*, e1801058.

([28.) Li, L. J., Wu, J., Chen, Z., Weir, N. L., Tsai, M. Y., Albert, P., and Zhang, C. (**2022**) Plasma phospholipid polyunsaturated fatty acids composition in early pregnancy and fetal growth trajectories throughout pregnancy: Findings from the US fetal growth studies-singletons cohort, *EBioMedicine 82*, 104180.

([29.) Chen, Y., Qiu, X., and Yang, J. (**2021**) Comparing the In Vitro Antitumor, Antioxidant and Anti-Inflammatory Activities between Two New Very Long Chain Polyunsaturated Fatty Acids, Docosadienoic Acid (DDA) and Docosatrienoic Acid (DTA), and Docosahexaenoic Acid (DHA), *Nutr Cancer 73*, 1697-1707.

([30.) Robinson, L. E., and Mazurak, V. C. (**2013**) N-3 polyunsaturated fatty acids: relationship to inflammation in healthy adults and adults exhibiting features of metabolic syndrome, *Lipids 48*, 319-332.

([31.) Saito, H., and Ioka, H. (**2019**) Lipids and Fatty Acids of Sea Hares Aplysia kurodai and Aplysia juliana: High Levels of Icosapentaenoic and n-3 Docosapentaenoic Acids, *J Oleo Sci 68*, 1199-1213.

([32.) AbuGhazaleh, A. A., Holmes, L. D., Jacobson, B. N., and Kalscheur, K. F. (**2006**) Short communication: Eicosatrienoic acid and docosatrienoic acid do

not promote vaccenic acid accumulation in mixed ruminal cultures, *J Dairy Sci 89*, 4336-4339.

([33.) Innis, S. M., Vaghri, Z., and King, D. J. (**2004**) n-6 Docosapentaenoic acid is not a predictor of low docosahexaenoic acid status in Canadian preschool children, *Am J Clin Nutr 80*, 768-773.

([34.) Kretzer, C., Jordan, P. M., Bilancia, R., Rossi, A., Gür Maz, T., Banoglu, E., Schubert, U. S., and Werz, O. (**2022**) Shifting the Biosynthesis of Leukotrienes Toward Specialized Pro-Resolving Mediators by the 5-Lipoxygenase-Activating Protein (FLAP) Antagonist BRP-201, *J Inflamm Res 15*, 911-925.

([35.) Schebb, N. H., Kühn, H., Kahnt, A. S., Rund, K. M., O'Donnell, V. B., Flamand, N., Peters-Golden, M., Jakobsson, P. J., Weylandt, K. H., Rohwer, N., Murphy, R. C., Geisslinger, G., FitzGerald, G. A., Hanson, J., Dahlgren, C., Alnouri, M. W., Offermanns, S., and Steinhilber, D. (**2022**) Formation, Signaling and Occurrence of Specialized Pro-Resolving Lipid Mediators-What is the Evidence so far?, *Front Pharmacol 13*, 838782.

([36.) Gilbert, N. C., Newcomer, M. E., and Werz, O. (**2021**) Untangling the web of 5-lipoxygenase-derived products from a molecular and structural perspective: The battle between pro- and anti-inflammatory lipid mediators, *Biochem Pharmacol 193*, 114759.

([37.) Lehmann, C., Homann, J., Ball, A. K., Blöcher, R., Kleinschmidt, T. K., Basavarajappa, D., Angioni, C., Ferreirós, N., Häfner, A. K., Rådmark, O., Proschak, E., Haeggström, J. Z., Geisslinger, G., Parnham, M. J., Steinhilber, D., and Kahnt, A. S. (**2015**) Lipoxin and resolvin biosynthesis is dependent on 5-lipoxygenase activating protein, *Faseb j 29*, 5029-5043.

([38.) Mashima, R., and Okuyama, T. (**2015**) The role of lipoxygenases in pathophysiology; new insights and future perspectives, *Redox Biol 6*, 297-310.

([39.) Pidgeon, G. P., Lysaght, J., Krishnamoorthy, S., Reynolds, J. V., O'Byrne, K., Nie, D., and Honn, K. V. (**2007**) Lipoxygenase metabolism: roles in tumor progression and survival, *Cancer Metastasis Rev 26*, 503-524.

([40.) Zeng, M., and Cao, H. (**2018**) Fast quantification of short chain fatty acids and ketone bodies by liquid chromatography-tandem mass spectrometry after facile derivatization coupled with liquid-liquid extraction, *J Chromatogr B Analyt Technol Biomed Life Sci 1083*, 137-145.

([41.) Di Pasquale, M. G. (**2009**) The essentials of essential fatty acids, *J Diet Suppl 6*, 143-161.

([42.) Srivastava, L. M. (2002) CHAPTER 19 - Seed Germination, Mobilization of Food Reserves, and Seed Dormancy, In *Plant Growth and Development* (Srivastava, L. M., Ed.), pp 447-471, Academic Press, San Diego.

([43.) Prigge, S. T., Boyington, J. C., Faig, M., Doctor, K. S., Gaffney, B. J., and Amzel, L. M. (**1997**) Structure and mechanism of lipoxygenases, *Biochimie 79*, 629-636.

([44.) Andreou, A., and Feussner, I. (**2009**) Lipoxygenases - Structure and reaction mechanism, *Phytochemistry 70*, 1504-1510.

([45.) Nelson, M. J., and Seitz, S. P. (**1994**) The structure and function of lipoxygenase, *Curr Opin Struct Biol 4*, 878-884.

([46.) Tran, M., Signorelli, R. L., Yamaguchi, A., Chen, E., Holinstat, M., Iavarone, A. T., Offenbacher, A. R., and Holman, T. (**2023**) Biochemical and hydrogen-deuterium exchange studies of the single nucleotide polymorphism Y649C in human platelet 12-lipoxygenase linked to a bleeding disorder, *Arch Biochem Biophys 733*, 109472.

([47.) Armstrong, M., van Hoorebeke, C., Horn, T., Deschamps, J., Freedman, J. C., Kalyanaraman, C., Jacobson, M. P., and Holman, T. (**2016**) Human 15-LOX-1

active site mutations alter inhibitor binding and decrease potency, *Bioorg Med Chem 24*, 5380-5387.

([48.) Tallima, H., and El Ridi, R. (**2018**) Arachidonic acid: Physiological roles and potential health benefits - A review, *J Adv Res 11*, 33-41.

([49.) Hanna, V. S., and Hafez, E. A. A. (**2018**) Synopsis of arachidonic acid metabolism: A review, *J Adv Res 11*, 23-32.

([50.) Wang, B., Wu, L., Chen, J., Dong, L., Chen, C., Wen, Z., Hu, J., Fleming, I., and Wang, D. W. (**2021**) Metabolism pathways of arachidonic acids: mechanisms and potential therapeutic targets, *Signal Transduct Target Ther 6*, 94.

([51.) Borngräber, S., Browner, M., Gillmor, S., Gerth, C., Anton, M., Fletterick, R., and Kühn, H. (**1999**) Shape and specificity in mammalian 15-lipoxygenase active site. The functional interplay of sequence determinants for the reaction specificity, *J Biol Chem 274*, 37345-37350.

([52.) Schwarz, K., Borngräber, S., Anton, M., and Kuhn, H. (**1998**) Probing the substrate alignment at the active site of 15-lipoxygenases by targeted substrate modification and site-directed mutagenesis. Evidence for an inverse substrate orientation, *Biochemistry 37*, 15327-15335.

([53.) Tsai, W. C., Aleem, A. M., Tena, J., Rivera-Velazquez, M., Brah, H. S., Tripathi, S., D'Silva, M., Nadler, J. L., Kalyanaraman, C., Jacobson, M. P., and Holman, T. (**2021**) Docking and mutagenesis studies lead to improved inhibitor development of ML355 for human platelet 12-lipoxygenase, *Bioorg Med Chem 46*, 116347.

([54.) Aleem, A. M., Tsai, W. C., Tena, J., Alvarez, G., Deschamps, J., Kalyanaraman, C., Jacobson, M. P., and Holman, T. (**2019**) Probing the Electrostatic and Steric Requirements for Substrate Binding in Human Platelet-Type 12-Lipoxygenase, *Biochemistry 58*, 848-857.

([55.) Newcomer, M. E., and Brash, A. R. (**2015**) The structural basis for specificity in lipoxygenase catalysis, *Protein Sci 24*, 298-309.

([56.) Gilbert, N. C., Bartlett, S. G., Waight, M. T., Neau, D. B., Boeglin, W. E., Brash, A. R., and Newcomer, M. E. (**2011**) The structure of human 5-lipoxygenase, *Science 331*, 217-219.

([57.) Gilbert, N. C., Gerstmeier, J., Schexnaydre, E. E., Börner, F., Garscha, U., Neau, D. B., Werz, O., and Newcomer, M. E. (**2020**) Structural and mechanistic insights into 5-lipoxygenase inhibition by natural products, *Nat Chem Biol 16*, 783-790.

([58.) Rådmark, O., Werz, O., Steinhilber, D., and Samuelsson, B. (**2007**) 5-Lipoxygenase: regulation of expression and enzyme activity, *Trends Biochem Sci 32*, 332-341.

([59.) Perry, S. C., van Hoorebeke, C., Sorrentino, J., Bautista, L., Akinkugbe, O., Conrad, W. S., Rutz, N., and Holman, T. R. (**2022**) Structural basis for altered positional specificity of 15-lipoxygenase-1 with 5S-HETE and 7S-HDHA and the implications for the biosynthesis of resolvin E4, *Arch Biochem Biophys 727*, 109317.

([60.) Wecksler, A. T., Garcia, N. K., and Holman, T. R. (**2009**) Substrate specificity effects of lipoxygenase products and inhibitors on soybean lipoxygenase-1, *Bioorg Med Chem 17*, 6534-6539.

([61.) Yamaguchi, A., van Hoorebeke, C., Tourdot, B. E., Perry, S. C., Lee, G., Rhoads, N., Rickenberg, A., Green, A. R., Sorrentino, J., Yeung, J., Freedman, J. C., Holman, T. R., and Holinstat, M. (**2023**) Fatty acids negatively regulate platelet function through formation of noncanonical 15-lipoxygenase-derived eicosanoids, *Pharmacol Res Perspect 11*, e01056.

([62.) Yeung, J., Tourdot, B. E., Adili, R., Green, A. R., Freedman, C. J., Fernandez-Perez, P., Yu, J., Holman, T. R., and Holinstat, M. (**2016**) 12(S)-HETrE, a 12-

Lipoxygenase Oxylipin of Dihomo-γ-Linolenic Acid, Inhibits Thrombosis via

Gαs Signaling in Platelets, *Arterioscler Thromb Vasc Biol 36*, 2068-2077.

([63.) Yeung, J., Hawley, M., and Holinstat, M. (**2017**) The expansive role of

oxylipins on platelet biology, *J Mol Med (Berl) 95*, 575-588.

([64.) Tsai, W. C., Kalyanaraman, C., Yamaguchi, A., Holinstat, M., Jacobson, M. P.,

and Holman, T. R. (**2021**) In Vitro Biosynthetic Pathway Investigations of

Neuroprotectin D1 (NPD1) and Protectin DX (PDX) by Human 12-

Lipoxygenase, 15-Lipoxygenase-1, and 15-Lipoxygenase-2, *Biochemistry 60*,

1741-1754.

([65.) Yamaguchi, A., Stanger, L., Freedman, C. J., Standley, M., Hoang, T., Adili,

R., Tsai, W. C., van Hoorebeke, C., Holman, T. R., and Holinstat, M. (**2021**)

DHA 12-LOX-derived oxylipins regulate platelet activation and thrombus

formation through a PKA-dependent signaling pathway, *J Thromb Haemost

19*, 839-851.

([66.) Perry, S. C., Horn, T., Tourdot, B. E., Yamaguchi, A., Kalyanaraman, C.,

Conrad, W. S., Akinkugbe, O., Holinstat, M., Jacobson, M. P., and Holman,

T. R. (**2020**) Role of Human 15-Lipoxygenase-2 in the Biosynthesis of the

Lipoxin Intermediate, 5S,15S-diHpETE, Implicated with the Altered

Positional Specificity of Human 15-Lipoxygenase-1, *Biochemistry 59*, 4118-4130.

([67.) Freedman, C., Tran, A., Tourdot, B. E., Kalyanaraman, C., Perry, S., Holinstat, M., Jacobson, M. P., and Holman, T. R. (**2020**) Biosynthesis of the Maresin Intermediate, 13S,14S-Epoxy-DHA, by Human 15-Lipoxygenase and 12-Lipoxygenase and Its Regulation through Negative Allosteric Modulators, *Biochemistry 59*, 1832-1844.

([68.) Fredman, G., Van Dyke, T. E., and Serhan, C. N. (**2010**) Resolvin E1 regulates adenosine diphosphate activation of human platelets, *Arterioscler Thromb Vasc Biol 30*, 2005-2013.

([69.) Vijil, C., Hermansson, C., Jeppsson, A., Bergström, G., and Hultén, L. M. (**2014**) Arachidonate 15-lipoxygenase enzyme products increase platelet aggregation and thrombin generation, *PLoS One 9*, e88546.

([70.) Vasquez-Martinez, Y., Ohri, R. V., Kenyon, V., Holman, T. R., and Sepúlveda-Boza, S. (**2007**) Structure-activity relationship studies of flavonoids as potent inhibitors of human platelet 12-hLO, reticulocyte 15-hLO-1, and prostate epithelial 15-hLO-2, *Bioorg Med Chem 15*, 7408-7425.

([71.) Robinson, S. J., Hoobler, E. K., Riener, M., Loveridge, S. T., Tenney, K., Valeriote, F. A., Holman, T. R., and Crews, P. (**2009**) Using enzyme assays to

evaluate the structure and bioactivity of sponge-derived meroterpenes, *J Nat Prod 72*, 1857-1863.

([72.) Perry, S. C., Kalyanaraman, C., Tourdot, B. E., Conrad, W. S., Akinkugbe, O., Freedman, J. C., Holinstat, M., Jacobson, M. P., and Holman, T. R. (**2020**) 15-Lipoxygenase-1 biosynthesis of 7S,14S-diHDHA implicates 15-lipoxygenase-2 in biosynthesis of resolvin D5, *J Lipid Res 61*, 1087-1103.

([73.) Ikei, K. N., Yeung, J., Apopa, P. L., Ceja, J., Vesci, J., Holman, T. R., and Holinstat, M. (**2012**) Investigations of human platelet-type 12-lipoxygenase: role of lipoxygenase products in platelet activation, *J Lipid Res 53*, 2546-2559.

([74.) Tourdot, B. E., Conaway, S., Niisuke, K., Edelstein, L. C., Bray, P. F., and Holinstat, M. (**2014**) Mechanism of race-dependent platelet activation through the protease-activated receptor-4 and Gq signaling axis, *Arterioscler Thromb Vasc Biol 34*, 2644-2650.

([75.) Tsai, W. C., Gilbert, N. C., Ohler, A., Armstrong, M., Perry, S., Kalyanaraman, C., Yasgar, A., Rai, G., Simeonov, A., Jadhav, A., Standley, M., Lee, H. W., Crews, P., Iavarone, A. T., Jacobson, M. P., Neau, D. B., Offenbacher, A. R., Newcomer, M., and Holman, T. R. (**2021**) Kinetic and structural

investigations of novel inhibitors of human epithelial 15-lipoxygenase-2, *Bioorg Med Chem 46*, 116349.

([76.) Kobe, M. J., Neau, D. B., Mitchell, C. E., Bartlett, S. G., and Newcomer, M. E. (**2014**) The structure of human 15-lipoxygenase-2 with a substrate mimic, *J Biol Chem 289*, 8562-8569.

([77.) Gan, Q. F., Browner, M. F., Sloane, D. L., and Sigal, E. (**1996**) Defining the arachidonic acid binding site of human 15-lipoxygenase. Molecular modeling and mutagenesis, *J Biol Chem 271*, 25412-25418.

([78.) Droege, K. D., Keithly, M. E., Sanders, C. R., Armstrong, R. N., and Thompson, M. K. (**2017**) Structural Dynamics of 15-Lipoxygenase-2 via Hydrogen-Deuterium Exchange, *Biochemistry 56*, 5065-5074.

([79.) Ramon, S., Baker, S. F., Sahler, J. M., Kim, N., Feldsott, E. A., Serhan, C. N., Martínez-Sobrido, L., Topham, D. J., and Phipps, R. P. (**2014**) The specialized proresolving mediator 17-HDHA enhances the antibody-mediated immune response against influenza virus: a new class of adjuvant?, *J Immunol 193*, 6031-6040.